Diploma thesis

Investigation of Anhydrides and Epoxides as Alternative Ring-Opening Copolymerization Monomers in Photopolymerization

conducted at the

Research Group for Polymer Chemistry and Technology,

Institute of Applied Synthetic Chemistry (IAS),

Vienna University of Technology (TU Vienna)

under the supervision of

Univ.Ass. Dr.techn. Katharina Ehrmann, MSc

Univ.Prof. Dipl.-Ing. Dr.techn. Robert Liska

by

Theresa Ammann, BSc

11701260

_____

Theresa Ammann, BSc

Danksagung

Eine Diplomarbeit entsteht nicht von allein über Nacht – viele Stunden Arbeit sind nötig, man erlebt Erfolge und Misserfolge, Begeisterung und Frustration. Und ohne die vielen Personen, die einen auf diesem Weg begleiten und unterstützen, würde man es nie bis zur Zielgeraden schaffen. Deshalb möchte ich mich an dieser Stelle bei allen bedanken, die mich ins Ziel gebracht haben.

Zuerst möchte ich mich bei **Robert** bedanken für die Möglichkeit, die Arbeit in seiner Forschungsgruppe an einem super spannenden Thema zu schreiben. Danke, dass du ohne zu zögern ja gesagt hast, als ich dich um eine Diplomarbeit gefragt habe, und mir mit deiner Erfahrung immer den richtigen Weg gewiesen hast.

Ein besonderer Dank gilt meiner Betreuerin **Kathi**. Danke, dass du so involviert in meiner Arbeit warst: Du wusstest immer Bescheid, was ich mache und was ich brauche. Du hast mich gefordert, aber mir auch das Gefühl gegeben, dass meine Arbeit wichtig ist und ich tolle Ergebnisse liefere. Bei Problemen habe ich mich nie allein gelassen gefühlt, denn du hast mir immer mögliche Auswege gezeigt.

Bedanken möchte ich mich auch bei **Carola**, die mit mir im Zuge eines Wahlpraktikums in der FBMC Initiatoren gekocht hat. Du hast mir gezeigt, wie spannend Polymerchemie sein kann, und mich außerdem in diese supernette, tolle Forschungsgruppe eingeführt.

Damit ein riesiges Dankeschön an **alle Mitglieder der FBMC**! Ein gutes Arbeitsklima hilft enorm dabei, konzentriert und mit Freude an einem Thema zu arbeiten. Ihr wart immer da für mich, wenn ich Fragen zu meiner Reaktion oder Messgeräten hatte (und habt Unmengen NMR für mich gemessen). Aber auch die lustigen, entspannten Momente außerhalb des Labors haben dafür gesorgt, dass ich jeden Tag voller Energie im Labor gestanden bin. Ob beim Kochen in der Küche, bei Institutsausflügen oder bei sonstigen sozialen Events, es war immer lustig und ich bin gerne mit euch unterwegs. Danke an meine Diplomanden-Kollegen **Björn, Edma, Philip Sgarz** und **Kristina** – zusammen lässt sich der Weg immer einfacher beschreiten. Danke an das H45 – **Carola, Klaus, Toni, Olja, Tina, Miriam** - ihr wart einfach immer für mich da (und nicht nur wegen der räumlichen Nähe 😉). **Dani, Chrissie** und **Flo M.**, danke für die vielen gemeinsamen Koch-Sessions und für eure offene, inklusive und freundliche Art. Danke an **Michi, Flo P., Larissa, Anna, Selina, Jelena, Markus, Kaja, Daniel, Haidi** und **Philip Schwarzl** für viele schöne gemeinsame Erinnerungen. Danke auch an **Walter, Jürgen** und **Dagmar** für die organisatorische Unterstützung, und an **Patrick, Stefan** und **Davide** für hilfreiches Feedback während der Arbeit.

An dieser Stelle nochmal ein riesiges Dankeschön an meinen Bench-Buddy **Toni.** Ich kann gar nicht zählen, wie oft du die Worte „Hey Toni" während meiner Zeit hier gehört hast. Egal welche Frage (und ich meine wirklich jede mögliche Frage – angefangen von Chemikalienlagerplätzen zu organisatorischen Details oder wissenschaftlichen Fragen), du hattest immer ein offenes Ohr und eine gute Antwort für mich parat. Du hast dir Zeit genommen, um mich in jeder Situation zu unterstützen und zu motivieren, und hast dich zu einem extrem tollen Vorbild und einer super Freundin für mich entwickelt.

Ein Dank gilt auch Leuten abseits der FBMC, die mir bei Messungen geholfen haben. Danke an **Dominik Laa** für die Druckversuche. Danke an **Thomas Koch** für die Zugversuche. Und danke an **Irena Jelenkovic-Didic** für die Hilfe mit den LC-MS Messungen.

Schlussendlich möchte ich mich auch noch bei den Menschen außerhalb des universitären Umfeldes bedanken – bei meiner Familie und meinen Freunden. Besonders hervorheben möchte ich meine Eltern **Brigitte** und **Michael**, die mir das Studium ermöglicht haben: Ihr seid einfach zu gute Eltern, deshalb komme ich immer noch gerne heim, esse euren Kühlschrank leer und quatsche euch voll. **Klara**, danke fürs Zuquatschen und dass du mir neue Sichtweisen zeigst. Danke **Judith** fürs Einkaufen und Kochen, für viele abendliche Gespräche und Aktivitäten außerhalb der Universität. Danke **Martina** – was soll ich sagen, du bist immer für mich da, und egal ob Theaterbesuch, Kletterhalle oder Grillabend, du stehst immer ganz oben auf meiner Einladungsliste.

Abstract

Polyesters are interesting polymers due to their versatility and degradability. This degradability furthermore allows for the potential development of recycling processes, resulting in significant environmental and economic benefits. Therefore, utilization of this material class for a variety of manufacturing technologies is highly relevant.

Light-based 3D printing has been established as method for producing highly complex, specialized parts in an environmentally and economically advantageous way due to minimal energy efforts, waste production and lead times. Recently, hot lithography has been introduced as an interesting new technique that solves some of the persisting problems of light-induced 3D printing such as low reactivity, and therefore opens the technology to utilization of new polymerization mechanisms.

The ring-opening copolymerization (ROCOP) of epoxides and anhydrides is a comparably recently discovered reaction mechanism to produce polyesters. It offers several advantages over traditional synthesis methods, as it combines the mild reaction conditions typical for ring-opening polymerizations with good tunability of polymer properties due to a broad monomer scope, analogue to polycondensation reactions. Even though many different catalysts have been found for ROCOP, no attempts of directly using light to trigger the copolymerization reaction have been made to date.

In this work, photoacid generators (PAGs) and photobase generators (PBGs) were investigated as possible catalysts for the ROCOP reaction of epoxides and anhydrides that can be triggered by light and as such be used in hot stereolithography. While PAGs proved to not only catalyze the copolymerization reaction, but also enabled the side reaction of epoxides to polyethers, PBGs solely catalyze the ROCOP reaction. Therefore, linear and crosslinked photopolymer systems were further optimized using PBG as catalyst. The influence of temperature, light intensity, PBG concentration, and monomer and PBG structures regarding the stability of the formulations and the properties of the produced polyesters were investigated. For linear systems, the chain length of the produced polymers was determined using size exclusion chromatography, while the conversion of monomers was determined *via* NMR analysis. RT-FT-NIR photorheology was used for investigating crosslinked systems, and revealed large differences when using different monomers. Crosslinked materials exhibited high strength, but also high brittleness and a high glass transition temperature of 187 °C, which is typical for a thermoset material. Printing tests were only partially successful since polymerization was also observed for non-irradiated areas. Some explanations such as diffusion-based overpolymerization could be excluded, but further investigations remain necessary to elucidate this effect. Finally, a degradation study revealed that the polyesters could indeed be degraded.

Kurzfassung

Polyester sind extrem vielfältige Polymere, die auch abbaubar sind. Das ermöglicht die Entwicklung von Recycling-Prozessen und bietet damit sowohl umwelttechnische als auch ökonomische Vorteile. Deshalb ist der Einsatz verschiedener Herstellungstechnologien für diese Materialien sehr interessant.

3D Druck ist eine etablierte Methode, um hochkomplexe, individualisierte Teile mit geringem Energieaufwand, geringer Müllproduktion und kurzen Druckzeiten zu erzeugen. Die neue Entwicklung „Hot Lithography" löst einige der bestehenden Probleme mit lichtinduziertem 3D Druck, wie etwa geringe Reaktivität. Dadurch wird es möglich, auch neue, unreaktivere Systeme zu entwickeln.

Eine relativ neue Methode für die Polyestersynthese ist die ringöffnende Copolymerisation (ROCOP) von Epoxiden mit Anhydriden. Dieser Mechanismus bietet viele Vorteile gegenüber traditionellen Synthesemethoden, denn er kombiniert die typischen milden Reaktionsbedingungen der ringöffnenden Polymerisation mit den vielfältigen Polymereigenschaften, die durch viele verschiedene Monomere ermöglicht werden, ähnlich wie in Polykondensationsreaktionen. Obwohl bereits viele verschiedene Katalysatoren für die ROCOP gefunden wurden, gibt es bis jetzt noch keine Berichte zu einer direkten lichtinduzierten ROCOP Reaktion.

In dieser Arbeit wurden sowohl Photosäuregeneratoren (PAG) als auch Photobasengeneratoren (PBG) als mögliche Katalysatoren für die ROCOP untersucht, da sie durch Licht aktiviert werden und daher in „Hot Lithography" Verfahren eingesetzt werden können. Leider hat sich herausgestellt, dass PAG neben der Copolymerisation auch die Nebenreaktion von Epoxiden zu Polyethern ermöglicht. PBG andererseits katalysieren ausschließlich die Copolymerisation und wurden daher in linearen und vernetzten Systemen eingesetzt, welche anschließend optimiert wurden. Der Einfluss von Temperatur, Lichtintensität, PBG Konzentration sowie Monomer und PBG Struktur auf die Stabilität der Formulierungen und die Eigenschaften der synthetisierten Polyester wurde untersucht. Mittels Größenausschlusschromatographie wurde die Kettenlänge der erzeugten Polymere in linearen Systemen ermittelt, während die Umsätze mittels NMR-Analyse bestimmt wurden. RT-FT-NIR Photorheologie wurde für die Untersuchung vernetzter Systeme verwendet und hat große Reaktivitätsunterschiede bei der Verwendung verschiedener Monomere aufgezeigt. Die vernetzten Polymere weisen hohe Stärke, aber auch hoher Sprödigkeit sowie eine hohe Glasübergangstemperatur von 187 °C auf. Drucktests waren nur teilweise erfolgreich, da die Formulierung auch abseits der belichteten Bereiche aushärtete. Während es möglich war, einige Erklärungen wie diffusionsbasierte Überpolymerisation auszuschließen, sind weitere Versuche zur Erklärung des Effekts nötig. Der Abbau der Polymere wurde in einer grundlegenden Studie gezeigt.

TABLE OF CONTENTS

INTRODUCTION

1   SUSTAINABLE POLYMERS

Polymers are an indispensable part of daily life, with applications ranging from packaging and commodity products to medical devices. Like in every other field, scientists nowadays thrive to develop sustainable polymers to tackle the climate crisis and other environmental problems.[1] Sustainability, however, is a complex concept, as it involves many different aspects (Figure 1). Firstly, most polymers are produced from fossil fuels, which are a finite, nonrenewable resource. Therefore, finding renewable biomass-derived sources to replace fossil fuels is inevitable. Then, of course the polymer production must be performed in an environmentally friendly way, implementing the principles of green chemistry. This includes avoiding toxic chemicals and solvents where possible, and reducing waste production, transportation, and storage. Furthermore, energy-efficient production techniques should be developed and implemented into mainstream processes. Lastly, thought must be given to end-of-life management of materials, both to avoid accumulation of harmful products in the environment and enable reuse of the products.[2, 3] One technique that already inherently possesses many sustainable aspects is 3D printing, since it allows for energy-efficient, individualized production of parts while avoiding waste production and solvents. However, the end-of-life behavior of the products still has to be addressed.

Figure 1. Sustainability entails many different aspects including the use of renewable feedstocks, sustainable processing and good end-of-use behavior. Figure reproduced from ref[4] without changes. Copyright n.d. by Jin Research Group.

1.1 End-of-Life Solutions for Polymers

In order to address several problems of petrol-based chemistry, for example environmental persistence and resource recovery, appropriate end-of-life fates for products is a very hot topic for polymer researchers.

Degradability describes the possibility of changing the chemical and/or physical structure of the polymer chain under the influence of environmental factors, which leads to a decrease of molecular weight of the polymer by formation of smaller degradation molecules and thus a change of its properties.[5] This is especially important for environmental reasons, since the production of biodegradable plastics reduces the long-term accumulation of synthetic plastics in the environment, especially in oceans and soil, that harm organisms.[6]

Thermoset materials are irreversibly covalently crosslinked and can therefore not be readily degraded. Only if hydrolysable links such as ester, carbonate, amide, urea or urethane groups are introduced, (bio)degradable thermoset polymers can be obtained.[1] Other degradation modes are for example oxidative or enzymatic degradation.[7, 8]

A more advanced way of reducing the persistency footprint of polymers in our environment is to recycle materials. This can either be done by reprocessing the final polymer, for example thermally, or by decomposing the polymer into its components and closing the loop from degradation products to monomers for renewed polymerization. While thermoplastic materials can be recycled relatively easily by melting and reshaping at elevated temperatures (e.g., PET), this does not hold true for permanently crosslinked thermosets. In thermosets, degradation into regenerable degradation components is the foundation to establishing a recycling process. For this, the polymer does not only need to be degradable, but it must also be possible to transform the degradation products back into the original monomers to close the recycling loop (Figure 2). Unfortunately, many thermosets are not recyclable even if they contain degradable bonds. For example, polyester-containing monomers for photopolymerization are typically linked *via* terminal (meth)acrylates or epoxy groups. This leads to a degradable but unrecyclable polymer since recovery of the monomers is not possible. Nevertheless, even though recycling is difficult, there are several reports that focus on the up- or downcycling of those components. In contrast to recycling processes, the original monomers do not get reformed in these processes. Instead, slightly different products of lower value (downcycling) or higher value (upcycling) are obtained. [1, 2, 9]
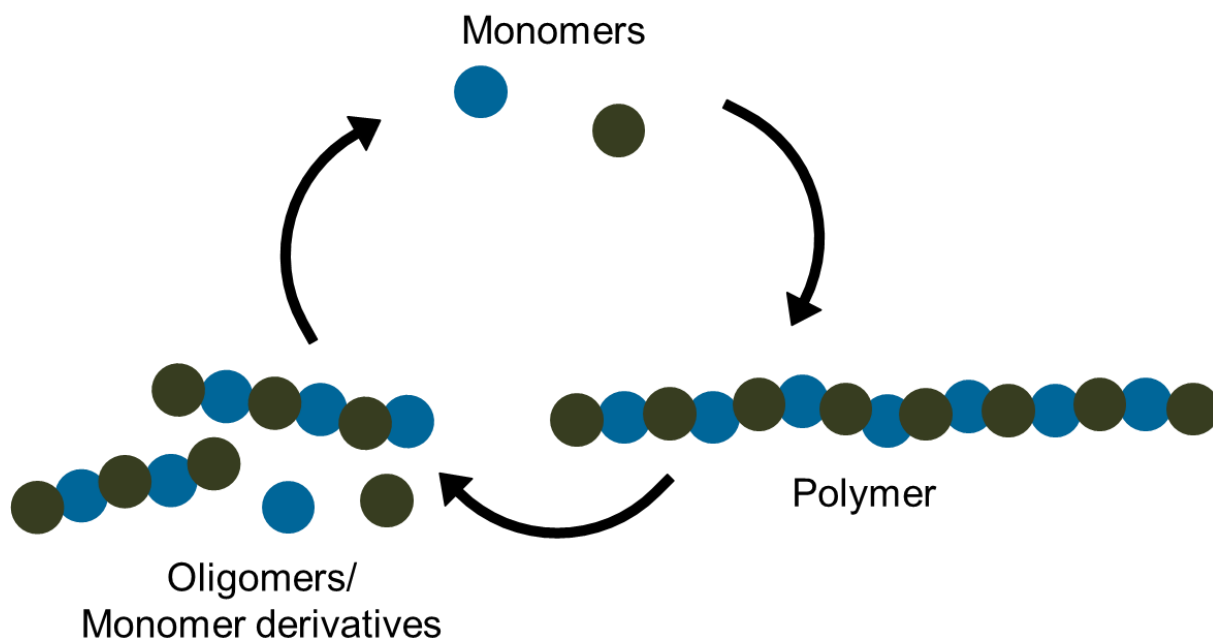
Figure 2. Schematic recycling loop for polymers.

1.2 Polyesters

Polyesters are polymers that contain ester groups in their backbone, and are therefore applicable for degradation and furthermore interesting because of their biocompatibility.[10] The most prominent example of a polyester is poly(ethylene terephthalate) (PET, Figure 3). However, the focus of science is shifting away from petrol-based chemistry towards greener chemistry. Studies about biodegradable polyesters such as poly(lactic acid) (PLA, Figure 3) and poly(caprolactone) (PCL, Figure 3), and monomers extracted from renewable resources are becoming increasingly popular.[10]

In general, aromatic moieties in the polyester backbone enhance thermal stability, mechanical strength, glass transition temperature, and chemical stability.[11] Therefore, PET is not easily biodegradable due to its aromatic groups, but aliphatic polyesters such as PLA and PCL are.
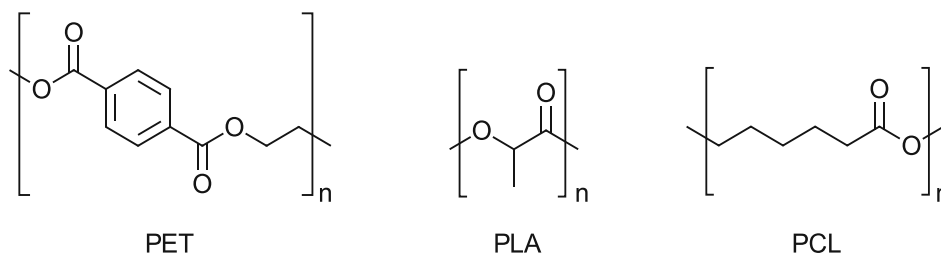

Figure 3. Structure of poly(ethylene terephthalate) (PET), poly(lactic acid) (PLA) and poly(caprolactone) (PCL) as examples for prominent polyesters.

1.2.1 Synthesis Methods

Several different reactions can be used to obtain polyesters. The most commonly used synthesis in industry is the step-growth polymerization - more precisely polycondensation - of diols and dicarboxylic acids (Figure 4a). Difunctional hydroxy carboxylic acids are also potential monomers for this reaction type.[12] Due to the wide scope of available monomers, polyesters with a wide range of properties can be produced this way. However, disadvantages of this polymerization type are plentiful: harsh reaction conditions, highly precise stoichiometry (equimolar functional groups) and energy-intensive removal of the low-mass side products, usually water, are required in order to obtain high conversions and high molecular weight polymers. This is due to the fact that the condensation reaction is an equilibrium reaction, which means removing water shifts the equilibrium towards polymer production. This reaction type is initiated by high temperatures, and usually catalysts based on manganese, antimony or zinc oxides or acetates are employed additionally.[13, 14]

Another important reaction to produce polyesters is a chain-growth reaction called ring-opening polymerization (ROP, Figure 4b), which requires cyclic esters such as ε-caprolactone as monomers. The ring size of the monomers influences the reactivity, since the release of ring strain is the main driving force of this reaction. However, only a limited number of monomers are available. Since the modification of such monomers is rather complicated, it is difficult to adjust the properties of the resulting polyester. Furthermore, aromatic cyclic esters often suffer from poor polymerizability. However, the reaction conditions in this case are much milder, the stoichiometry is irrelevant and no condensation byproducts are formed. This reaction can be initiated either by nucleophiles, which results in an anionic polymerization mechanism, or by electrophiles, which results in a cationic polymerization mechanism.[13, 15, 16]

Recently, there has been an increase in reports focusing on another chain-growth reaction type: The ring-opening copolymerization (ROCOP) of epoxides with anhydrides (Figure 4c) combines the advantages of the two mechanisms discussed above. Since a number of anhydrides and epoxides are readily available and those monomers can also be modified easily, a wide scope of different polymer properties is accessible. It is also easier to substitute just one comonomer to manipulate the properties of the resulting polyester while the catalyst and reaction conditions remain similar.[17] At the same time, the characteristic mild reaction conditions of ROP can be used. Many different catalysts have been reported for this reaction mechanism, most commonly organometallic catalysts, but also organocatalysts.[13, 15, 18-23]
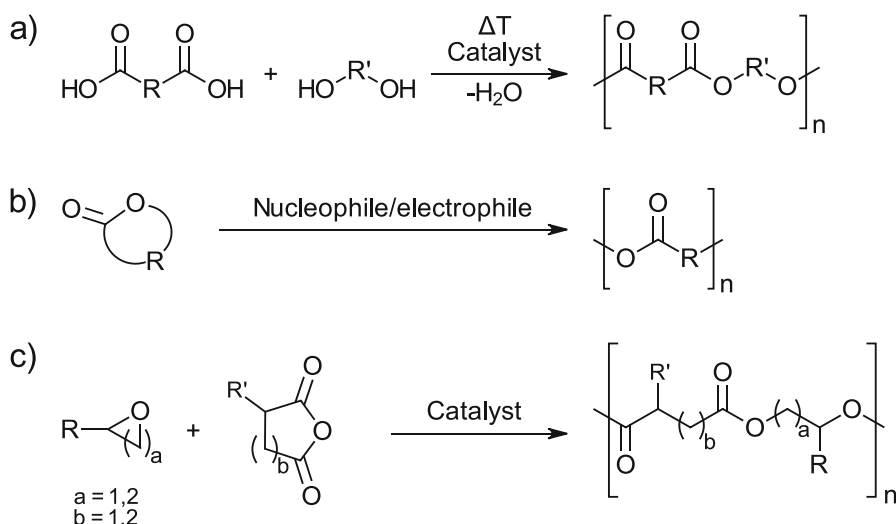
Figure 4. Different polymerization reactions for producing polyesters. a) Condensation reaction between diacids and diols (step-growth mechanism). b) Ring-opening polymerization (ROP) of cyclic esters (chain-growth mechanism). c) Ring-opening copolymerization (ROCOP) of epoxides with anhydrides (chain-growth mechanism).

1.2.2 Properties and Applications

Polyesters are both important thermoplastic and thermoset polymers.[11] The field of applications is wide and ranges from mundane applications (packaging, fibers, films) to more sophisticated applications, for example in the field of biomedicine (tumor-imaging, biomedical self-healing materials, …).[20, 21] Due to their tunable properties, polyesters are used in many different fields such as textile, automotive, medical, electronic and construction sectors.[24]

Thermoset polyesters are usually unsaturated polyesters with good chemical resistances, good electrical insulation properties and fast curing. Therefore, they are used as civil/structural engineering materials, ships materials, composites, construction, piping, storage tanks, protective coatings, and automotive paints.[24] They are very versatile and can possess a wide range of chemical and mechanical properties, dependent on the use of different monomers, initiators and additives. For example, fire-resistance or electrical resistance can be introduced.[25]

Thermoplastic polyesters including PET are mainly used as textile fibers and bottles.[24] One subgroup are elastomers, which are highly elastic and viscoelastic materials. Elastomers are for example used in automotive, aerospace, construction, electronics, healthcare, and biomedicine applications.[26]

2   ADDITIVE MANUFACTURING TECHNOLOGIES

Additive Manufacturing Technologies (AMTs), better known as 3D-printing, were first introduced in the 1980s and are important methods for the fabrication of complex 3D structures, which are printed in a layer-by-layer fashion. First, a computer-aided design (CAD) is generated and sliced into different layers, which are then processed using an AMT to obtain the final product (Figure 5).[27] This is in contrast to other known manufacturing techniques, namely subtractive and formative manufacturing. In subtractive manufacturing, material is selectively removed until the desired shape of the part is obtained, while materials are shaped *via* bending, casting or forging in formative manufacturing.[28, 29] However, using those methods leads to material waste and is typically very energy intensive, leaving AMTs as more efficient and resource-friendly alternative. Furthermore, the printing of highly complex structures becomes possible. While the low throughput is disadvantageous for some applications, 3D printing outperforms many of the other techniques in many other applications. Especially prototyping can be performed in an economically and ecologically favorable way.[27, 30]

There are a number of different AMTs, which can be classified in a number of different ways, for example classification according to the supply phase (gas-, solid- or liquid-based techniques), manufacturing process (curing, sheet, dispensing, sintering or binding process) or the type of manufactured prototype (visual, functional, material or production prototype).[29]
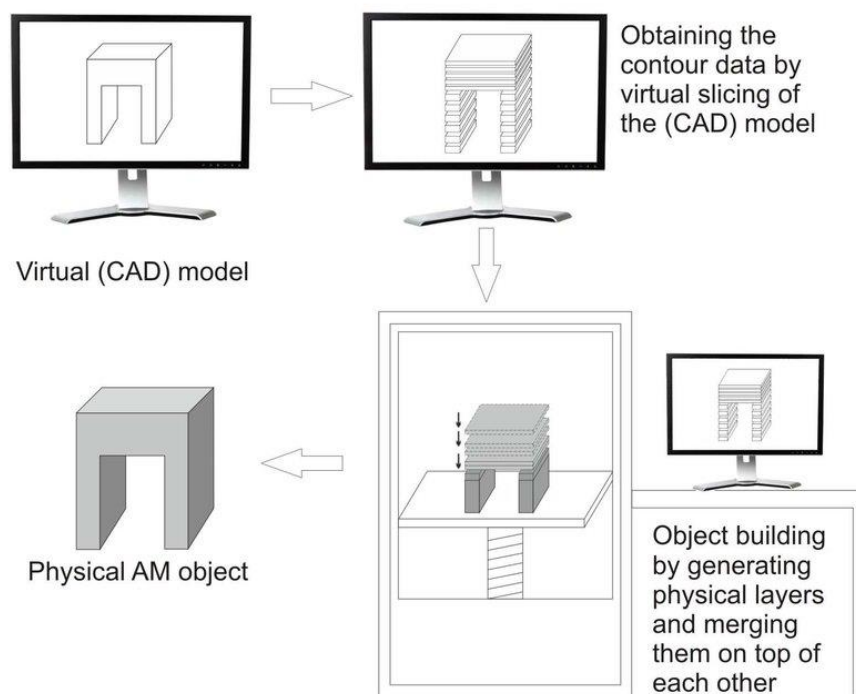

Figure 5. Principle of additive manufacturing technologies (AMTs). Figure reproduced from ref[28] without changes. Copyright 2015 by Coll Antropol.

6

Fused Deposition Modeling

Fused deposition modeling is one technique classified as AMT (Figure 6). Here, thermoplastic polymers are required that are molten and then extruded through a nozzle onto a platform in a layer-by-layer fashion. The hot filament bonds to the previous layer and hardens immediately upon cooling.[29]

However, complex structures might need support structures printed from a second nozzle that have to be removed afterwards, or might not be accessible at all since the resolution is also lower compared to other techniques like stereolithography or traditional injection molding processes. Furthermore, the material scope is limited since only thermoplastic polymers can be processed this way.[31]
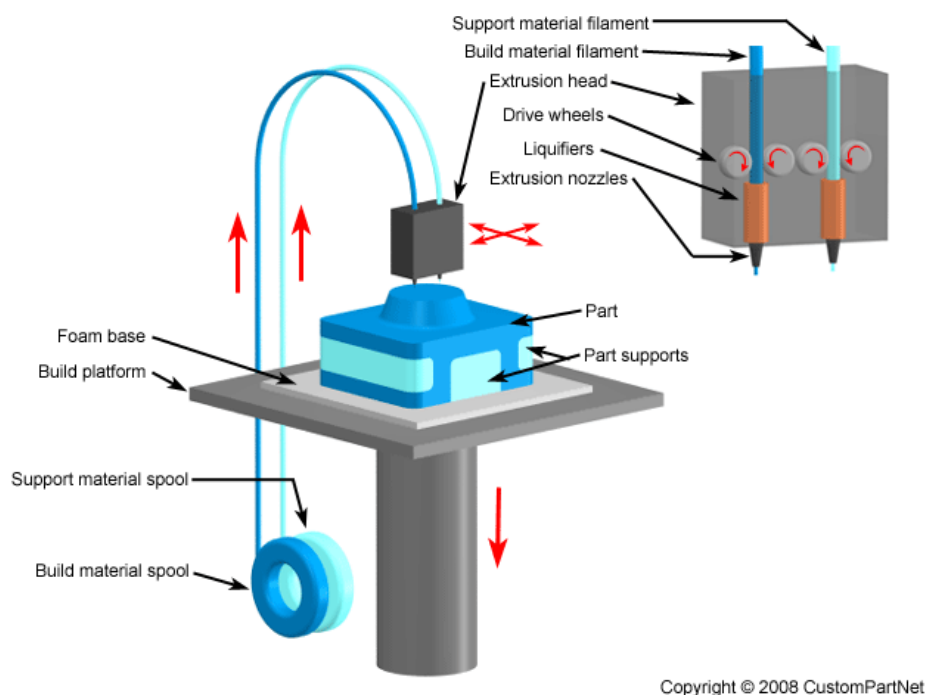
Figure 6. Scheme representing fused deposition modeling (FDM). Figure reproduced from ref[32] without changes. Copyright 2008 by CustomPartNet.

Stereolithography

Another important class of AMTs are lithography-based AMTs (L-AMTs), were a liquid photoreactive formulation is cured in a layer-by-layer fashion using light, which results in very good spatial resolution and thus the possibility to print highly complex parts. The photoreactive formulations for L-AMTs contain polymerizable monomers or prepolymers and a photoinitiator that starts the polymerization process after irradiation with light. Other components like photosensitizers, reactive diluents or additives such as inhibitors or fillers might be included as well.[29, 33, 34]

Depending on the light source, L-AMTs can be further divided into laser-stereolithography (L-SL, Figure 7a) or digital light processing-based stereolithography (DLP-SL, Figure 7b). In both of these

techniques, the photocurable formulation is placed in a vat, which is why these techniques are often summarized as vat photopolymerization techniques. A building platform is then moved in the z-direction towards the bottom of the vat until the desired gap size that corresponds to the layer thickness of the printed part is reached. In L-SL, a laser is then used to solidify the first layer by moving it in the x,y-plane and tracing the wanted shape. On the other hand, in DLP-SL a system of mirrors is used to guide the light from an LED source onto the sample surface, printing a whole layer simultaneously. This method is thus much more time-efficient, but at the same time the resolution is limited by the mirrors and subsequently the pixels available. In both cases, the building platform is then lifted up in z-direction, allowing new formulation to fill the gap, and the next layer is printed.[27, 29] The process described here is the more popular top-down approach, in which the sample gets irradiated from a light source below and the part is built in a top-down manner. However, the light source can also be located on the top, and the part thus printed in a bottom-up manner.[35]
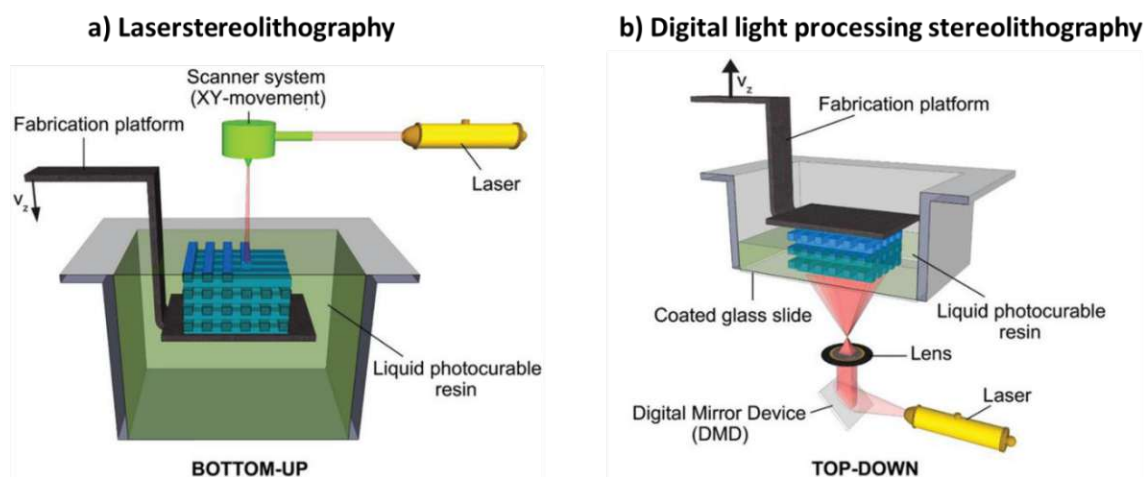
Figure 7. Vat photopolymerization schemes: a) Laser-stereolithography in a bottom-up approach. b) Digital light processing-based stereolithography in a top-down approach. Figure reproduced from ref[35] without changes. Copyright 2020 by Wiley-VCH GmbH.

An interesting new development is hot lithography, where the formulation is heated to higher temperatures during the printing process.[36] This new technique widens the scope of accessible materials, since viscous monomers or systems with low reactivity at room temperature become available. This leads to the possibility of producing tougher materials by avoiding the use of low molecular weight monomers that lead to highly crosslinked and thus brittle materials. Furthermore, higher reactivity leads to reduced printing times and therefore higher throughputs. Unfortunately, classical radical systems are limited in their application due to stability issues at high temperatures, so a focus is put into developing new systems, for example cationic polymerizations with highly stable monomers.[36, 37]

8

3 PHOTOPOLYMERS

Photopolymerization is the fundamental concept used in stereolithography. It describes the curing of liquid formulations initiated by light rather than heat. For this, a photoreactive formulation needs a photoinitiator that starts the polymerization, and polymerizable monomers or prepolymers. Chain-extending monomers are monomers that can react with other monomers to form linear polymers, while crosslinkers contain more functional groups so they can react with at least two or three other monomers in chain- and step-growth reactions, respectively, and act as crosslinks between the linear chains to form a polymer network. Furthermore, other components like reactive diluents, photosensitizers or other additives such as pigments of fillers might be added. Reactive diluents are monomers that reduce the viscosity of the formulation for easier handling thereof, but still contain reactive groups and as such are incorporated in the formed polymers. Photosensitizers are defined as molecules that can absorb light and transfer the excitation to the photoinitiator molecules, which might not have sufficient light absorption in the relevant wavelength area.[34]

3.1 Epoxides as Monomers

Epoxides are well-known monomers in macromolecular chemistry. Epoxy resins describe prepolymers containing more than one epoxy group. By crosslinking these resins *via* different curing agents, they form thermosetting polymers.[38, 39] Epoxy resins show good mechanical properties, low shrinkage and good chemical and thermal resistance.[40] Important applications for epoxy resins include high-performance composites, electronic boards, adhesives and coatings.[39]

Epoxide groups show rather high ring-strain and therefore high reactivity towards ring-opening reactions. They can undergo either step-growth polymerization or chain-growth ring-opening polymerization. In step-growth polymerization, co-reactants such as multifunctional amines, acids or isocyanates react with the multifunctional epoxides in a ring-opening addition reaction (Figure 8). The reactivity of such systems is determined by the nucleophilicity of the co-reactant and the electrophilicity of the epoxide. Usually, such systems are cured thermally.[39]
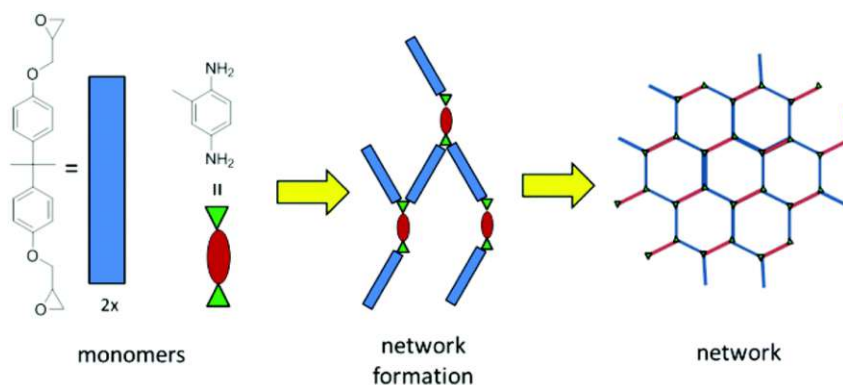
Figure 8. Step-growth polymerization of epoxides with amines as co-reactants. Figure reproduced from ref[41] without changes. Copyright 2016 by Royal Society of Chemistry.

Due to the polar oxygen-carbon-bonds, epoxides can also undergo either cationic or anionic ring-opening polymerization, which are chain-growth polymerization reactions (Figure 9). Thus, these reactions follow the classical three steps of a chain-growth polymerization: initiation, propagation and termination. Cationic photopolymerizations are commonly initiated by onium salts and more popular than anionic photopolymerizations, which are initiated by photobase generators that typically release tertiary amines as active catalytic species. On the other hand, the anionic mechanism allows for easy copolymerization with other cyclic monomers.[39, 41]
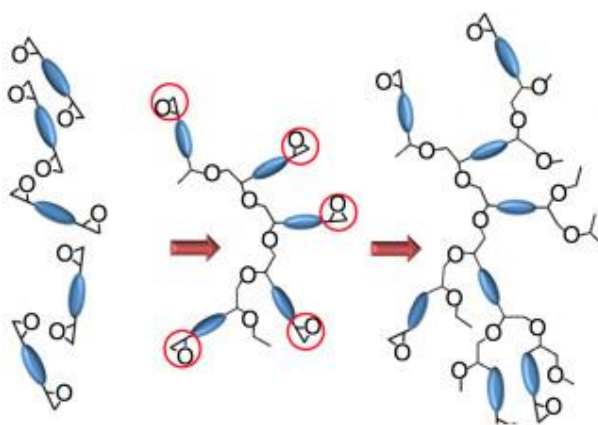
Figure 9. Chain-growth polymerization (anionic or cationic) of epoxides. Figure reproduced from ref[39] without changes. Copyright 2016 by Elsevier Ltd.

3.2 Photoinitiators and -catalysts

Photoinitiators (PIs) are an important part of a photocurable formulation as they start the reaction by transforming irradiation into chemical energy. For this, the photoinitiator needs a chromophore, which absorbs light of a certain wavelength. This absorption causes the molecule to go from a ground state (S_0) into an excited singlet state (S_1), followed by a number of possible relaxation pathways (Figure 10). One of those pathways leads to the molecule in an exited triplet state (T_1), which can then undergo an unimolecular fragmentation reaction generating radicals thus starting the polymerization process.[42, 43]
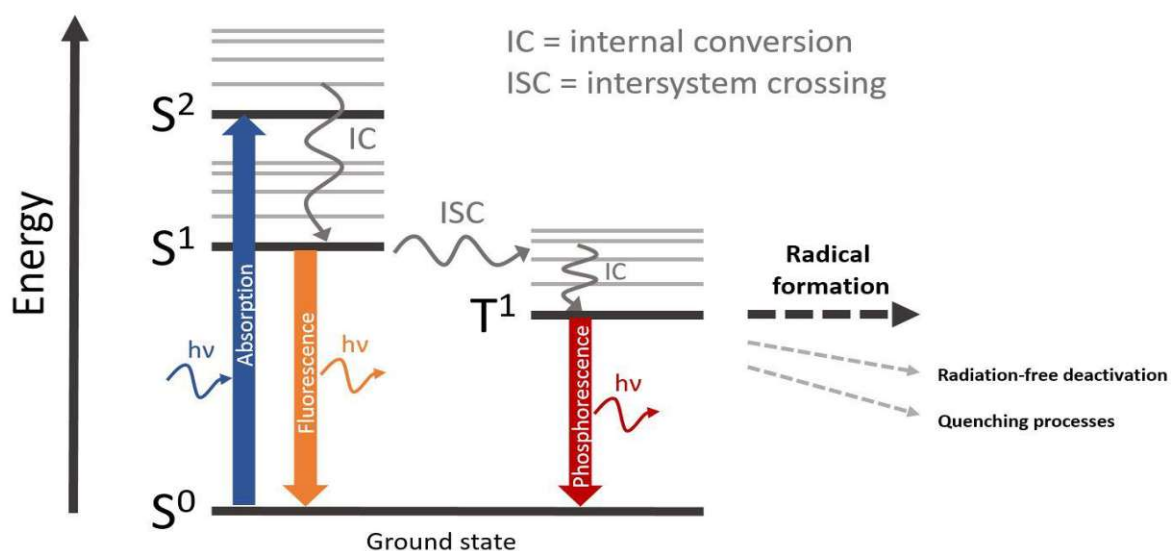
Figure 10. Jablonski diagram depicting the excitement of a molecule from a ground state S^0 into an excited singlet state S^2. Relaxation can happen via internal conversion and fluorescence, or after intersystem crossing via phosphorescence or initiation of chemical reactions. Figure reproduced from ref[44] without changes. Copyright 2019 by TU Wien.

However, not all reactions are initiated by radical formation. Other possibilities to initiate a photopolymerization reaction include the generation of acids or bases as active species through light, which then start cationic or anionic polymerization reactions. This is shown for the example of epoxides in Figure 11. These ionic polymerization reactions have the big advantage of insensitivity towards oxygen compared to free radical polymerizations, and usually also result in lower shrinkage of the materials after curing.
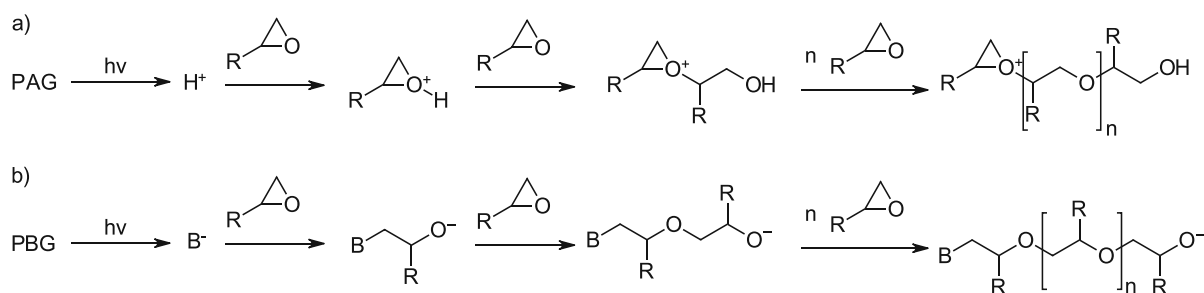
Figure 11. a) Cationic polymerization catalyzed by a photoacid generator (PAG). b) Anionic polymerization catalyzed by a photobase generator (PBG).

Photoinitiators that release strong Broensted- or Lewis acids upon irradiation are called photoacid generators (PAGs), or photobase generators (PBGs) if they release bases upon irradiation.[45-47] PAGs and PBGs must fulfill several requirements, including good stability before irradiation, non-toxicity of the PAGs/PBGs and their released compounds, and a high photoinitiation efficiency for which strong absorption of the light in the employed wavelengths is required.[46]

3.2.1 Photoacid generators

As already mentioned, PAGs work by releasing an acid upon irradiation by light. For this, PAGs must contain a chromophore that allows for the excitation of the PAG into an excited singlet state. Since this state is very instable, homolytic or heterolytic cleavage follow, in which cations or radical cations are formed. The cleavage products of the homolytic cleavage can also be transformed into the heterolytic cleavage products *via* electron transfer. Regardless of the mechanism, the produced intermediates then abstract protons from a hydrogen donor in the reaction mixture (monomer, solvent or impurity) to generate super acids, which initiate the cationic polymerization reactions (Figure 12).[47, 48] More detailed mechanisms have been developed that also take into account the intersystem crossing from the singlet to the triplet excited state, and solvent-caging.[49]
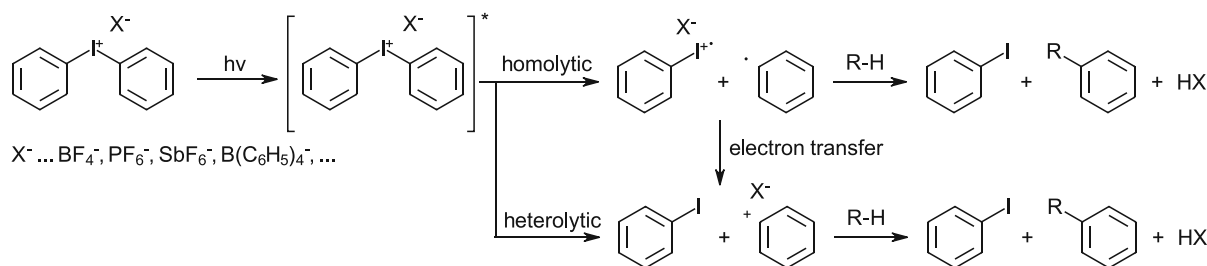
Figure 12. Homolytic or heterolytic photodecomposition of an iodonium salt and release of the super acid.

The earliest discovered class of PAGs are onium salts, which were investigated by Crivello *et al.* in the 1970s.[50] Up to date, they are still state of the art in industry. The ions in a PAG salt have different roles: While the cation influences photochemistry-related properties like absorption maximum or thermal stability, the anion determines all polymer-related properties such as initiation efficiency and acid strength.[51]

Especially triarylsulfonium or diaryliodonium are used as cations in onium salts employed as PAGs (Figure 13). This is due to their relatively easy preparation methods, their high stability and high photochemical efficiency, with triarylsulfonium outperforming diaryliodonium in both thermal stability and reactivity.[51, 52] Diaryliodonium salts usually require high energies for the bond cleavage, which is why electron donating groups are often introduced in the *para* position to help shift the absorption to higher wavelengths.[46] Shifting of the absorption wavelength is however not only possible by introducing electron-shifting substituents, but also by introducing more chromophoric groups.[47] Besides sulfonium and iodonium, other commonly used cations for onium salts include phosphonium and pyridinium (Figure 13).[48]

Sulfonium salt   Iodonium salt   Pyridinium salt   Phosphonium salt
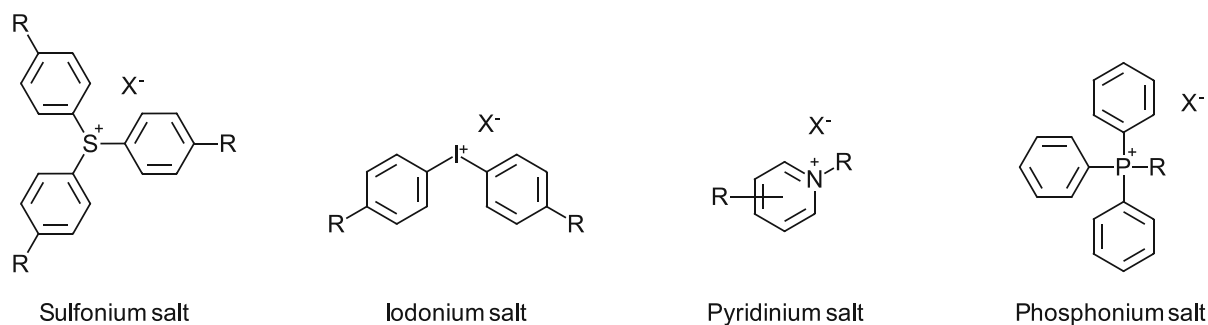
Figure 13. Examples of onium salts with different cations that can be used as PAGs.

Anions need to exhibit non-nucleophilicity to avoid immediate quenching with the cationic species. However, high acid strength of the produced acid is required for an efficient initiation, which is inversely dependent on the nucleophilicity of the anion (Figure 14). Therefore, perfluorometallates are highly interesting, for example the anions BF_4^-, PF_6^-, AsF_6^-, and SbF^- are often used. However, the more reactive anions AsF_6^-, and SbF^- are toxic and thus cannot be used for certain applications.[51, 52]
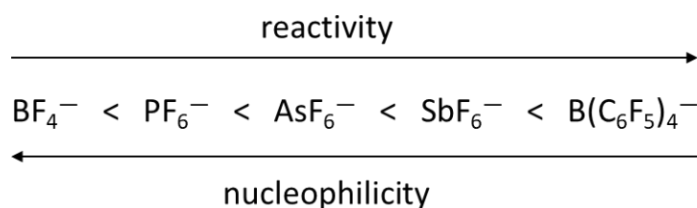
Figure 14. Nucleophilicity vs. reactivity of different perfluorometallates commonly used as anions X⁻ in photoacid generators.

Besides onium salts, there are also non-ionic PAGs, which often show better solubility in monomers, but less thermal stability. Non-ionic PAGs contain C-O, S-O or N-O bonds that dissociate upon irradiation and lead to the formation of an acid by abstraction of a proton (Figure 15).[53] They are mainly derived from arylsulfonates, including nitrobenzyl esters or iminosulfonates.[46]
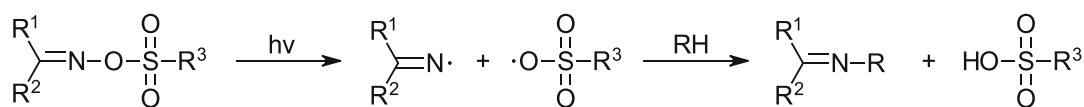
Figure 15. Photodecomposition of an iminosulfonate as example for a non-ionic PAG.

PAGs are usually used to initiate cationic polymerization reactions, which can even continue in the dark after the irradiating has stopped if long-lived acids are produced.[54] Typical monomers include epoxy, vinyl ether or oxetane monomers, which are non-toxic compared to (meth)acrylates often employed in radical polymerizations (Figure 16). The produced materials often have good mechanical

13

strength, good adhesion and chemical and thermal resistance, and are used as coatings or adhesives.[46, 49]

Epoxy   Oxetane   Vinylether
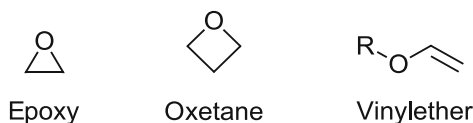
Figure 16. Typical monomers for cationic polymerizations.

Nowadays, research focuses on the development of PAGs that absorb at longer wavelengths. Another new development is the two photon absorption, where two photons are absorbed simultaneously by the PAG and therefore allows for more spatial control over the polymerization.[53]

3.2.2   Photobase generators

PBGs work by releasing an active base upon irradiation. However, they are still less investigated than PAGs, even though they have very advantageous characteristics including air-stability and inertness towards metals. Therefore, they are suitable for application in sectors that heavily rely on metals, such as automotive or electronic industries.

The concept of organic PBGs was first explored in 1990 by Cameron *et al.*[55], who used a photosensitive carbamate to generate basic amines upon irradiation (Figure 17). Carbamates are primary or secondary amines protected with a photolabile protection group. They undergo photodecarboxylation upon irradiation and release the free amine. The released primary and secondary amines are usually only weak bases and as such relatively inefficient in the activation of anionic polymerizations.[46] However, in 2014, Xi *et al.*[56] demonstrated that the strong base 1,1,3,3-tetramethylguanidine could also be photocaged *via* a carbamate bond.
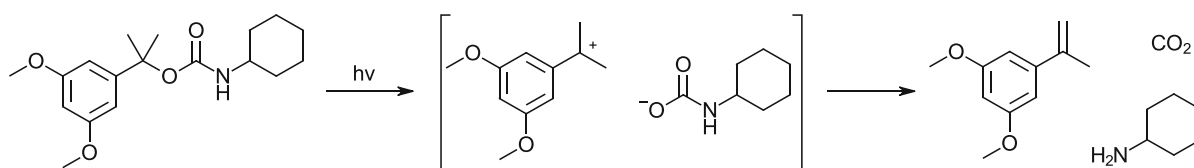
Figure 17. Photosensitive carbamate used by Cameron et al.[55] to generate a basic amine upon irradiation.

Besides carbamates, different salts, for example quaternary ammonium salts, are also commonly used as PBGs. In this case, a tertiary amine is bonded to a chromophore and undergoes C-N bond cleavage upon irradiation to release the amine (Figure 18). However, many of these compounds show low solubility, thermal stability and stability in organic solvents.

14
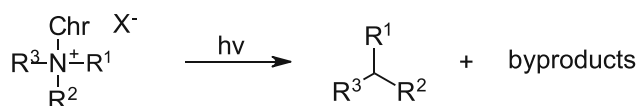
Figure 18. Photolysis of quaternary onium salts to release tertiary amines.

Later developments overcame those problems by introducing salts that contain the protonated, inactive base that only gets activated by deprotonation upon irradiation. Especially borates that can rearrange upon irradiation and deprotonate the base turned out to be good anions since they also tolerate strong bases such as phosphazenes and carbenes (Figure 19a). Later, carboxylate containing chromophores were introduced that also release the base by deprotonation, in this case however by decarboxylation instead of rearrangements (Figure 19b). These developments expanded the scope of possible PBGs tremendously, and nowadays there are even a few commercially available PBGs (Figure 19c).[45, 46]
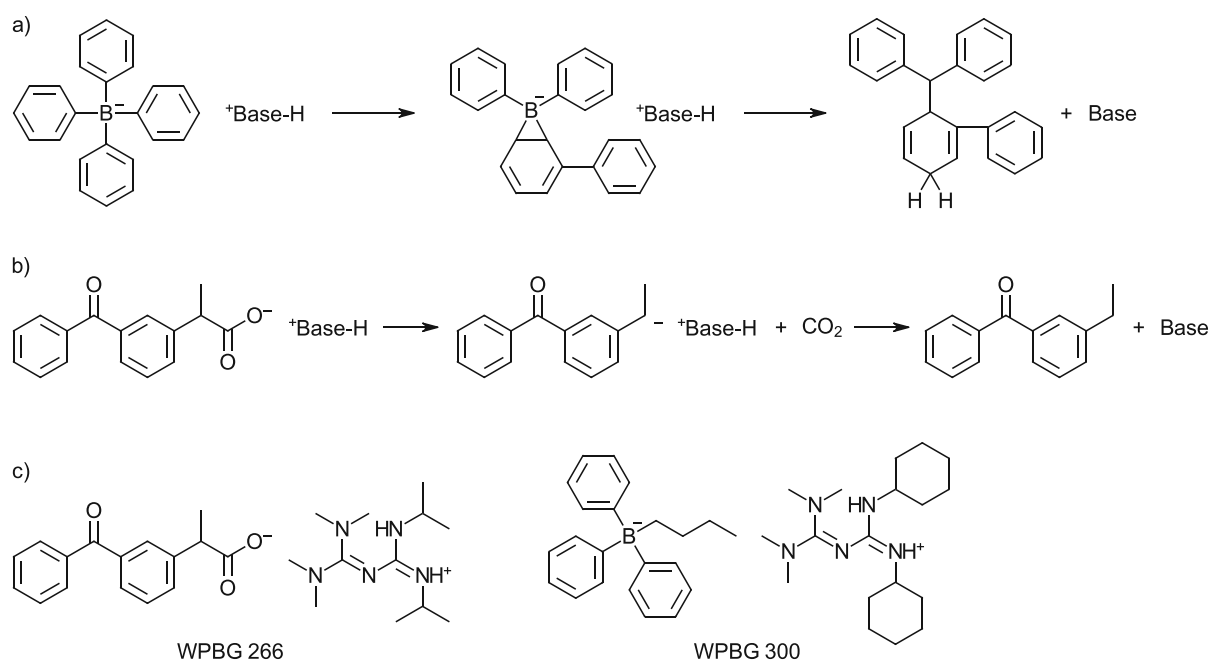
Figure 19. Mechanism of photodecomposition of a) borate-based PBGs that deprotonate the base through rearrangements, or b) carboxylate-based PBGs that deprotonate the base through decarboxylation. c) Examples of commercial PBGs.

PBGs can be employed for photo-induced anionic polymerizations, which enables the curing of monomers that would otherwise not be accessible through traditional radical polymerizations. Examples include thiol-Michael additions or thiol-epoxy polymerizations. However, quaternary ammonium salts can also be used for radical polymerizations since radicals get produced in the photodecomposition. Finally, PBGs can also be used for the photoinduced depolymerization of polymers such as polyolefinsulfones.[45]

16

OBJECTIVE

In recent years, 3D printing has been identified as an ecologically and economically favorable means of production because complex parts can be produced with minimal energy efforts and lead times. Thus, research in this area has devoted much effort to broadening the scope of accessible materials for this technology.

One major drawback of most thermosets is limited recyclability and degradability, since polymer networks need bonds that can be easily cleaved for that. In this regard, pure polyester networks offer an ideal opportunity. They are produced commercially by condensation reactions of multifunctional carboxylic acids with multifunctional alcohols or ring-opening polymerization of cyclic esters. However, another method called ring-opening copolymerization (ROCOP) has been reported that combines many of the advantages of the methods mentioned before, such as wide monomer scope and controlled reaction conditions. While many different catalysts including both organometallic catalysts and organocatalysts have been reported for the initiation of ROCOPs, no attempts of using photocatalysts have been published to date.

Therefore, this report will focus on the photocatalyzed copolymerization reaction between epoxides and anhydrides into degradable polyesters. Either photoacid generators (PAGs) or photobase generators (PBGs) are viable candidates for the photoinitiation process. Since there is no precedent reaction known to date, the first part of this thesis focuses on the elucidation of the copolymerization behavior when using either of those photocatalysts.

Based on these results, optimization regarding conversion and stability of monomers, polymerization times and chain length of the produced polyesters at varying temperatures and irradiation intensities, concentration and type of photocatalyst, and monomer structures will be done.

Finally, multifunctional monomers will be explored to obtain crosslinked systems. The (thermo)mechanical properties and degradability of these materials will be investigated. Furthermore, printing tests will show if these materials are utilizable for 3D printing applications.

STATE OF THE ART

1 RECYCLING IN 3D PRINTING

3D printing techniques are already considered as an environmentally friendly means of production, since they are an energy-efficient way of producing highly individualized parts while avoiding the use of solvents and the production of waste. Introducing recyclable materials makes this method even more sustainable. Unfortunately, not much progress has been made in this regard.

In order to allow for recycling processes to take place, the materials have to be biodegradable. Therefore, thermoplastic polymers that are known for their biodegradability can be used as precursors. However, many of those polymers are only degradable to a certain extent since the crosslinks are usually permanent.[35] Furthermore, the non-reversible nature of typical photoinduced bond formations, as in radical photopolymerization, renders photopolymers nonrecyclable or downcyclable at best.

Hence, a new class of polymers called covalent adaptable networks (CANs) were developed. The covalent bonds in this case are reversible and as such can be triggered by molecules, temperature, light or other forms of irradiation to adapt to a new form. CANs can further be classified according to their mechanism that differs between dissociative and associative bond exchanges (Figure 20). The dissociative mechanism allows for thermal reprocessing, while the associative mechanism retains the same number of dynamic covalent bonds since bond-breaking and bond-forming occurs in the same step. Materials that follow the associative mechanism are also called vitrimers.[35, 57, 58]

These bond-exchange mechanisms can include transesterifications, transalkylations, transaminations, transcarbonations, disulfide or imine exchanges. Vitrimers can be produced in many different 3D printing methods including DLP, SLA or FDM printing, and many different polymer systems have been reported, consisting for example of (meth)acrylates, epoxides, cyclic esters, isocyanates, aldehydes, vinyl and allyl monomers, acids, anhydrides and thiols.[59]
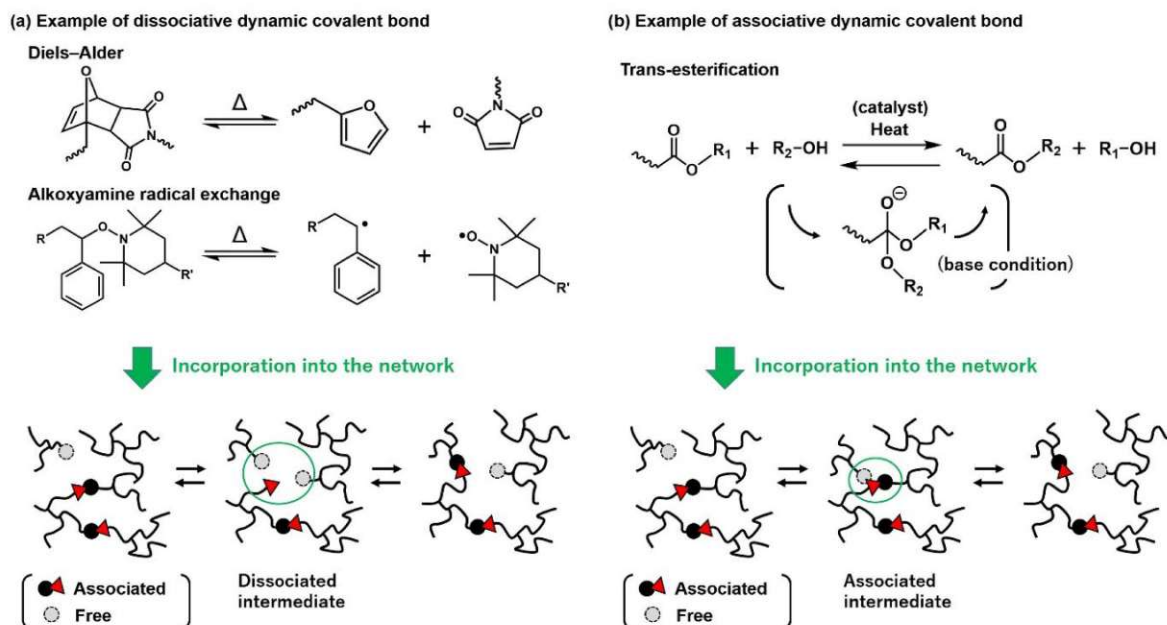
Figure 20. Examples of covalent adaptable networks (CANs) following a) the dissociative or b) the associative mechanism, and a schematic depiction of the difference in the bond-exchange mechanism. Figure reproduced from ref[60] without changes. Copyright 2020 by MDPI.

There have been reports on reprintable resins based on bond-exchange mechanisms, but new virgin monomers also needed to be added.[61] For example, Zhu *et al.*[62] reported the synthesis of a linear poly(isobornyl acrylate) that is soluble in the monomer used for production (isobornyl acrylate), and this solution can then be reused as new liquid formulation in the same printing setup.

There are also several reports that focus on chemical recyclability of polymers back to their liquid monomers.[63] Examples include the thermal depolymerization of poly(γ-butyrolactone) back to the monomer γ-butyrolactone,[64] the acidic depolymerization of poly(hexahydrotriazine)s into their bisaniline monomers,[65] or the acidic depolymerization of poly(diketoenamine)s into the triketone monomers and the amines after ion-exchange processes on a resin (Figure 21).[66]
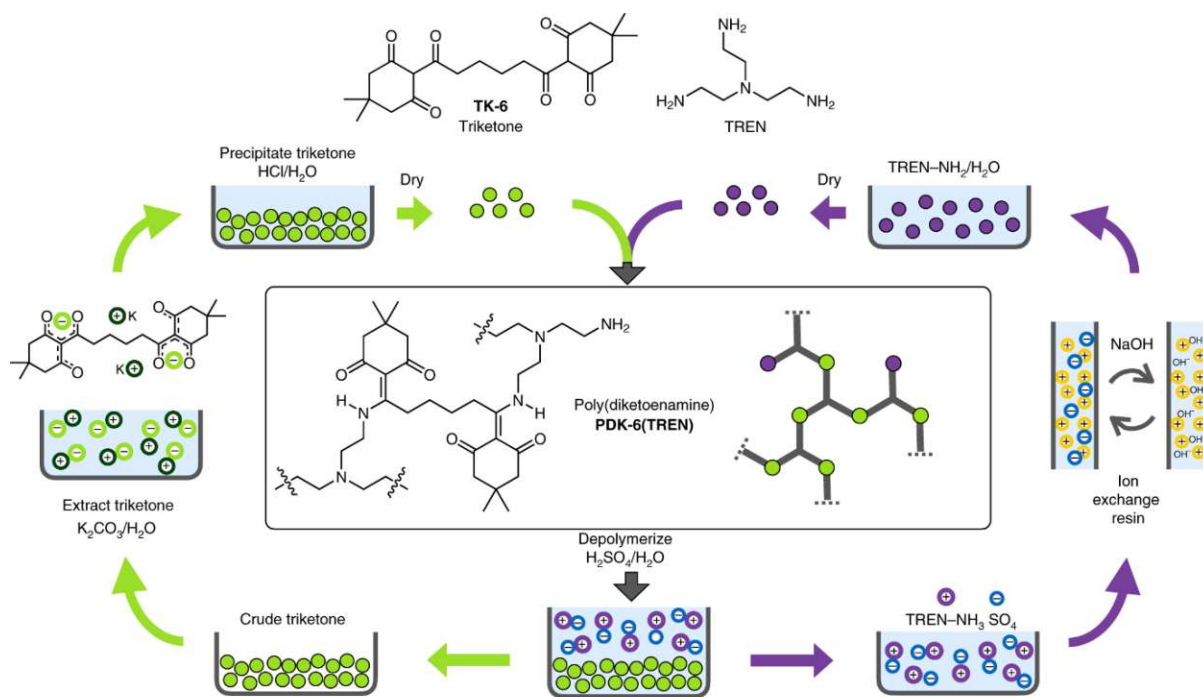
Figure 21. Schematic representation of chemical recyclability of poly(hexahydrotriazine)s through depolymerization into their triketone and amine monomers with subsequent purification steps. Figure reproduced from ref[66] without changes. Copyright 2019 by Springer Nature.

Polyesters have already been the focus of recycling attempts before 3D printing was even developed. PET, one of the most abundant polymers, is also one of the most recycled ones. Since it is a thermoplastic, it can be reprocessed thermally, but loses some value during this process which makes it a downcycling mechanism.[7] However, light-based 3D printing produces thermoset materials, and therefore other recycling mechanisms have to be used. Since polyesters contain a reactive ester carbonyl, they can undergo chemical depolymerization under acidic, basic or enzymatic conditions.[67] However, since most polyester networks are formed by irreversibly crosslinking with other molecules such as (meth)acrylates or epoxides, these polymers are usually only semi-degradable.

2 POLYESTERS IN 3D PRINTING

There are several different ways to produce polyesters with 3D printing methods, including material extrusion and light-based printing techniques.

For fused deposition modeling, thermoplastics are required. Indeed, polylactide (PLA) materials are widely used, which however suffer from poor thermal stability, even though 3D printing improves the mechanical properties compared to PLA produced by traditional injection-molding.[68] Therefore, co-polyesters or composites are possible high-performance alternatives.[69, 70]

For light-based printing techniques, there are more possibilities for designing polyester systems. First attempts focused on the employment of polyesters that were modified to contain functional groups

21

that can be photopolymerized radically, for example (meth)acrylate groups. Invernizzi *et al.* [71] functionalized both polycaprolactone (PCL) and 2-ureido-4[1*H*]-pyrimidinone (UPy) with methacrylate end groups, and then 3D-printed those compounds on a DLP printer by adding the radical photoinitiator 2,4,6-trimethylbenzoyl-diphenyl-phosphinoxide (TPO-L). The obtained materials showed thermally triggered shape-memory and self-healing properties due to the self-assembling UPy units that can form hydrogen-bonds. The same approach with methacrylated PCL was used for producing tissue engineering scaffolds that showed improved metabolic activity in combination with bioactive glass.[72] It has also been shown that other monomers can be incorporated into the network to influence material properties, for example anhydrides can be used to form poly(ester anhydride)s before methacrylation and light-intitiated crosslinking.[73] Besides methacrylate groups, acrylate groups have also been successfully used to functionalize PCL and then crosslink it using a two-photon polymerization approach.[74]

Instead of functionalizing polyesters to enable radical crosslinking, it is also possible to use unsaturated monomers so the double bond is already incorporated into the polyester (= unsaturated polyester UPE). For example, Lammel-Lindemann *et al.*[75] used isosorbide in combination with (un)saturated diesters (diethyl adipate and diethyl fumarate) to give 3D-printable polymers with higher tensile strength. Barker et al.[67] used step-wise melt polycondensation for the polymerization of different saturated and unsaturated anhydrides with diethylene glycol to obtain UPEs that were subsequently photopolymerized by adding phenylbis(2,4,6-trimethylbenzoyl) phosphine oxide (BAPO) as initiator under solvent-free conditions. The produced polymers were also able to undergo depolymerization afterwards.

While there are many different ways of producing polyesters that contain functional groups which can be used for photopolymerization, it is also possible to exploit the cationic ring-opening polymerization of lactones to directly synthesize polyesters *via* photopolymerization at elevated temperatures. This was first reported by Mete et al.[76] who used a sulfonium salt as PAG to polymerize ε-caprolactone upon light-triggering the process. These first reactions still required higher temperatures for sufficient reactivity and difunctional crosslinkers for reducing the gelation time. The concept of cationic ROP was further explored by Kojic et al.[77], who used spiro-orthoesters for hot stereolithographic 3D printing of pure poly(ether-ester) networks, using bifunctional spiro-orthoesters or epoxides for crosslinking (Figure 22). Due to spiro-orthoesters expanding during polymerization, a significant reduction of volumetric shrinkage is observed in these materials. Macroscopic, well-defined 3D figures were printed from this approach.
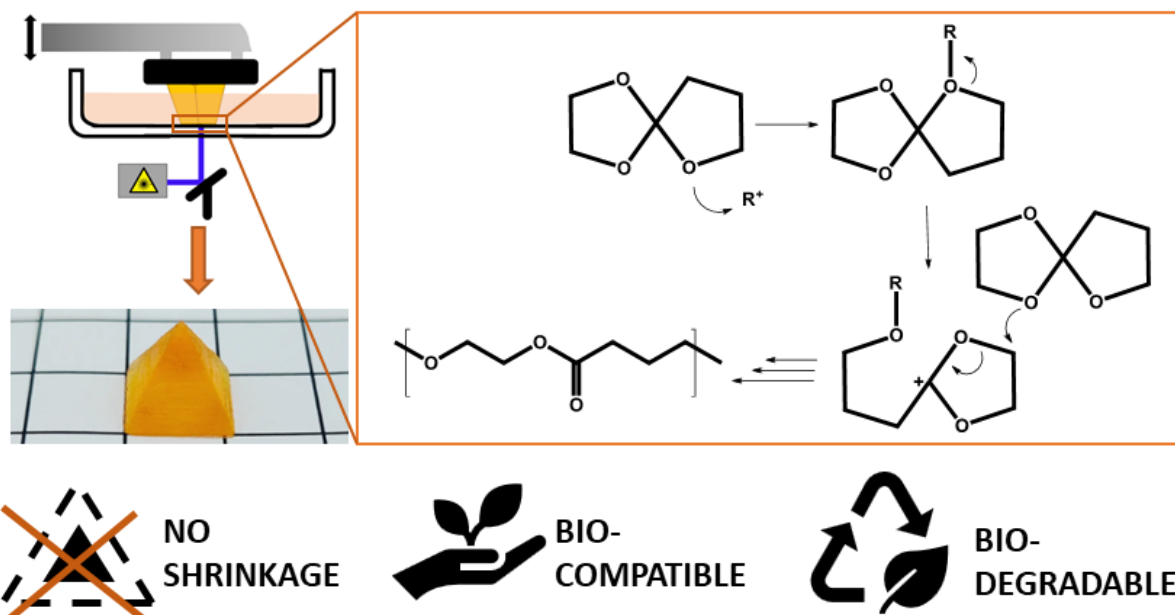
Figure 22. Schematic representation of the cationic ring-opening polymerization (ROP) of spiro-orthoesters to produce 3D printed poly(ether-ester) networks with nearly no shrinkage. Figure reproduced from ref[77] without changes. Copyright 2023 by Royal Society of Chemistry.

3 RING-OPENING COPOLYMERIZATION

Ring-opening copolymerization ROCOP of epoxides and anhydrides has gained more interest in recent years, since it combines many of the advantages of both step-growth and chain-growth reactions: high-molecular weight polymers with low dispersities can be produced through a controlled reaction mechanism using mild conditions, while at the same time easy tunability of properties of the produced polyesters can be achieved due to a large scope of available monomers.[17]

A recent study compared the classical polycondensation of ethylene glycol (EG) and succinic acid (SAc) with the novel ROCOP approach using ethylene oxide (EO) and succinic anhydride (SA), that both yield poly(ethylene succinate) as product, with regard to preprocessing, polymerization technique, post-processing and the properties of the produced polymers.[78] While the monomers can be used without purification in the polycondensation reaction, extensive purification is required for the ROCOP. This is due to the fact that protic impurities lead to chain-transfer reactions and thus reduced molecular weights of the polymers. This behavior was indeed observed by many different groups because it results in bimodal mass distributions, depending on the initiation being started by the catalyst or by the hydrolyzed anhydride, in which case the chain grows in two directions instead of one (Figure 23).[13, 17, 20, 23, 79, 80]
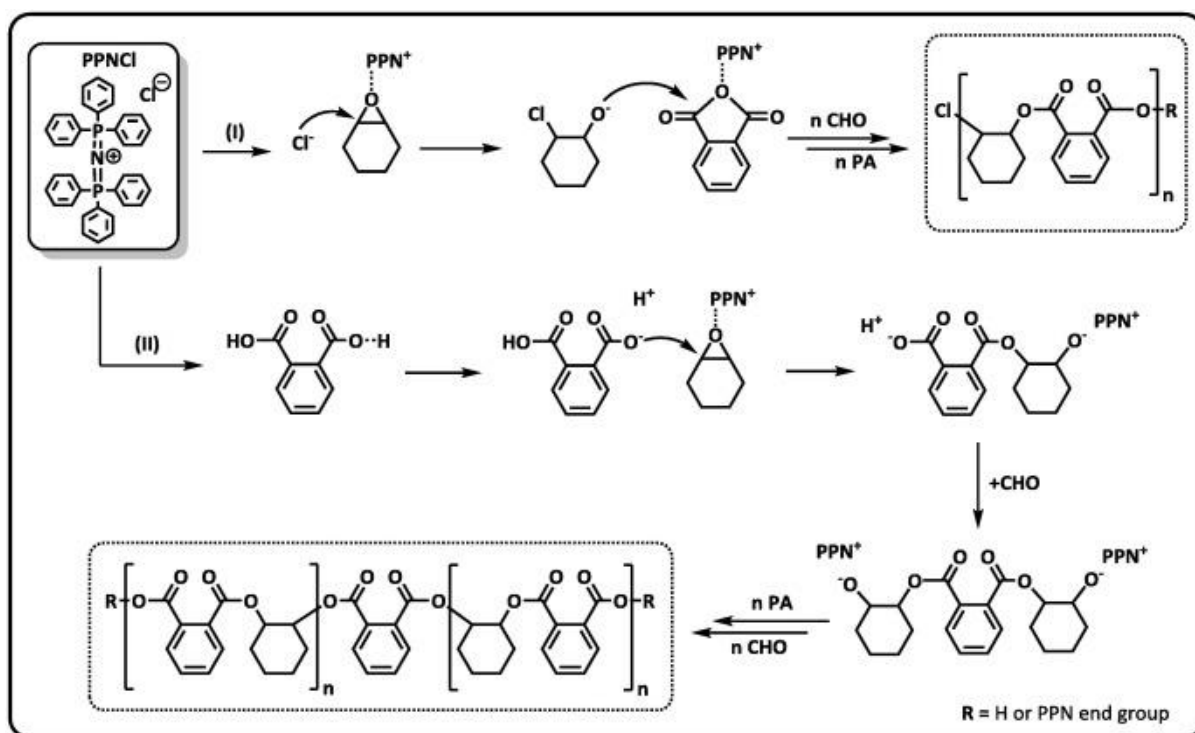
Figure 23. Different initiation mechanism by the catalyst PPNCl or phthalic acid resulting in bimodal mass distribution. Figure reproduced from ref[17] without changes. Copyright 2017 by Elsevier Ltd.

With regard to polymerization conditions, ROCOP requires much milder reaction conditions and less time. In the polycondensation reaction, excess diols have to be removed under high-vacuum, while excess epoxide, which is usually used to achieve lower viscosity in ROCOP reactions, has to be removed there. The properties of the produced polymers can be adjusted in both cases, however, the polycondensation is still better investigated and thus results in slightly better and more reproducible polymer production. Overall, the report concludes that at the moment ROCOP cannot compete with the polycondensation, but offers some advantages of its own like the possibility to produce highly stereoregular polyesters. Thus, more research has to be done for this reaction to be truly competitive on a large scale.[78]

The ROCOP reaction was first reported by Fischer in 1960.[81] They discovered that tertiary amines had been used by other research groups to catalyze the anhydride-epoxide reaction. However, tertiary amines do not only influence the rate of the reaction, but also the mechanism: using this catalyst suppresses the homopolymerization of epoxides and thus the epoxide and anhydride react in a strictly bifunctional way towards each other to give linear polyesters. This new reaction can therefore be a powerful tool to prepare linear polyesters that can easily be modified by introducing various substituents along the polymer backbone. Indeed, using equimolar quantities of terminal epoxides and acid anhydrides results in 99% polyester formation. A reaction mechanism was proposed (Figure 24): First, the amine activates the acid anhydride, which then reacts with the epoxide. After

this, anhydride and epoxide react with the growing chain alternately. Several advantages were reported for this reaction:

- No formation of volatile side products and thus no need for distillation during polymerization.
- Good control of molecular weights of polymers by introducing hydrogen impurities.
- The reaction rate is independent of monomer concentration up to certain conversion rates.
- The reaction is very specific, allowing an excess of epoxides serving as solvent without influencing the product formation and purity.
- End-groups are dependent on which monomer is used in excess.
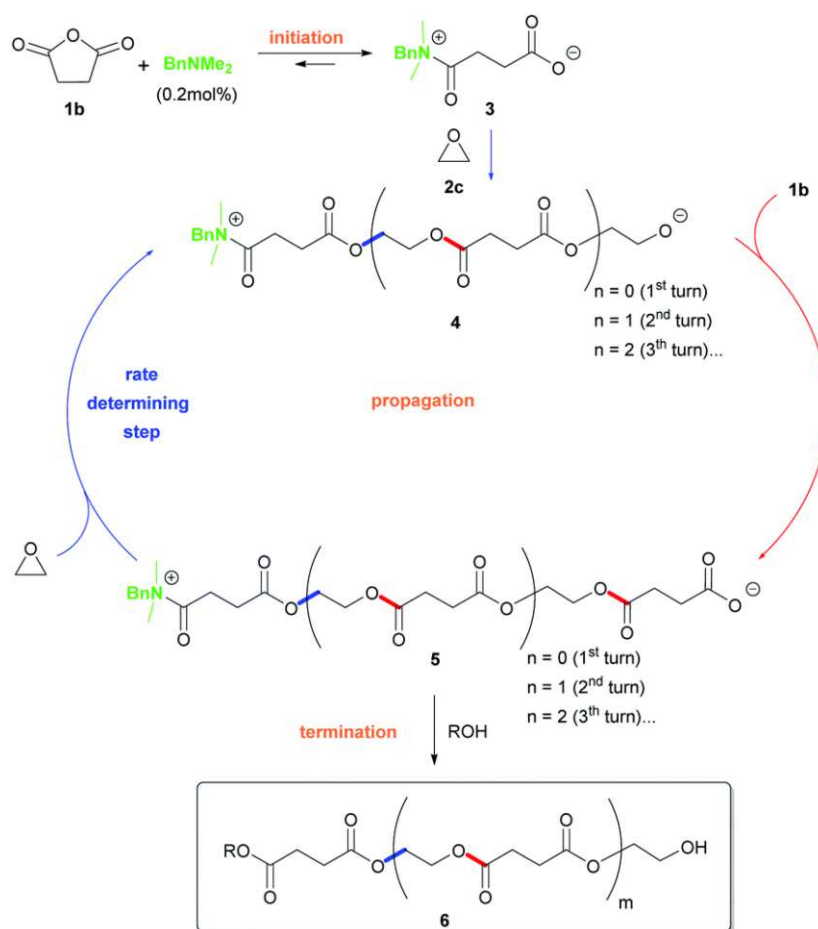
Figure 24. Proposed reaction mechanism by Fischer[81] for the amine-catalyzed reaction between acid anhydrides and terminal epoxides. Figure reproduced from ref[79] without changes. Copyright 2021 by Royal Society of Chemistry.

However, the reaction still suffered from harsh reaction conditions (100 °C, several hours) and relatively low molecular weight products (up to 18 kDa). Further lowering of the molecular weight of the products is observed when hydroxyl impurities are present, as the anhydride will react with them and start new chains. Furthermore, using epoxides such as cyclohexene oxide or alkyl epoxy stearates promotes side reactions like homopolymerization and isomerization.

Even though different catalysts for the ROCOP of epoxides and anhydrides including inorganic salts and metal-alkyl initiators were found over the next years,[82] the next major breakthrough was only achieved much later in 2007 by Coates *et al.*[83] with the discovery of a new catalyst (BDI)ZnOAc (BDI = β-diiminate, Figure 25). This catalyst allowed the synthesis of polyesters with high molecular weights up to 55,000 g mol^{-1} and narrow dispersity ≤ 1.5 under mild conditions (50 °C, 2 h, 20 µmol catalyst).
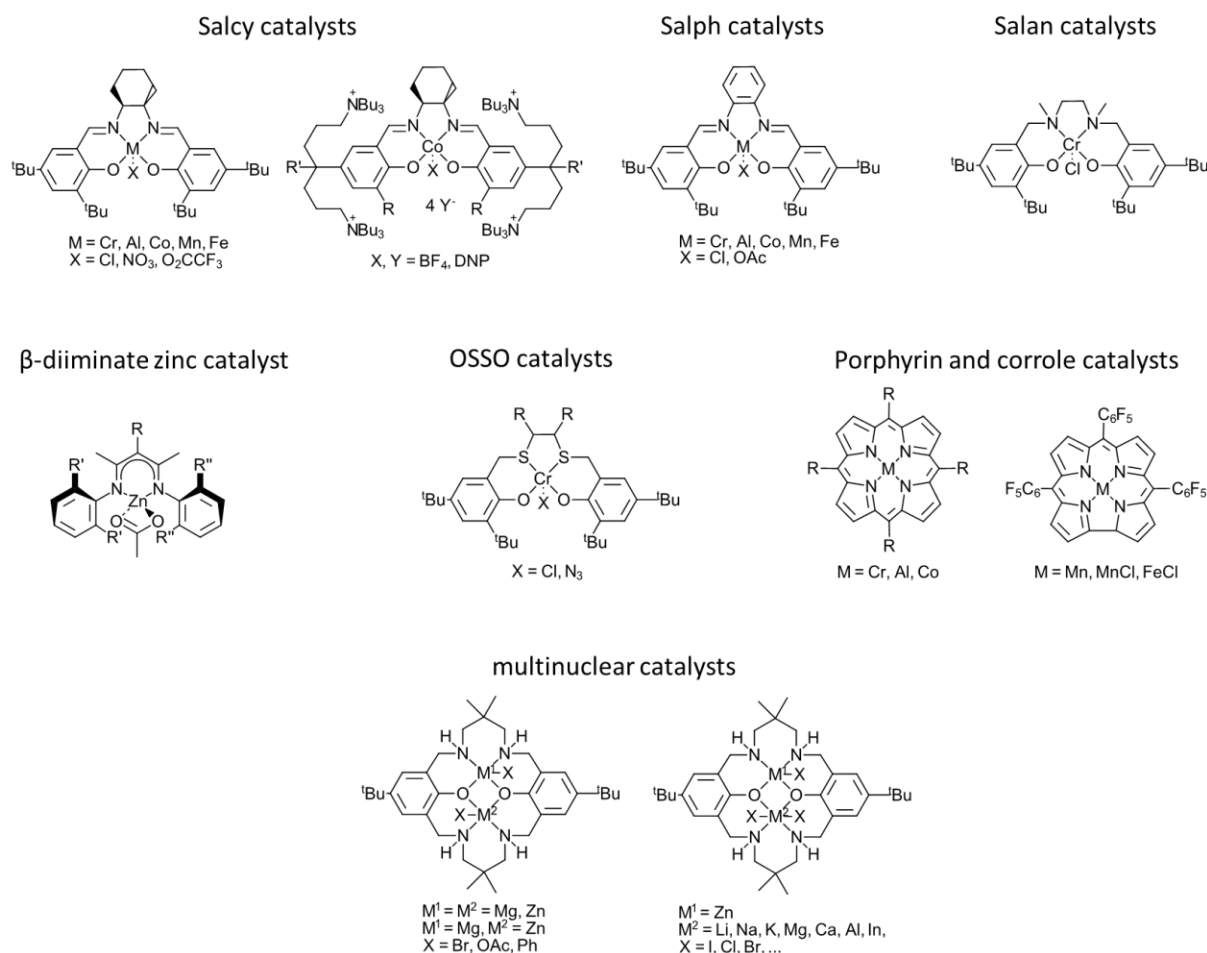
Figure 25. Examples of organometallic catalysts for the ring-opening copolymerization of epoxides and anhydrides reported in literature.[18, 19]

This rekindled the interest in ROCOP reactions. The focus remained on transition-metal complexes for a long time, and numerous different catalysts have been developed (Figure 25). The elemental steps of the ROCOP reaction catalyzed by metal catalysts LMX (L = ligand, M = metal center, X = initiating species) are depicted in Figure 26. In the initiation step, the initiator MX coordinates with the epoxide to form an alkoxide intermediate that then reacts with the anhydride to form an alkoxide-carboxylate intermediate. During propagation, the monomers are added sequentially by first forming a metal alkoxide with the epoxide that then attacks another anhydride to form the metal carboxylate. The metal carboxylate can then attack another epoxide to reform the metal alkoxide. Termination is only

26

achieved by changing the reaction conditions or adding water or acids. Besides propagation, a possible side-reaction is the homopolymerization of epoxides which leads to the formation of polyether segments. Furthermore, when a protic substance is added, chain-transfer reactions occur, resulting in a decrease of molecular weight.[20, 82]
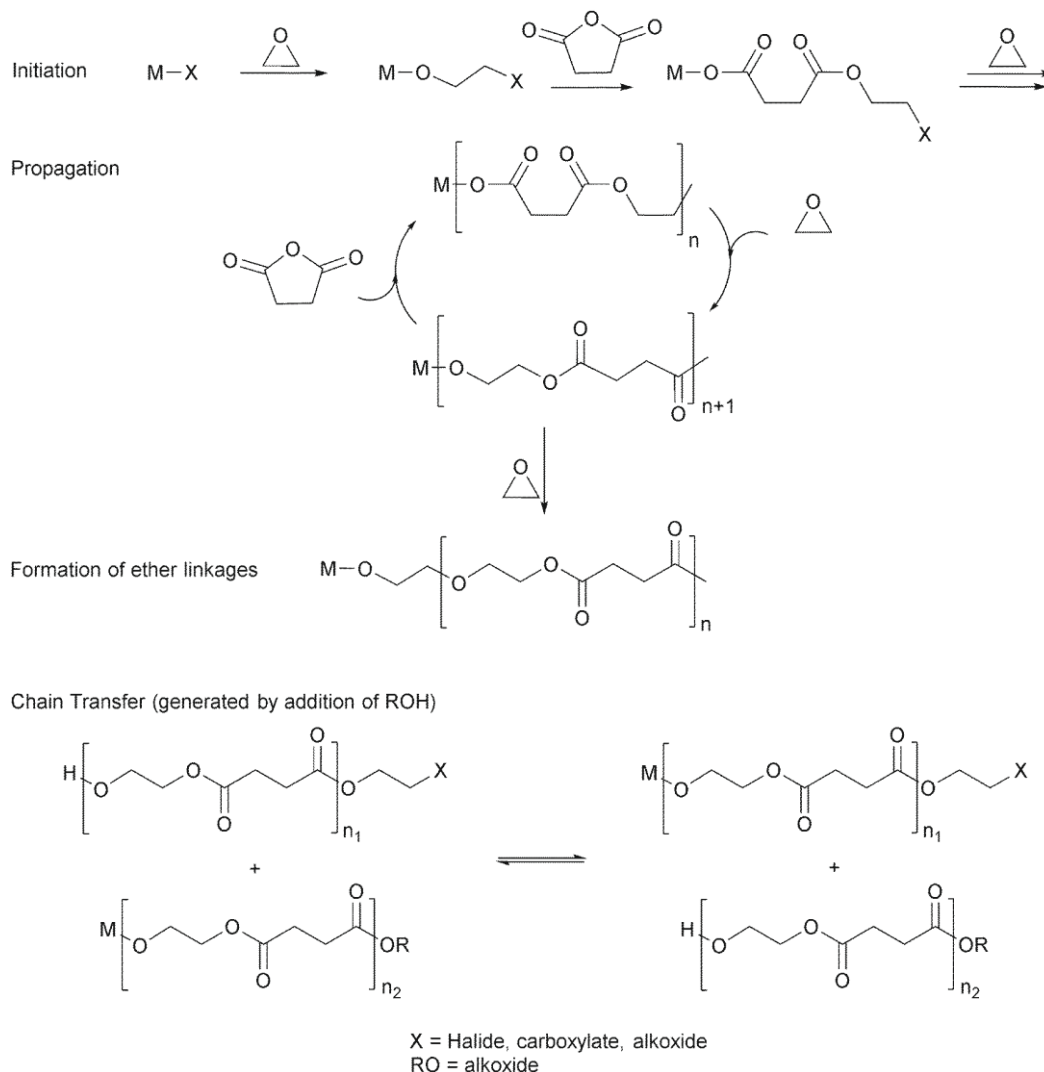
Figure 26. General reaction mechanism showing the elemental steps for the metal-catalyzed ring-opening copolymerization ROCOP between epoxides and anhydrides. Figure reproduced from ref[82] without changes. Copyright 2015 by Royal Society of Chemistry.

Many convincing results were also achieved with regard to stereo-controlled, block and functional polyesters.[84] For example, Niknam *et al.*[85] describes the deployment of dinuclear chromium complexes with [OSSO] type ligands and small amounts of PPNCl as cocatalyst for the terpolymerization of various epoxides with CO_2 and phthalic anhydride. It was revealed that reaction of the epoxide/anhydride coupling is faster than the epoxide/CO_2 coupling, therefore terpolymerization leads to poly(ester-*block*-carbonate) copolymers. The produced blockcopolymers have an increased T_G compared to pure polycarbonates. However, it is also possible to get statistical

terpolymers when selecting a different catalyst, for example a bimetallic complex containing Cr as one metal center and different binucleating ligands as reported by Stühler *et al*.[80]

While many organometallic catalysts suffer from a complicated multistep synthesis and low air-stability, there are also findings of easy-to-synthesize, air-stable Ni and Cu complexes.[86] However, other disadvantages of metal catalysts still persist, including coloration of the polymer and toxic metal residues, which restrict their application in certain fields, for example medical applications.[20]

Therefore, metal-free organocatalysts were investigated to overcome those challenges and provide a large number of cheap, less toxic catalysts with low sensitivity towards moisture and oxygen.[79] As already mentioned, tertiary amines were originally identified as possible catalysts for the ROCOP reaction in 1960.[81] In the following years, there were a few more studies describing tertiary amines[87-90], quarternary onium salts[89-91] and phosphazenes[14, 90, 92] as catalysts in the ROCOP reaction. However, it was not until 2016 that a major breakthrough was achieved by Zhang *et al.*[93] combining the onium salt as initiator with the Lewis acid triethylborane (TEB) as activator for a metal-free synthesis of polycarbonates from epoxides and CO_2. The Lewis acid needs to be moderate so that it is mild enough to not facilitate the homopolymerization of epoxides, but at the same time strong enough to activate the epoxide for easier attack by the carbonate anion of the growing polymer chain. NBu_4Cl (tetrabutylammonium chloride)/TEB was discovered as best catalyst system, with high activity (TON close to 500) and selectivity (up to 97%). This resulted in further investigation of metal-free Lewis pairs (Figure 27), which turned out to not only be highly active, but also give excellent stereo- and regioselectivity.

In 2018, Ji *et al.* [94] used $Zn(C_6F_5)_2$/DMAP (4-(dimethylamino)pyridine) to produce perfectly alternating copolymers with ester linkages >99% in a controlled manner using phthalic anhydride (PA) and cyclohexene oxide (CHO) as monomers. The homopolymerization was efficiently suppressed in this system, since no polyether formation was observed when increasing the reaction time or using an excess of CHO. The right matching of the Lewis acid (LA)/Lewis base (LB) pair is, however, very important, since other combinations resulted in high polyether contents. While exchanging the LA did not result in major changes, changing the LB to DBU or MTBD retained the good selectivity but resulted in reduced reactivity. Furthermore, the molar ratio of LA/LB is very important since it greatly affects the chemoselectivity. The solvent also has a distinct impact on the reaction; using polar solvents reduces the reactivity due to proton transfer from the α-H of the anhydride to the organic base and thus its inactivation. Interestingly, this $Zn(C_6F_5)_2$/DMAP catalyst system was also able to insert the epoxide regioselectively.

Tertiary amines

DBU TBD MTBD DABCO TMG TEAA DMAP pyrr23 pyrz34

Quarternary onium salts

N(Bu)₄Cl N(Bu)₄Br DTMeAB P(Ph)₄Cl P(Ph)₄Br

Phosphazenes

t-BuP₁ t-BuP₄ CTPB PPNCl

Lewis acids

TEB TPB TFPB
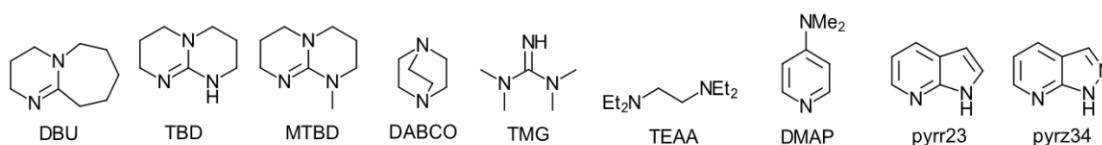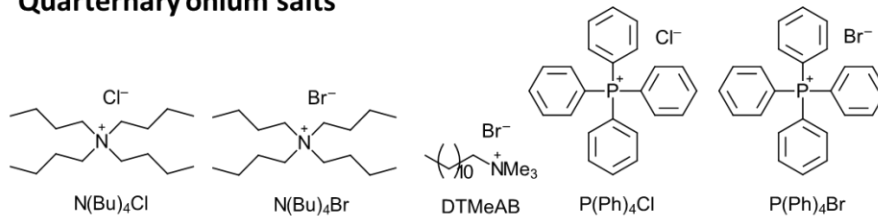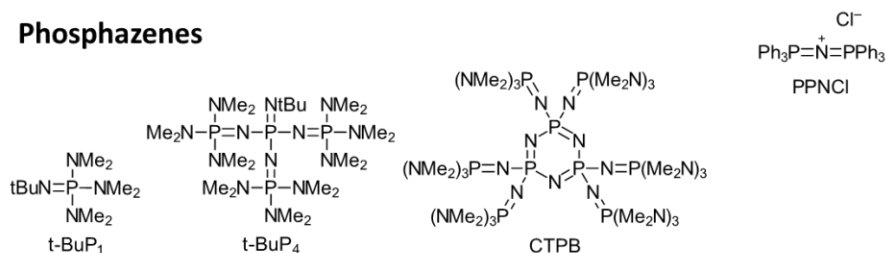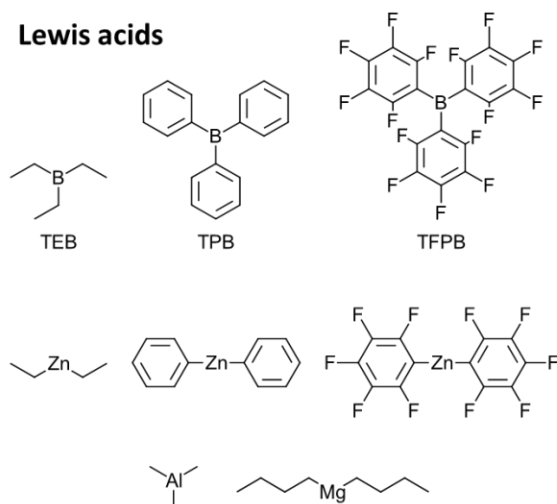
(Thio)urea derivatives

R = Cy, Ph R = Cy, Ph
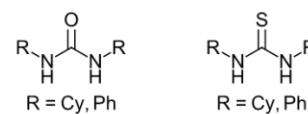
Figure 27. Organocatalysts reported in literature.[13, 20, 22, 23] Lewis acids are not active on their own but have to be used in combination with Lewis bases to give active Lewis pair catalysts.

Later in 2018, Hu *et al.*[22] further looked into the matching of LA/LB pairs. They reported different organoborane compounds as cocatalysts together with quaternary onium salts as highly active catalysts in the copolymerization of propylene oxide (PO) and maleic anhydride (MA) or PA with a TOF of 102 or 303 h⁻¹. The effect of acidity, type and size of Lewis pairs on the catalytic activity and selectivity was tested, and they discovered that strong Lewis acidity and big steric hindrance resulted in lower conversion. Furthermore, onium salts with Br⁻ instead of Cl⁻ showed higher activity due to Br⁻ being the better leaving group. However, the type and size of the cation did not have any obvious

influence. Finally, they were also able to produce block-copolymers with low polydispersity by sequential addition of different anhydrides.

As already mentioned before, the molar ratio of LA/LB is very important, which can be explained by looking closer at the reaction mechanism. If a quaternary onium salt is used, the reaction follows an anionic pathway (Figure 28), whereas a zwitterionic pathway occurs when using a Lewis base like tertiary amines. (Figure 29). Either way, the Lewis acid has two different roles: it forms an ate-complex with the Lewis base that then acts as the active catalytic species, and if used in excess it also activates the epoxide towards ring-opening. It is also important to note that the LA is not able to catalyze the ROCOP reaction on its own.[20, 23]
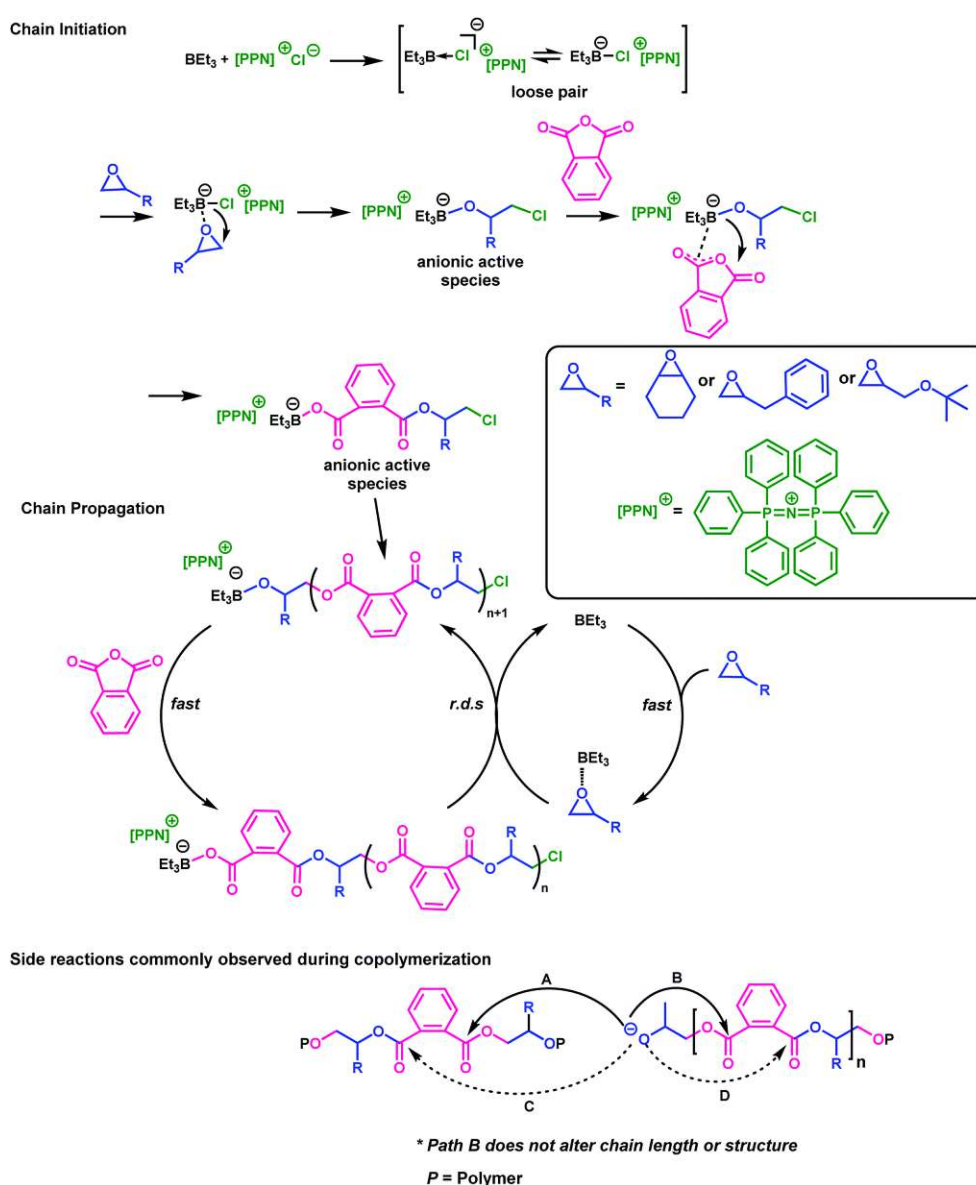
Figure 28. Proposed reaction mechanism for the anionic ring-opening copolymerization (ROCOP) of epoxides with phthalic anhydride (PA) catalyzed by TEB/PPNCl Lewis pair. Figure reproduced from ref[20] without changes. Copyright 2018 by Royal Society of Chemistry.
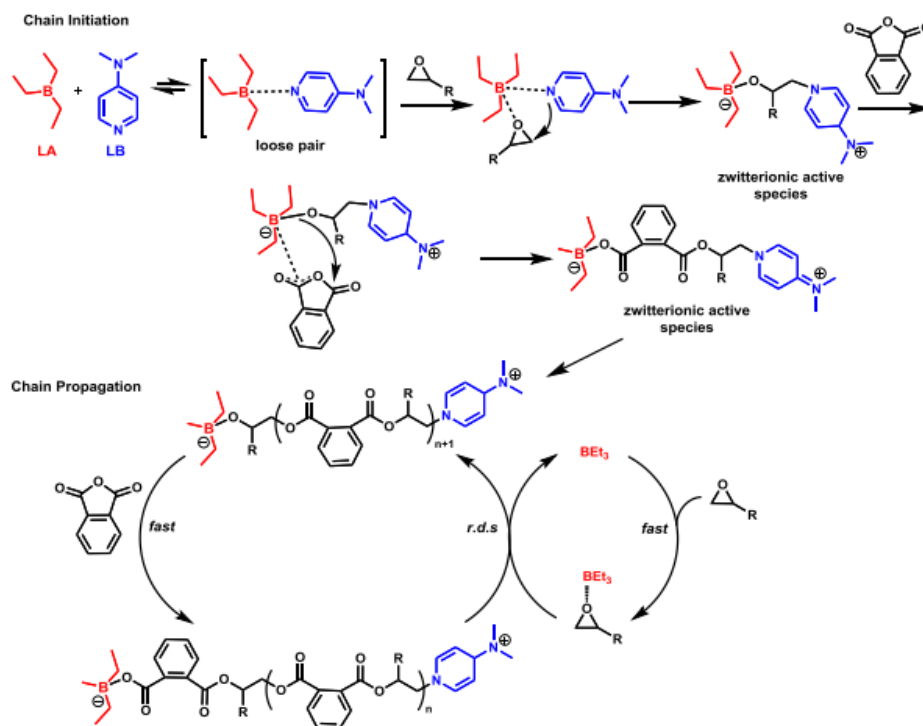
Figure 29. Proposed reaction mechanism for the zwitter-ionic ring-opening copolymerization (ROCOP) of epoxides with phthalic anhydride PA catalyzed by TEB/PPNCl Lewis pair. Figure reproduced from ref[20] without changes. Copyright 2018 by Royal Society of Chemistry.

Recently, (thio)ureas have also been explored as cocatalysts to avoid some of the problems still associated with the Lewis acids used as cocatalysts so far, like the toxicity and spontaneous combustion of TEB in air. The U1/PPNCl pair turned out to be the most active combination, leading to perfectly alternating copolymers with a TOF of 456 h^{-1} using the monomers CHO and PA. The catalytic activity of (thio)ureas is consistent with their basicity because higher acidity of the (thio)urea reduces the nucleophilic activity of the organic base anion towards monomer ring-opening. Furthermore, it was shown that lower nucleophilicity of the organic bases resulted in higher activity, which might be contributed to stronger bases interacting stronger with the (thio)urea and thus lower dissociation and consequently attack on the monomer.[13] It is also possible to use (thio)ureas in combination with PPNCl as a self-switchable polymerization catalysts that can catalyze both the ROCOP between epoxides and cyclic anhydrides as well as the ROP of cyclic esters (Figure 30). First, only ROCOP takes place due to lower activation barriers and more stable intermediates. However, once all anhydride is consumed, the polymerization switches to ROP of the cyclic ester, resulting in multiblock polyesters.[95]

31
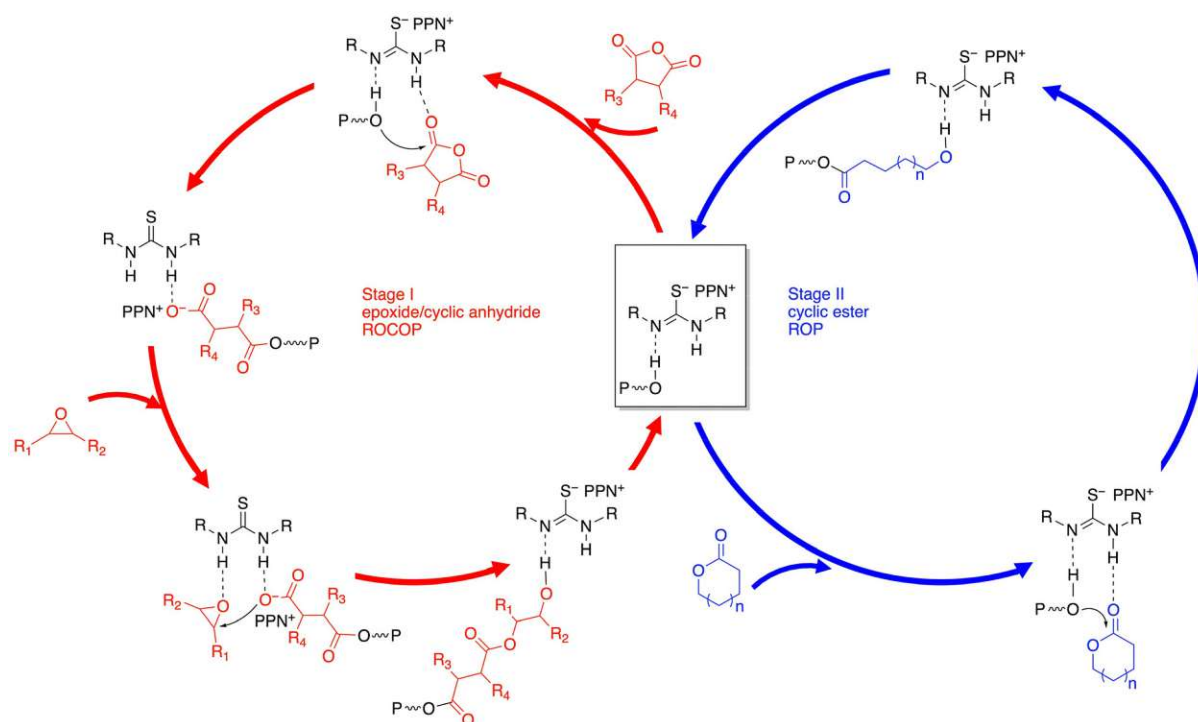
Figure 30. Proposed reaction mechanism for the self-switchable polymerization of epoxides, cyclic anhydrides and cyclic esters. Figure reproduced from ref[95] without changes. Copyright 2023 by Royal Society of Chemistry.

While most reports about organometallic catalysts focus on Lewis pairs, phosphazene superbases were also reported as effective single-component catalysts that could produce polyesters with a perfectly alternating monomer distribution and low dispersities. It was discovered that using two different phosphazene bases, t-BuP$_4$ or t-BuP$_1$, both resulted in full conversion of monomers into an alternating copolymer. However, when using the strong t-BuP$_4$ base, high polydispersity was discovered due to many inter- and intramolecular transesterification side reactions taking place. The mild base t-BuP$_1$, on the other hand, effectively suppressed all side reactions and gave polymers with low polydispersity. This behavior was attributed to the different basicity: while t-BuP$_4$ can deprotonate both the epoxide terminal (aliphatic hydroxyl) and anhydride terminal (benzoic carboxyl), the weaker t-BuP$_1$ base is only able to activate the PA-terminal, while it deactivates the EO by returning the proton (Figure 31). This proton shuttle between the t-BuP$_1$ and the growing chain results in high selectivity and control of the reaction. The living nature of this polymerization was proven and used in block-alternating copolymerization. When adding the monomers simultaneously instead of sequentially, it is also possible to obtain statistical-alternating copolymers.[14, 92]

Considering sustainability, the ROCOP reaction also offers a lot of advantages. For one, the monomers can be derived from natural sources. Terpenes such as limonene oxide can be used and offer the possibility of further modifications if they contain other functional groups.[96, 97] Furthermore, epoxidized oils such as castor oil or epoxidized fatty acids such as oleic acid have also been explored for ROCOP reactions.[98, 99] Finally, it is also possible to use oxetanes instead of epoxides, even though their lower ring-strain results in reduced reactivity.[100, 101] Such oxetanes can be derived from sugars, for example the D-xylose 3,5-anhydrosugar oxetane has been applied successfully in a copolymerization with different anhydrides.[100] Furthermore, as mentioned already in the last chapter, the products are polyesters that can degrade hydrolytically and therefore can be recycled subsequently through separation of degradation products and regeneration of monomers thereof.[96]

Even though this is a versatile reaction used in many different ways, there are not many reports on light-based 3D printing. In fact, this reaction has not been triggered by light at all until now. However, there are reports about photopolymerization of copolymers obtained by ROCOP of cyclic anhydrides and epoxides that also contain a double bond. After the copolymerization reaction, the polyesters still contain the double bonds, which can be crosslinked in a free radical polymerization or a thiol-ene reaction. However, when using free radical crosslinking, curing is slow and brittle materials are obtained. The thiol-ene mechanism, on the other hand, produces mechanically stable thermosets in a rapid pace, but also requires the addition of a thiol crosslinker.[84, 96] In either case, however, crosslinking based on radical photopolymerization mechanisms renders the resulting construct degradable, yet unrecyclable. Therefore, photopolymerization approaches which do not require irreversible crosslinking reactions would be highly desirable.

RESULTS AND DISCUSSION

Based on literature research, the task of this thesis was to determine if the synthesis of degradable polyesters using the ring-opening copolymerization (ROCOP) of epoxides and anhydrides is possible using light as trigger, making this sustainable system available for 3D printing applications. In this regard, either a photoacid generator (PAG) or a photobase generator (PBG) are viable catalyst options.

1 ELUCIDATION OF POLYMERIZATION BEHAVIOR

The first task of this thesis was determining if copolymerization is happening when using either a PAG or a PBG as catalyst, while at the same time avoiding side reactions. One such literature-known side reaction is the homopolymerization of epoxides to polyethers, which are not readily degradable and have different properties.

Therefore, a linear model system was established to investigate the polymerization behavior. Phenylglycidylether (PGE) and 4-methyl-1,2-cyclohexanedicarboxylic anhydride (MHHPA) were chosen as monomers (Figure 32) because they are liquid at room temperature and have a high boiling point so that loss of monomer can be minimized during the polymerization reaction at higher temperatures. Some of the older monomer batches showed impurities and thus were purified before use. As photocatalysts, Irgacure 290 and WPBG 266 were chosen due to their commercial availability (Figure 32). Furthermore, PBGs usually do not show sufficient absorption in the light range of a standard Hg broadband lamp (320-500 nm), and therefore a photosensitizer needed to be added. Isopropylthioxanthone (ITX, Figure 32) is a commonly used photosensitizer and has been used with PBGs before.[102, 103]

Formulations contained the monomers in a 1/1 (fg%/fg%) ratio to allow for quantitative conversion, where fg% corresponds to functional groups in each monomer. Furthermore, 2.5 mol% photocatalyst as well as 0.25 mol% ITX additionally when using PBGs were employed. Control experiments using only epoxide and 2.5 mol% photocatalyst (+ 0.25 mol% ITX when using PBG) were conducted as well to see if homopolymerization of the epoxide to polyether is happening at the selected conditions. Photo-DSC was chosen as easy, controllable and steady curing method, although no exothermic behavior was observed for this reaction. Since the reactivity is highly dependent on the temperature, different temperatures of 50, 100 and 150 °C were chosen. For irradiation, a broadband LED ranging from 320-500 nm with an intensity of 91 ± 1 mW cm^{-2} was used. Once the desired temperature was reached, the system was equilibrated for 4 min before irradiating twice for 5 min.

PGE

MHHPA

Irgacure 290

WPBG 266

ITX
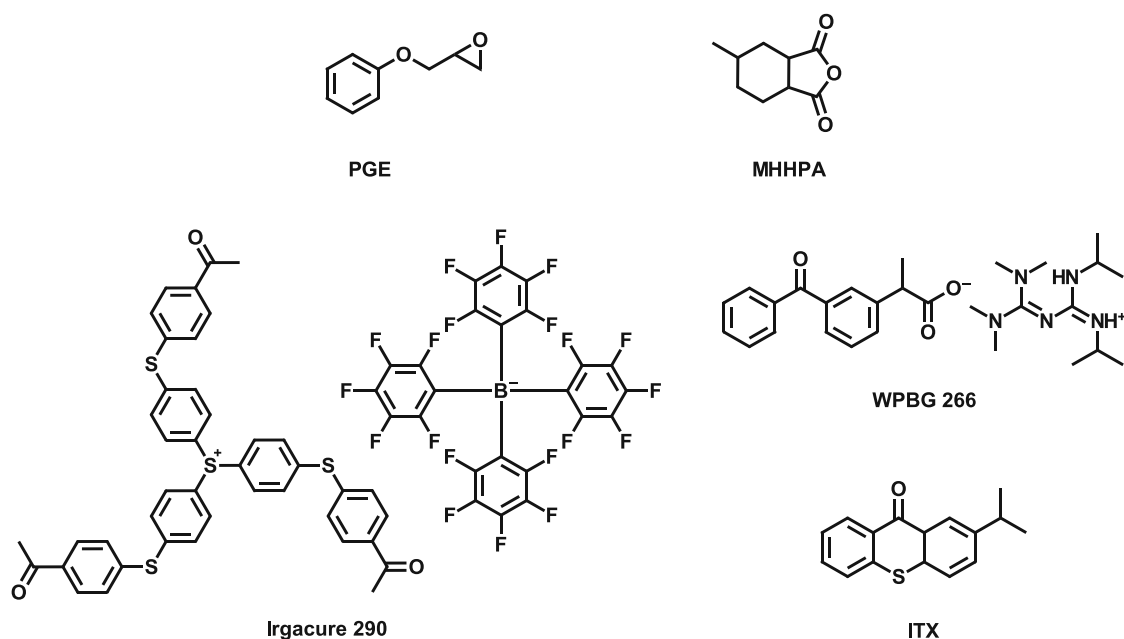
Figure 32. Structures of monomers and photocatalysts chosen for the model system.

1.1 Polymerization Process

NMR analysis was used to investigate the polymerization behavior of the ROCOP of epoxides and anhydrides initiated by PAGs or PBGs. For this, a formulation containing PGE/MHHPA 1/1 (fg%/fg%) and 2.5 mol% photocatalyst was used. Furthermore, a control experiment was performed using only the epoxide PGE and photocatalyst to determine if the literature-known side reaction homopolymerization of PGE to polyethers is possible at the employed reaction conditions.

The samples were cured on the photo-DSC by irradiating twice for 300 s with 91 ± 1 mW cm^{-2} at 50, 100 and 150 °C. Then, the cured samples from the photo-DSC were immediately dissolved in deuterated acetonitrile CD$_3$CN, since no overlap of signals was observed using this solvent. Even though anionic polymerization reactions are ideally "living" and as such retain their active chain ends, even traces of impurities such as water lead to termination.[104] Therefore, no additional quenching reagent was added when using PBGs. However, when using PAG as catalyst, the NMR solvent was spiked with 0.3 wt% pyridine in order to quench excess acid and stop the cationic polymerization process.

New signals or an altered shape of existing peaks, especially broadening, are signs of polymerization. Such signs of polymerization can be found when comparing both PAG- and PBG-catalyzed reactions after curing at 100 °C compared to the unreacted formulations (Figure 33a1, b1). However, the control experiment using only epoxide and photocatalyst only shows signs of polymerization for the photoacid-catalyzed system (Figure 33a2, b2), indicating the unwanted homopolymerization of epoxide to polyether is only possible in those systems.

36
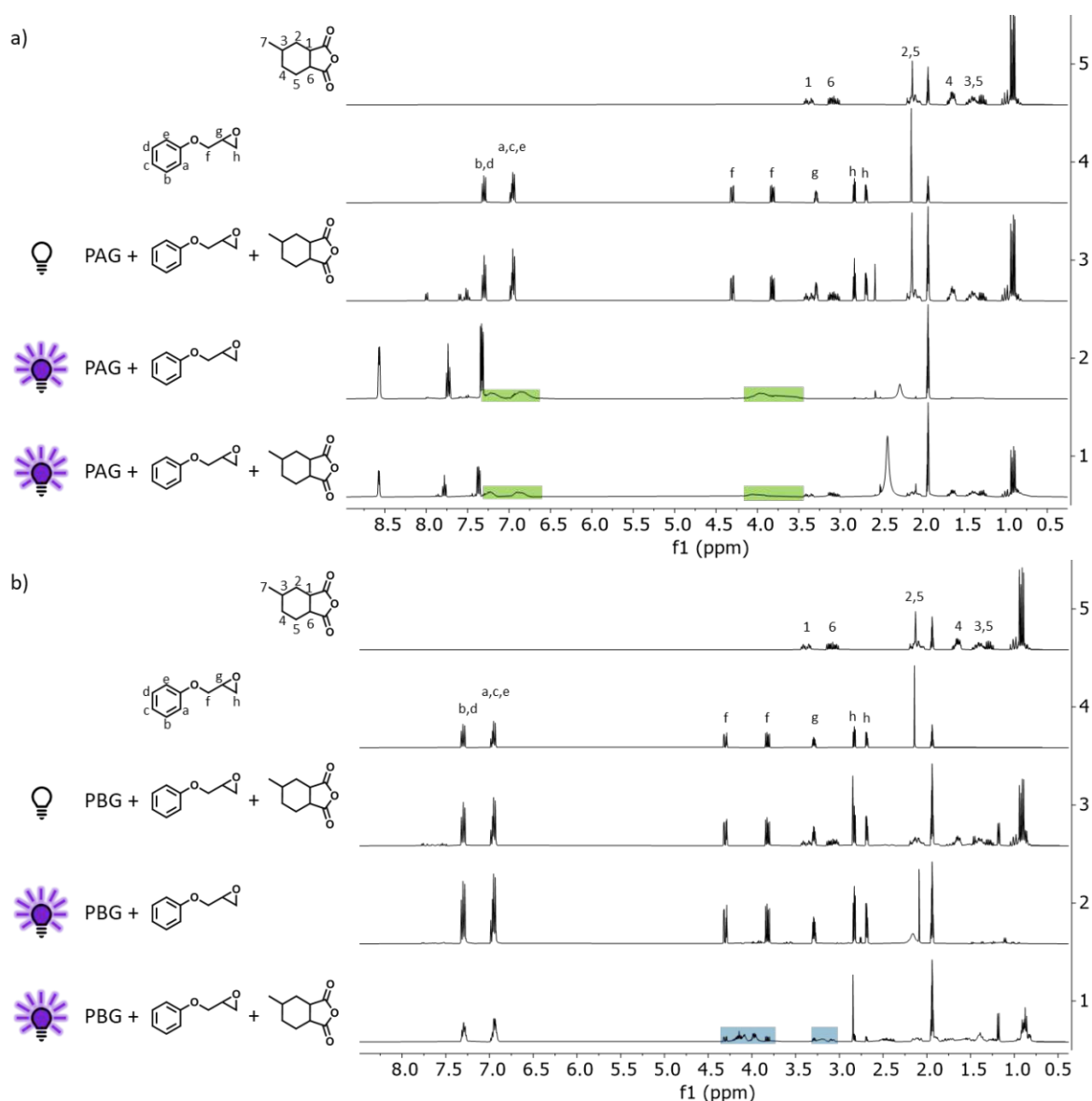
Figure 33. a) ^{1}H-NMR of PAG-catalyzed systems cured at 100 °C. 1) MHHPA, PGE + PAG cured at 100 °C. 2) PGE + PAG cured at 100 °C. 3) MHHPA, PGE + PAG formulation before irradiation. 4) PGE. 5) MHHPA. b) ^{1}H-NMR of PBG-catalyzed systems cured at 100 °C. 1) MHHPA, PGE + PBG cured at 100 °C. 2) PGE + PBG cured at 100 °C. 3) MHHPA, PGE + PBG formulation before irradiation. 4) PGE. 5) MHHPA.

The variation of curing temperature led to similar results (Figure S8, Figure S9, Figure S10, Figure S11). No matter the temperature, polymerization in the model system occurs using either PAG or PBG. However, the higher the temperature, the stronger the signs of polymerization. Especially the PBG-catalyzed system at 50 °C only shows very little to no signs of polymerization. The control experiment using only epoxide and photoinitiator, on the other hand, shows clear signs of polymerization at all temperatures when using PAG, but only at 150 °C when using PBG. This could indicate that 150 °C is sufficiently high for the homopolymerization of epoxides to happen even without any catalyst, although this was not further investigated and confirmed. Instead, further experiments were only carried out to a maximum of 100 °C, since no homopolymerization of epoxides is happening when using PBGs in this case. Overall, these results imply that PBGs might be better suited for the reaction.

However, even though homopolymerization is possible when using PAG, it is not clear whether this reaction is indeed happening in the model system, since the copolymerization could also be highly favorable and therefore suppress the homopolymerization if both anhydride and epoxide are available as monomers.

Therefore, it is important to determine the ratio of copolymerization to homopolymerization in the model system. According to Shimomura *et al.*[105], ROCOP of PGE and MHHPA leads to the formation of a new methine-H signal (-COOCH$_2$-C$\underline{H}$-) at around 5.3 ppm. This signal can indeed be found in all of the copolymerization experiments and indicates that at least some copolymer is formed (Figure S12 and Figure S13). However, using the NMR for quantification is quite hard due to many signals that could not be assigned beyond doubt.

Therefore, quantitative NMR was introduced. For this technique, an internal standard is added, which should be very stable and only show very few signals. Sigma-Aldrich[106] suggests several such possible internal standards, from which ethylene carbonate was chosen since it shows no overlap with other signals from either uncured or cured samples, and should be unreactive towards the monomers and polymer if added after irradiation.

For determining the conversion of monomers during polymerization, the signals belonging to the marked protons in Figure 34 were chosen and integrated since those signals show no overlap with signals of the polymer. To minimize errors, the exact same integral boundaries were used in each spectrum.
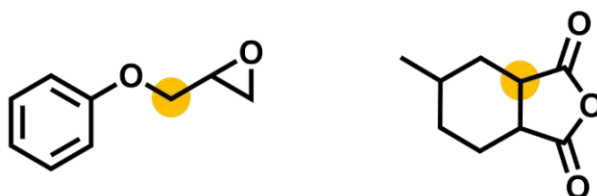
Figure 34. Monomers' protons analyzed in qNMR-measurements are highlighted in yellow.

The amount of the monomer in the sample can then be calculated using Equation 1.

$$X_A = \frac{I_A}{I_{iS}} \cdot \frac{N_{iS}}{N_A} \cdot \frac{M_A}{M_{iS}} \cdot \frac{m_{iS}}{m_P} \cdot 100 \tag{1}$$

X$_A$ .... percentage of analyte in sample (wt %)	Subscripts:
I........... integral	A .... analyte
N .... number of protons	iS .... internal Standard
M .... molecular weight (g/mol)	P.......... sample
m .... mass (mg)	

For PAG-initiated systems, the consumption of PGE is significantly higher than the consumption of MHHPA (Figure 35a, Table S9). This clearly shows that homopolymerization makes up a good part of the overall polymerization process, therefore rendering this system useless for the application of producing pure polyester systems. It is possible that using a less reactive epoxide could lead to better ratios of copolymerization to homopolymerization, which was, however, not investigated further. On the other hand, similar conversion of both PGE and MHHPA were observed when catalyzing the polymerization with PBG. Surprisingly, the MHHPA conversion was in fact even slightly higher than the PGE conversion (Figure 35b, Table S9). The reason for this is likely the reaction of MHHPA with traces of water to the corresponding acid, since acid signals of a similar integral size to make up the differences were found.

Another interesting detail is that the monomers only make up about 80 wt% in the PAG formulation and about 87 wt% in the PBG formulation. This is because the photoinitiators are rather big molecules. Therefore, 2.5 mol% PAG correspond to 18 wt%, and 2.5 mol% PBG correspond to 8 wt% of the formulations.
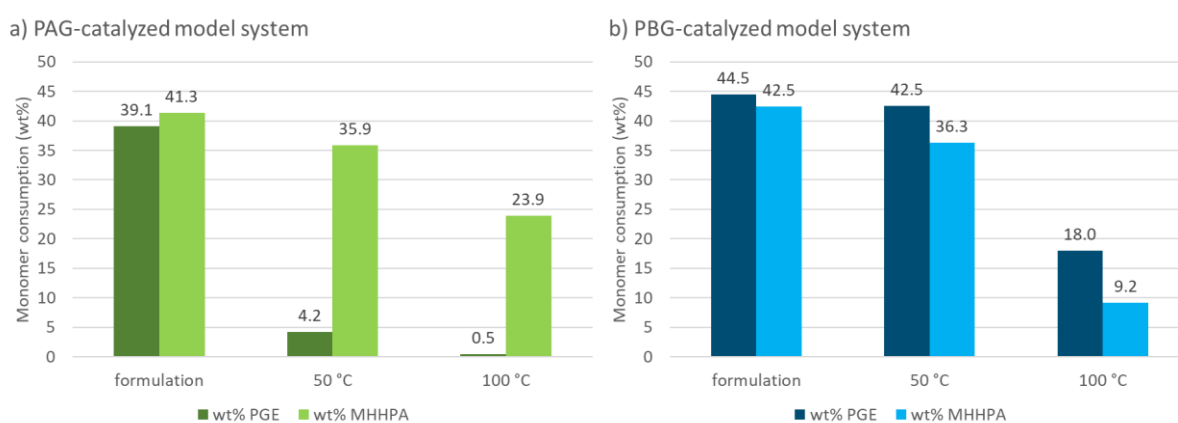
Figure 35. Monomer consumption in weight percent calculated from quantitative NMR results for the unirradiated formulation containing PGE/MHHPA 1/1 (fg%/fg%) as well as cured samples at 50 and 100 °C using a) photoacid generator Irgacure 290 or b) photobase generator WPBG 266. Data summarized in Table S9.

These results strongly suggest that using PBGs exclusively leads to the formation of polyester, while using PAGs leads to significant homopolymerization of the epoxides in parallel to copolymerization.

ATR-FTIR spectra were used to reinforce those results (Figure 36). According to Merck KGaA,[107] ester stretch vibrations can be found at 1210-1163 cm^{-1} (C-O) and 1750-1735 cm^{-1} (C=O), while aliphatic ether stretch vibrations can be found at 1150-1085 cm^{-1} (C-O). After curing of the model system, new signals appear in the ester region (1732.46 + 1702.59 cm^{-1} for PAG and 1688.77 cm^{-1} for PBG) that are neither visible for the formulation prior to irradiation nor in the control experiment, indicating polyester formation. On the other hand, new signals in the region of ether stretch vibrations are only

visible for PAG-catalyzed systems and especially dominant for the control experiment, while absent using PBG.
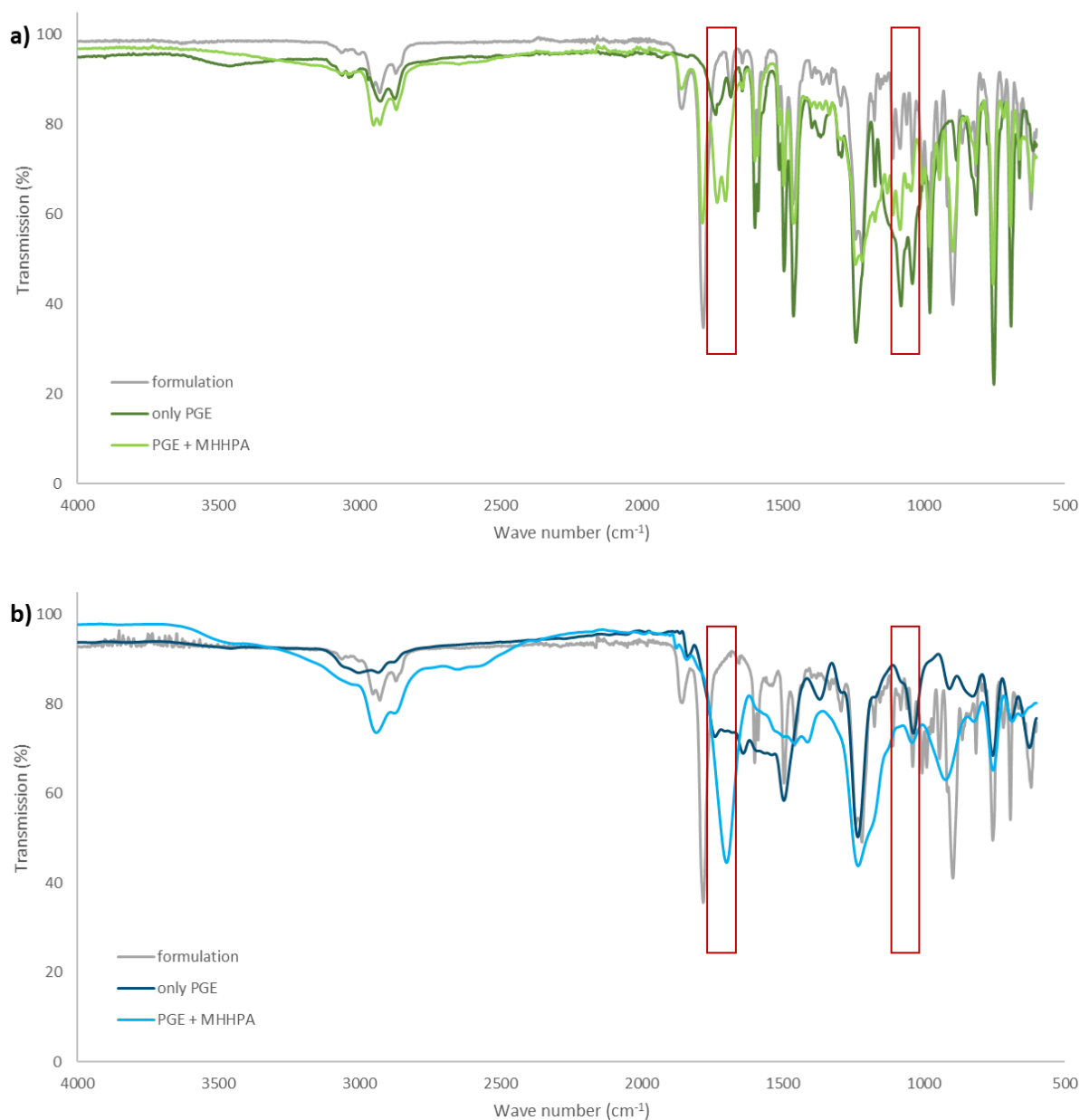
Figure 36. ATR-FTIR spectrum of the model system containing PGE/MHHPA 1/1 (fg%/fg%) cured at 100 °C catalyzed by a) photoacid generator Irgacure 290 or b) photobase generator WPBG 266.

1.2   Conversion of Monomers

During photopolymerization, complete conversion of monomers is desirable to achieve good properties of the resulting polymer. NMRs can be used to calculate the conversion of monomers by comparing the integrals of a decreasing and a constant monomer signal before and after curing

(Equation 2). However, this method is usually not completely accurate since different protons give different signal intensities dependent on their chemical surroundings. Furthermore, when many signals are involved, the likelihood of overlap of signals increases tremendously.

$$X_A = \frac{I_A}{I_{cs}} \cdot \frac{N_{cs}}{N_A} \cdot 100 \qquad (2)$$

X_A .... percentage of analyte in sample (wt %)   Subscripts:

I........... integral   A .... analyte (changing signal)

N .... number of protons   cs......... constant signal

Since it was shown in the previous chapter that MHHPA is reacting with trace amounts of water to the corresponding acid, thus making it unreliable for determining the conversion towards polymerization, only the conversion of PGE was determined from now on. Formulations containing PGE/MHHPA 1/1 (fg%/fg%) and 2.5 mol% photocatalysts as well as formulations containing only PGE and 2.5 mol% photocatalyst were cured on the photo-DSC at 50, 100 and 150 °C. Then, the cured samples were immediately quenched in NMR solvent.

Some trends are immediately visible (Figure 37, Table S10): First of all, the higher the temperature, the higher the conversion of epoxide, which will be investigated further at a later point. Furthermore, the conversions are higher for the model system when both epoxide and anhydride are present, which indicates that copolymerization definitely occurs to a certain degree. Finally, the monomer conversions are also higher when using PAG, which allows nearly quantitative conversions at 100 °C. To reach quantitative conversions using PBGs, 150 °C are necessary.
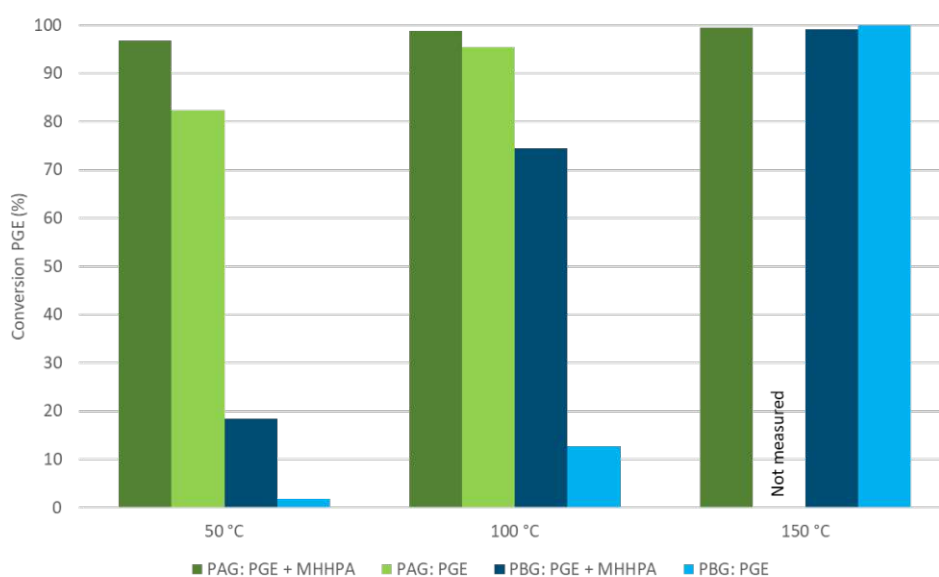
Figure 37. Epoxide conversion calculated from ^{1}H-NMRs when curing samples containing PGE/MHHPA 1/1 (fg%/fg%) + 2.5 mol% photocatalyst at different temperatures. Data summarized in Table S10.

41

In order to verify those results, quantitative NMR with ethylene carbonate as internal standard was employed (Figure 38, Table S11). Otherwise, the same procedure as described before was used. The monomer conversion is very similar when calculating it from either ^{1}H-NMR or quantitative ^{1}H-NMR, and thus both methods seem to be reliable for quantification purposes.

Furthermore, the percentage of copolymerization based on total conversion of PGE was calculated (Equation 3) and shows very little copolymerization for PAG-catalyzed systems, while PBG-catalyzed systems show almost exclusively copolymerization. It should also be mentioned that the extremely low conversion at 50 °C in the PBG system resulted in high susceptibility to errors, so that the calculated copolymerization amount is well above 100% and as such not meaningful.

$$S = \frac{X_{pol}}{Y_{mon}} = \frac{I_{pol}}{I_{cs}} \cdot \frac{N_{cs}}{N_{pol}} \cdot 100 \cdot \frac{1}{100 - \frac{I_{mon}}{I_{cs}} \cdot \frac{N_{cs}}{N_{mon}} \cdot 100} \tag{3}$$

S..........percentage of copolymerization based on total conversion of monomer (%)   Subscripts:

X..........percentage in sample (%)   pol...................copolymer

Y..........conversion (%)   mon.................monomer

I...........integral   cs.....................constant signal

N.........number of protons
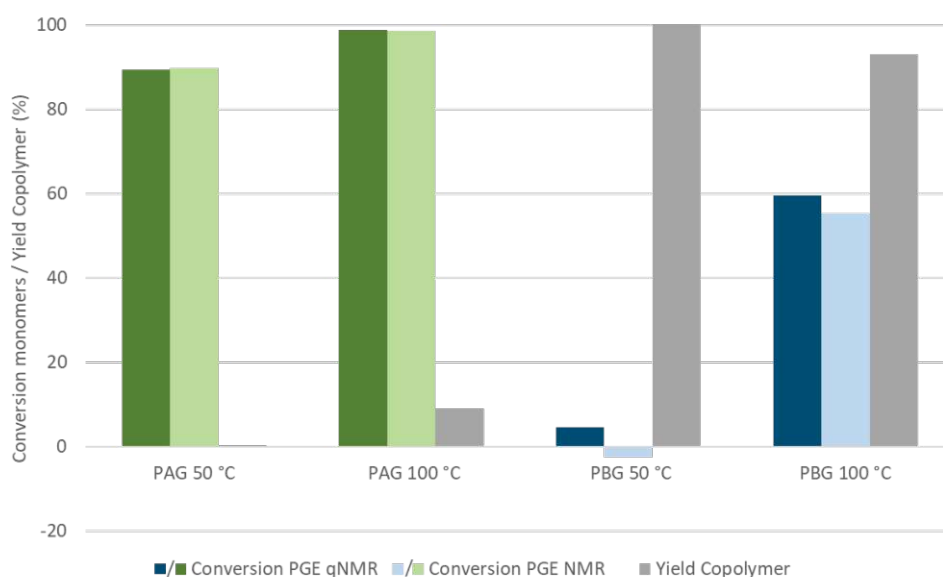
Figure 38. Comparison of monomer conversions calculated from ^{1}H-NMR and quantitative NMR when curing samples containing PGE/MHHPA 1/1 (fg%/fg%) + 2.5 mol% PBG or 2.5 mol% PAG at 50 or 100 °C. Data summarized in Table S11.

1.3 Chain Length of Polymers

In order to determine the chain length of the produced polymers, SEC-measurements were conducted using butylhydroxytoluol (BHT) as flowrate marker, and the results were based on external calibration with polystyrene standards and are therefore only approximations. The polymers were produced

using formulations containing PGE/MHHPA 1/1 (fg%/fg%) and 2.5 mol% photocatalysts as well as formulations containing only PGE and 2.5 mol% photocatalyst. The samples were cured on the photo-DSC by irradiating twice for 300 s with 91 ± 1 mW cm^{-2} at 50, 100 and 150 °C, and then immediately quenched in THF with 0.5 mg mL^{-1} BHT.

Figure 39 (Table S12) shows the number average molecular weight, M_n, of the peak corresponding to the highest molecular weight. In two cases, the flowrate marker was not found by the software. This indicates that some of the sample is of similar chain length so that the peaks overlap with the peak of the flowrate marker BHT. Therefore, the BHT peak which is usually used for referencing elution times cannot be distinguished from sample peaks, making these results more unreliable. Furthermore, the average degree of polymerization DP was calculated using Equation 4.

$$DP = \frac{M_n}{\overline{M_{monomer}}} \tag{4}$$

DP .... average degree of polymerization

M_n .... number average molecular weight of the polymer

$\overline{M_{monomer}}$ .... average molecular weight of the monomers
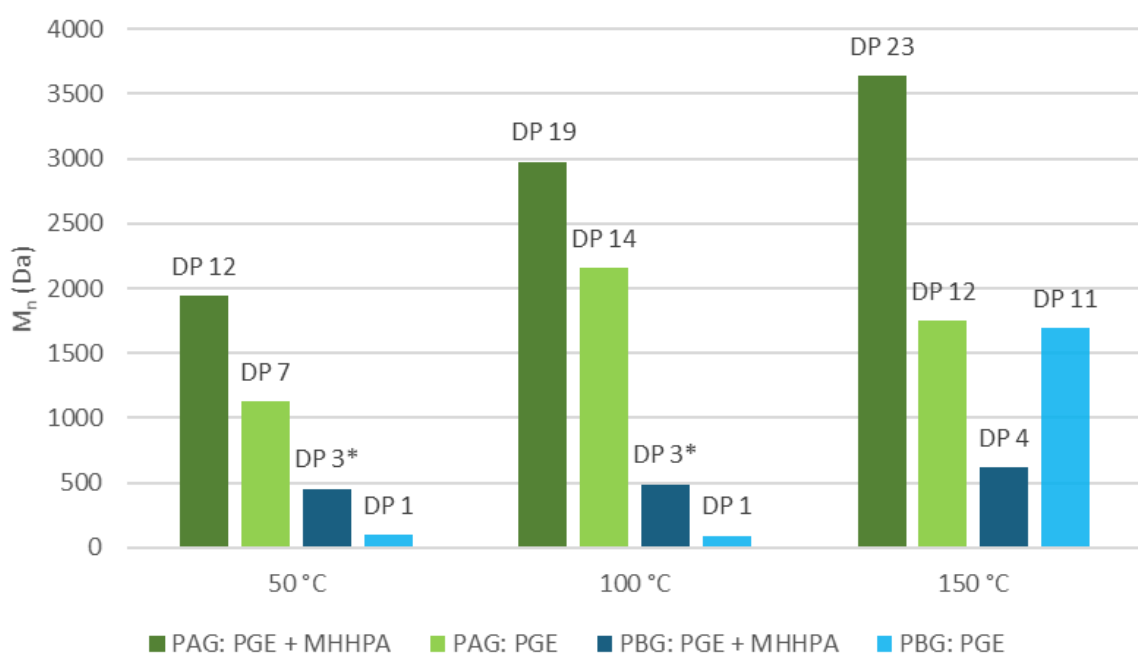
Figure 39. SEC results of the molecular weight and the average degree of polymerization (DP) of the model system containing PGE/MHHPA 1/1 (fg%/fg%) and the control experiment containing only PGE using either 2.5 mol% photoacid generator Irgacure 290 or 2.5 mol% photobase generator WPBG 266. Data summarized in Table S12.

These results show that the higher the temperature, the longer the polymers. Furthermore, PAG-catalysis leads to higher molecular weights than PBG-catalysis. The control system using only PGE also verifies that PAG-catalysis enables homopolymerization, though the molecular weights of the produced polyethers are not as high as the molecular weight of the polymers produced in the model system using both PGE and MHHPA. It is also clear that under PBG catalysis, homopolymerization of PGE is only happening from 150 °C on. Surprisingly, at 150 °C the molecular weight of the produced polyether chains in the control experiment using only PGE was even higher than the molecular weight for the produced polymers when using both PGE and MHHPA, indicating that the homopolymerization is favorable over the copolymerization at this temperature.

Unfortunately, while this supports the theory that only PBGs can be used to obtain pure polyester systems, the chain lengths of the polymers obtained from ROCOP are very short, and thus optimization is crucial.

1.4 Stability of Formulation

The stability of the monomers in the formulation is very important since the formulation needs to remain uncured at the designated printing temperature in the absence of light over prolonged time frames. Furthermore, in industry it is advantageous if formulations can be stored over longer time periods.

Preliminary stability tests of the model system using a formulation containing PGE/MHHPA 1/1 (fg%/fg%) and 2.5 mol% WPBG 266 + 0.25 mol% ITX were conducted using (quantitative) ^{1}H-NMR analysis. They drew a rather bleak picture, with first signs of polymerization at room temperature after 6 h, and over 50% PGE conversion after 2 h storage at 90 °C (Table S13).

Therefore, a more concise stability study was conducted using qNMR and rheology measurements to monitor the stability of a formulation containing PGE/MHHPA 1/1 (fg%/fg%) and 1 mol% WPBG 266 + 0.1 mol% ITX that was stored at 100 °C between measurements.

As expected from the preliminary studies, the measurements revealed severe stability problems (Figure 40, Table S15 and Table S16). After one hour, around 15% PGE were consumed, and the viscosity increased slightly from 0.01 to 0.05 Pa s. While this was not ideal, the stability dropped considerably after this, with an eightfold increase in viscosity from 0.05 to 0.41 Pa s over the next hour. At this point, already 35% PGE had been consumed. After just four hours, the PGE conversion of over 60% led to such high viscosities of nearly 500 Pa s that the formulation could hardly be processed anymore.

This instability of monomers is a severe problem for the usage of this particular formulation in hot stereolithography. Therefore, finding a different formulation with increased stability is key to establishing this system for hot stereolithography.
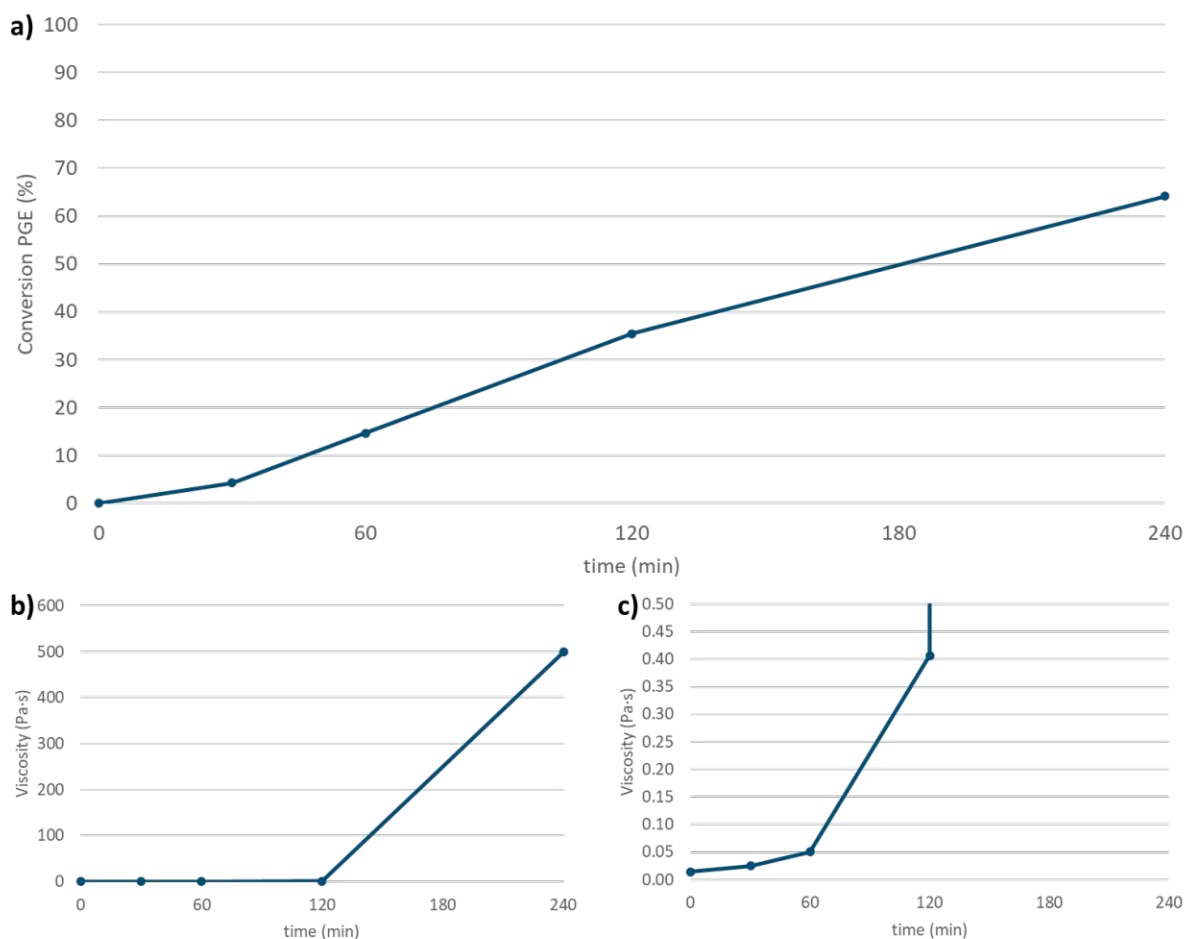
Figure 40. Stability of formulations at 100 °C containing PGE/MHHPA 1/1 (fg%/fg%) + 1 mol% WPBG 266 + 0.1 mol% ITX determined using a) qNMR analysis, b) rheology measurements (full-scale spectrum), c) rheology measurements (zoomed-in spectrum for more details). Data summarized in Table S15 and Table S16.

2 OPTIMIZING THE LINEAR MODEL SYSTEM

In the last chapter, photobase generators (PBGs) were established as possible catalysts for the light-triggered ring-opening copolymerization (ROCOP) of epoxides and anhydrides. However, low conversion of monomers and only small polymers were obtained, and major problems regarding stability were discovered. Therefore, optimization of the linear system consisting of phenylglycidylether (PGE) and 4-methyl-1,2-cyclohexanedicarboxylic anhydride (MHHPA) is crucial.

2.1 PBG Screening

It was shown in the last chapter that while the ROCOP between epoxides and anhydrides can be catalyzed by PBGs, the reactivity is low and monomers show insufficient stability when using a formulation containing PGE, MHHPA and WPBG 266. However, using different PBGs might help in both increasing the reactivity and the stability of the formulations.

Therefore, several different PBGs were tested. PBGs were chosen due to availability and include two commercial PBGs (WPBG 266 and WPBG 300), PDBN and two phosphazene bases (KP2T and BP2T) (Figure 41).
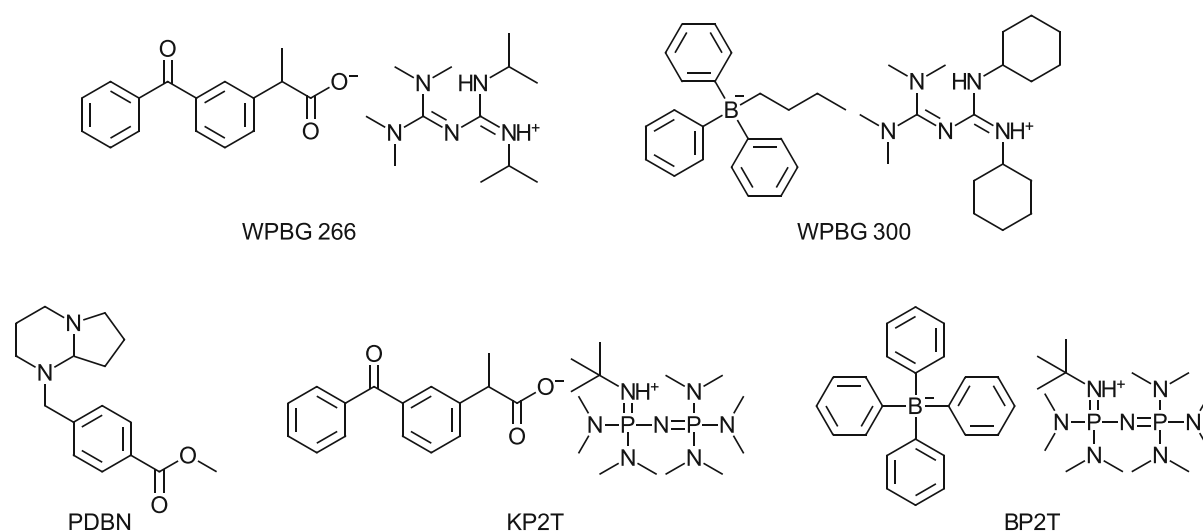
Figure 41. Chosen PBGs for reactivity and stability screening.

2.1.1 Reactivity Study

Using different PBGs might cause distinct differences in reactivity. This was investigated by measuring qNMRs to determine the monomer conversion, and SEC to determine the chain length of the produced polymers when using different PBGs (Table 1, Table S14). The samples contained PGE/MHHPA 1/1 (fg%/fg%), 1 mol% PBG and 0.1 mol% ITX and were cured on the photo-DSC at 100 °C by irradiating twice for 300 s with 91 ± 1 mW cm^{-2}.

Table 1. Monomer conversion, molecular weight of polymers (M_n) and average degree of polymerization (DP) using different PBGS.

PBG	Conversion PGE (%)	M_n (Da)	DP
WPBG 266	24	740	5
WPBG 300	23	1750	11
PDBN	13	560	4
KP2T	61	1260	8
BP2T	11	1260	8

The conversion of monomers seems to be dependent on the basicity of the released base (Figure 42). The highest conversions are achieved by using KP2T releasing a highly basic phosphazene base. Surprisingly, however, the phosphazene base BP2T shows very low conversion and therefore contradicts the trend. It is unclear what causes this huge difference in reactivity, but the anion seems to effect it significantly, too. Both commercial PBGs, WPBG 266 and WPBG 300, release biguanidines as bases which leads to similar conversion of monomers, while PDBN only shows about half of this conversion and thus is quite unreactive.

DBN
$pK_a = 23.9$ (ACN)[108]

Biguanidine
$pK_a = 27$ (ACN)[109]

Phosphazene
$pK_a = 33.5$ (ACN)[110]
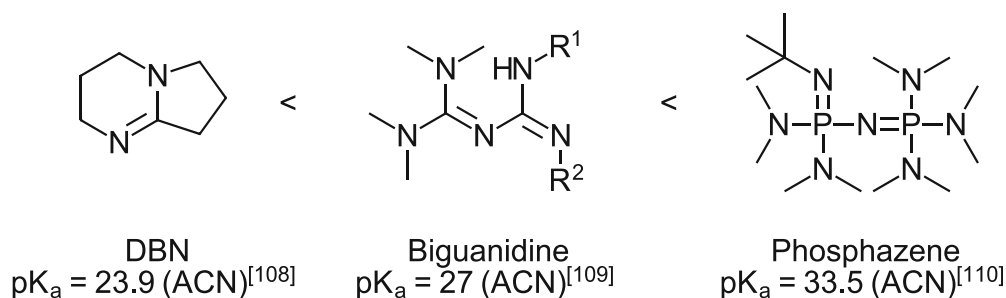
Figure 42. Basicity of bases released by photobase generators.[108-110]

Interestingly, the chain lengths of the produced polymers do not follow this trend. Biguanidine-based WPBG 300 exhibits the highest average degree of polymerization of 11. The two phosphazene bases KP2T and BP2T have similar chain lengths of approximately 8 monomers. The second biguanidin-based base WPBG 266 and DBN-based PDBN produce the shortest oligomer chains with only 4-5 monomers.

2.1.2 Stability Study

Since the choice of PBG has a big influence on the reactivity, it seems only reasonable that it will also influence the stability of the monomers in the formulation. This is especially important since the stability using WPBG 266 was not sufficient for the application in hot stereolithography (see p.44).

Therefore, a stability study was conducted using qNMR and rheology measurements to monitor the stability of formulations containing PGE/MHHPA 1/1 (fg%/fg%) and 1 mol% of different PBGs plus 0.1 mol% ITX that were stored at 100 °C between measurements (Figure 43, Table S15 and Table S16).

Fortunately, it is immediately apparent that using different PBGs does indeed result in different stabilities of the formulations. The PBG used so far, WPBG 266, shows mediocre stability compared to the other bases: PDBN and KP2T exhibit worse stability, while using WPBG 300 and BP2T results in more stable formulations.
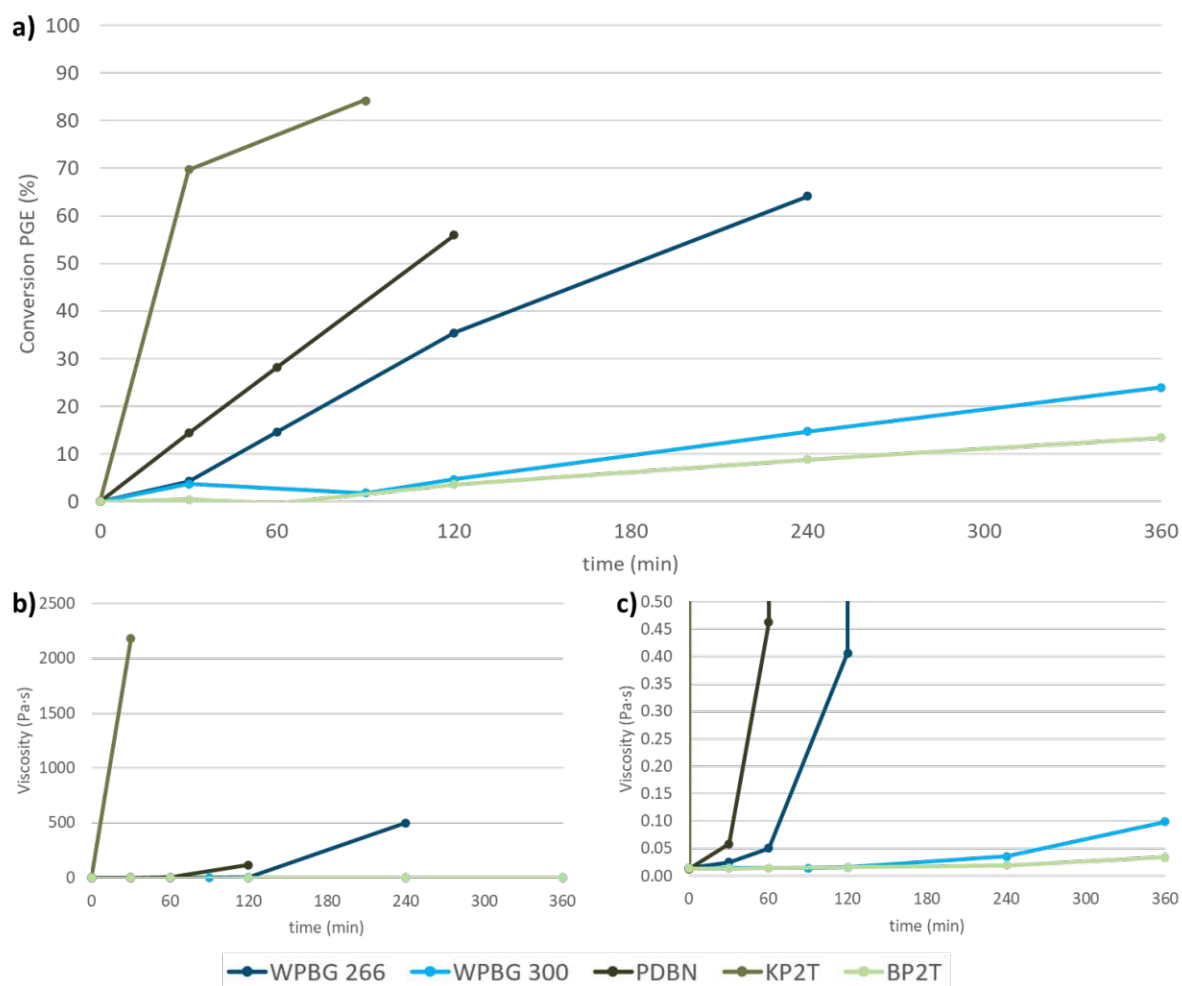
Figure 43. Stability of formulations at 100 °C containing PGE/MHHPA 1/1 (fg%/fg%) + 1 mol% of different PBGs + 0.1 mol% ITX measured using a) qNMR, b) rheology (full-scale spectrum), c) rheology (zoomed-in spectrum for more details). Data summarized in Table S15 and Table S16.

The low stability when using PDBN was expected since it contains a tertiary amine that can act as a basic initiator even without irradiation.

On the other hand, the low stability of KP2T especially compared to the other phosphazene base BP2T was quite surprising. Using KP2T leads to conversions above 70% and highly viscous formulations (> 2000 Pa s) after storage at 100 °C for only 30 min, which makes it impossible to use in hot stereolithography. However, the high reactivity of KP2T discovered in the last chapter might explain this incredibly low stability.

This could also explain the huge differences in stability to the other phosphazene base, BP2T, since this PBG showed very low reactivity even though the released base is stronger than bisguanidine or DBN bases. In fact, BP2T showed the best stability of all tested PBGs. The conversion of PGE stays below 10% for 4 h, and the viscosity does not even double during this time (increase from 0.0136 to

48

0.0195 Pa s), making this formulation a viable option for hot stereolithography. However, the low reactivity of this PBG is not ideal.

Therefore, the commercial PBG WPBG 300 was revealed as the most promising candidate. It shows similarly good monomer stability with PGE conversions below 15% and viscosities below 0.04 Pa s within four hours, and still processable formulation within six hours (< 25% conversion of PGE, viscosity < 0.1 Pa s). But contrary to BP2T, in the last chapter it was also shown that WPBG 300 shows decent reactivity and is even able to produce the longest polymer chains compared to all the other PBGs tested.

Finally, it is interesting to note that the stability does not seem to be influenced a lot by the basicity of the released bases. Instead, the counterion seems to have a more distinct influence: Borate makes for more stable systems, while ketoprofen decreases the stability but increases the reactivity. This is true for both guanidine-based PBGs (WPBG 266, WPBG 300) and phosphazene-based PBGs (KP2T, BP2T).

2.2   Concentration of PBG

The concentration of PBG can play a crucial role for both conversion of monomers and achievable chain length of the arising copolymer. It is expected that higher PBG concentration will lead to higher conversion but lower molecular weight since more chain starters are available.

To test the influence of the concentration of PBG on the polymerization, formulations containing PGE/MHHPA 1/1 (fg%/fg%) and either WPBG 266 or WPBG 300 in different concentrations were cured on the photo-DSC at 100 °C by irradiating twice for 300 s with 91 ± 1 mW cm^{-2}. The samples were then immediately quenched in solvent. In order to determine the conversion of monomers, samples were analyzed using quantitative ^{1}H-NMR measurements with ethylene carbonate as internal standard. To determine the chain length of the produced polymers, other samples were analyzed using SEC measurements with BHT as flowrate marker.

However, tests at 100 °C curing temperature showed that higher PBG concentrations lead to both better conversion of monomers (Figure 44, Table S17 and Table S18) and higher molecular weights (Figure 45, Table S19). One exception was the formulation with 2.5 mol% WPBG 266, which produced the shortest chains in the whole measurement series. This could, however, be a measurement error since the data for both measurement series was obtained from several different measurement runs. Therefore, slight differences in the reaction conditions or sample preparations could have led to this exception, especially because the differences in molecular weight are small on an absolute scale and

the differences therefore most likely in the margin of error. Since a trend was still clearly visible, measurements were not repeated.
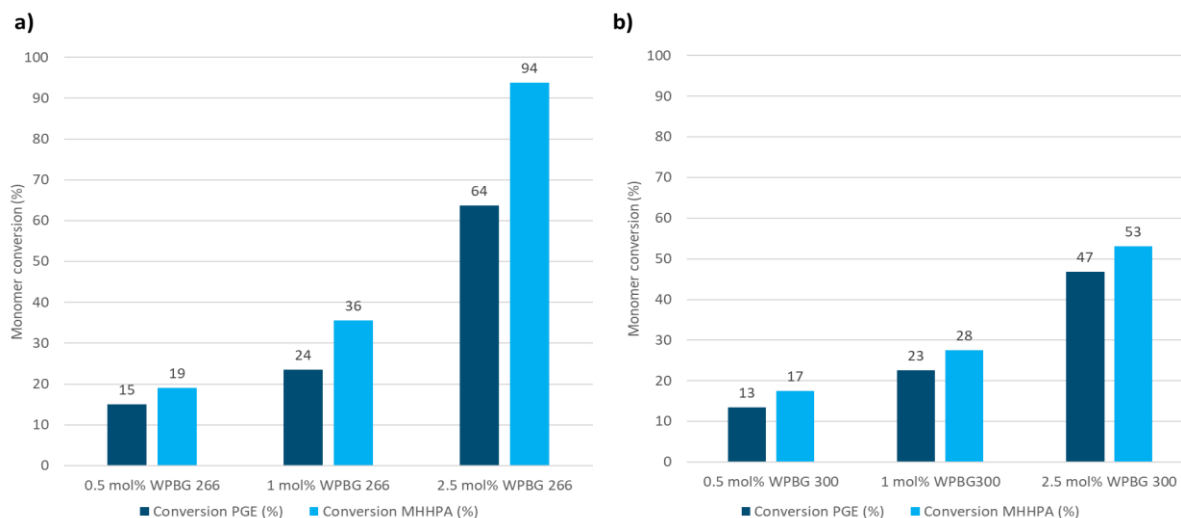
Figure 44. Conversion of monomers determined by quantitative NMR for different PBG concentrations (0.5, 1 or 2.5 mol%) using a) WPBG 266 or b) WPBG 300 as PBG at 100 °C curing temperature. Data summarized in Table S17 and Table S18.
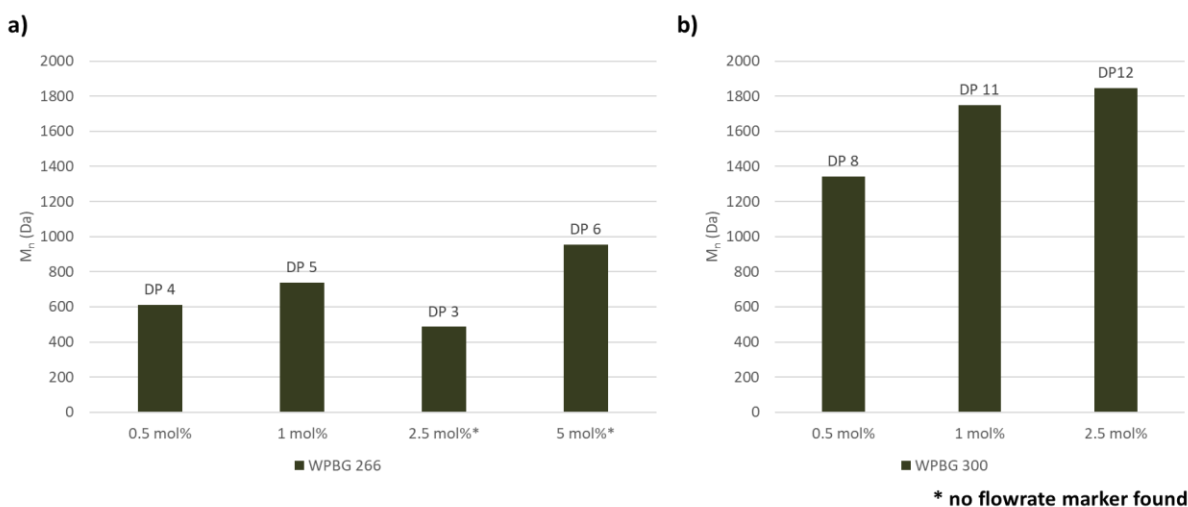
Figure 45. Highest M_n values determined by SEC measurements for different PBG concentrations (0.5, 1 or 2.5 mol%) using a) WPBG 266 or b) WPBG 300 as PBG at 100 °C curing temperature. Data summarized in Table S19.

The unexpected increase in molecular weight with higher PBG concentration could be caused by the overall low conversion of monomers. If a lot of unreacted monomers are still available for the copolymerization, they will still find enough monomers for the reaction even if the number of chain starters is increased.

Even though higher PBG concentrations are thus advantageous in all regards, it is still not recommended to use more than 2.5 mol% PBG since this already corresponds to 8-9 wt% PBG in the formulation, and the PBG remains in the produced polymer and is also an expensive component.

2.3 Temperature Screening

Conducting this reaction at elevated temperatures is necessary, since the reactivity is not high enough at room temperature to generate sufficient conversion. However, at the same time it was shown in chapter 1 that performing the reaction at 150 °C can lead to homopolymerization of the epoxide. Therefore, determining the optimal temperature for this reaction is crucial.

At first, temperatures between 50 and 100 °C were investigated. For this, samples containing PGE/MHHPA 1/1 (fg%/fg%) + 2.5 mol% WPBG 266 + 0.25 mol% ITX were cured in the photo-DSC, and the cured samples analyzed using qNMR (Figure 46, Table S20) and SEC measurements (Figure 47, Table S21).

As expected, higher temperatures lead to higher reactivity and thus higher conversion of the monomers (Figure 46). Furthermore, it can be seen that at least 70 °C are needed for any significant polymerization to occur. However, for good conversions above 50%, at least 100 °C are necessary.
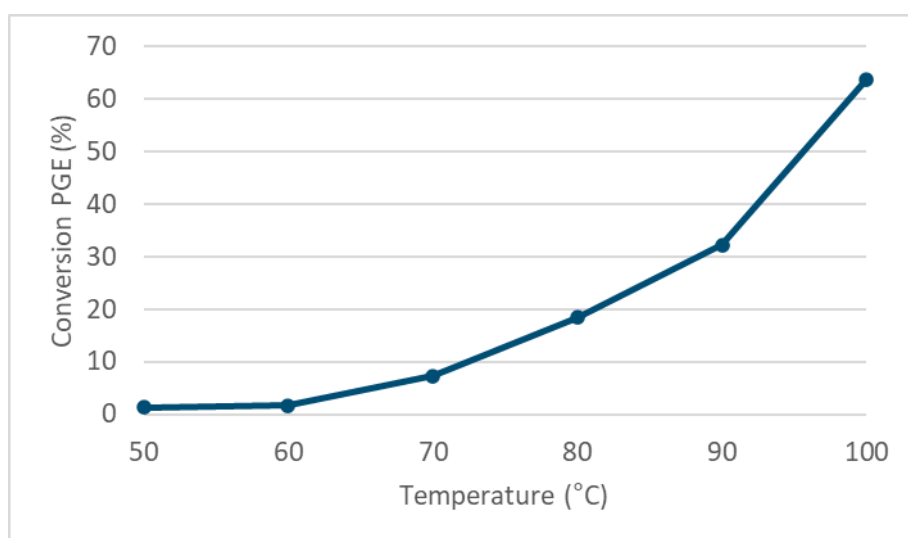
Figure 46. Conversion of PGE determined by qNMR after curing of samples containing PGE/MHHPA 1/1 (fg%/fg%) + 2.5 mol% WPBG 266 + 0.25 mol% ITX at different temperatures. Data summarized in Table S20.

SEC measurements confirmed these results (Figure 47, Table S21). In fact, polymers with more than one monomer unit were only observed in SEC measurements at temperatures of 90 °C and above, with 100 °C resulting in the longest chains.

However, during this SEC run, a strange peak at a retention volume of 20-25 mL was observed that corresponds to very high molecular weights. This peak has never been seen in measurements of this system before nor has it ever been measured after this experiment. The same solvent was used in other experiments, so impurities in the solvent can be ruled out as possible explanation. However, the peak is clearly visible in the first measurement, but gets smaller with every further measurement. This

could hint at a possible contamination of the column from a previous measurement, and thus this peak was ignored.
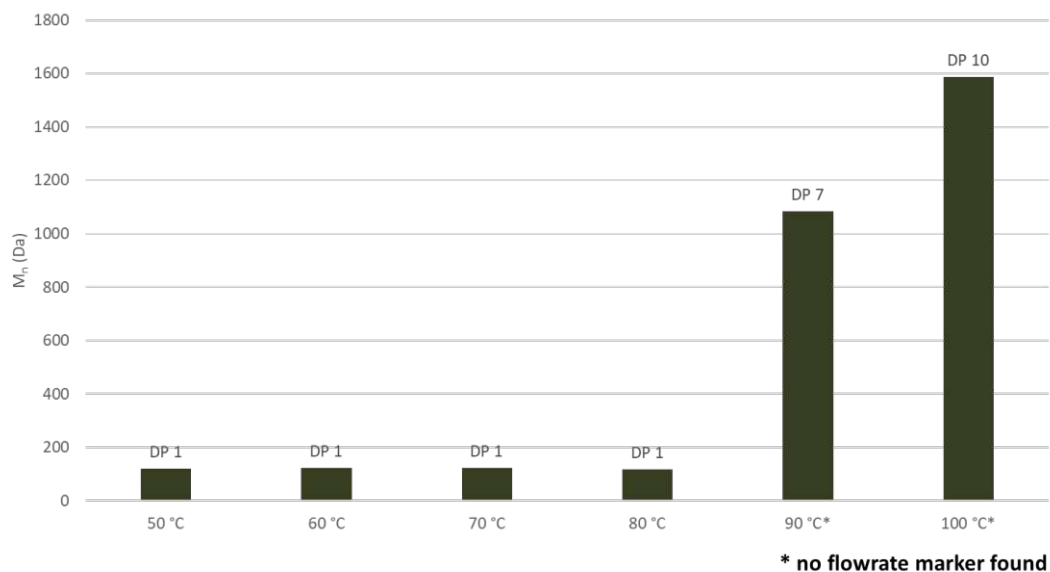
Figure 47. M_n and average degree of polymerization (DP) determined through SEC for samples containing PGE/MHHPA 1/1 (fg%/fg%) + 2.5 mol% WPBG 266 + 0.25 mol% ITX at different temperatures. Data summarized in Table S21.

Since temperature is such an important parameter and is also known to significantly influence the reaction time, another measurement series was conducted investigating the temperatures between 100 and 150 °C. This time, however, the better-suited PBG WPBG 300 was used instead of WPBG 266 (see chapter 2.1 PBG Screening). Samples containing PGE/MHHPA 1/1 (fg%/fg%) + 2.5 mol% WPBG 300 + 0.25 mol% ITX were cured in the photo-DSC at 100 °C by irradiating twice for 300 s with 91 ± 1 mW cm^{-2}, and the cured samples analyzed using qNMR measurements to determine the monomer conversion, and SEC measurements to determine the chain length of the produced polymers.

An increase of temperature from 100 to 120 °C leads to a significant jump in conversion, where nearly quantitative conversions are reached at temperatures ≥ 120 °C (Figure 48, Table S22), while the chain lengths of the produced polymers remain similar with a DP of 13-17 at temperatures above 120 °C (Table S23).
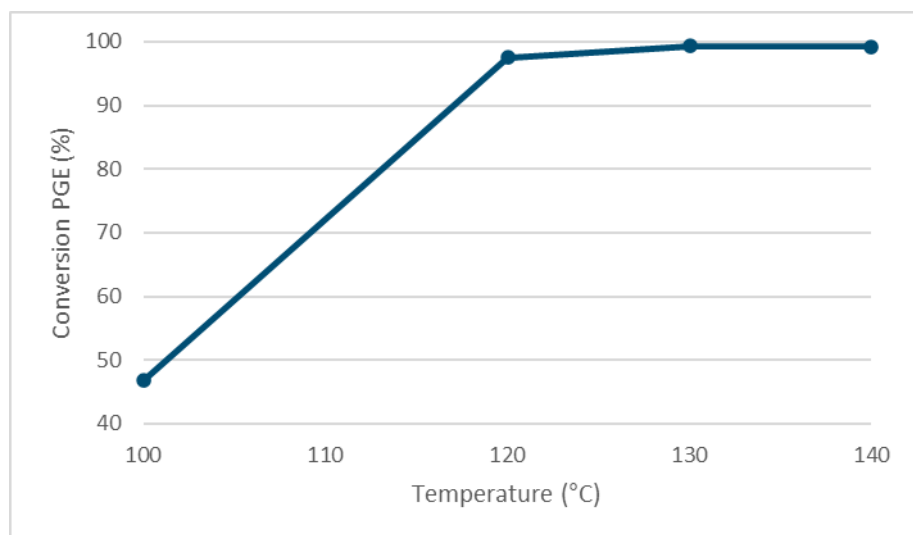
Figure 48. Conversion of PGE determined by qNMR after curing of samples containing PGE/MHHPA 1/1 (fg%/fg%) + 2.5 mol% WPBG 300 + 0.25 mol% ITX at different temperatures between 100 and 140 °C. Data summarized in Table S22.

At the same time, the control experiment using only epoxide gives no polymerization for 120 °C and only slight polymerization with a DP of 3-4 for 130 and 140 °C (Table S23). This indicates that no homopolymerization occurs. However, when looking at the ^{1}H-NMRs, the results are not as clear. qNMRs indicate conversions of PGE between 15 and 40% in the control experiments using only PGE as epoxide, which would point to some homopolymerization (Table S20).

Therefore, the NMRs of the copolymerization reaction were further investigated to determine the yield of copolymerization by comparing the integral of the newly found methine-H signal (-COOCH$_2$-C$\underline{H}$-) of the polyester to an unchanged integral of PGE. Indeed, these results seem to indicate worse copolymerization rates when using higher temperatures (Figure 49, Table S24). Therefore, a change in material properties has to be expected due to partial homopolymerization when increasing the temperatures above 100 °C.
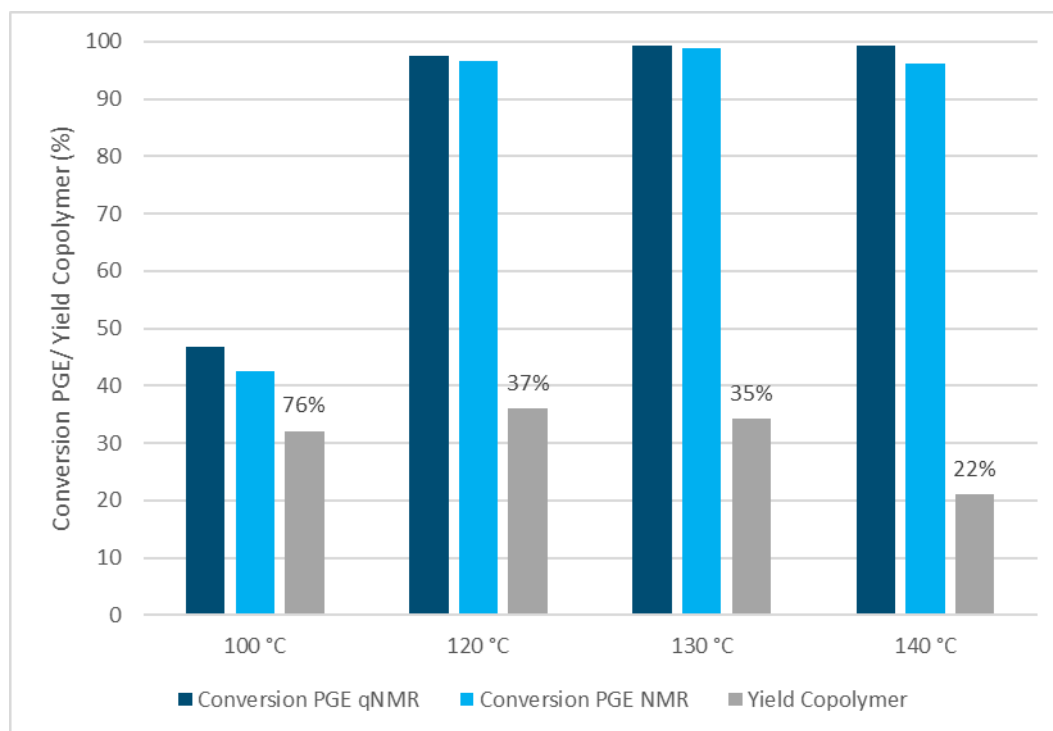
Figure 49. Comparison of conversion calculated from ¹H-NMR and qNMR for samples containing PGE/MHHPA 1/1 (fg%/fg%) + 2.5 mol% WPBG 300 + 0.25 mol% ITX at different temperatures between 100 and 140 °C. Selectivity of copolymerization reaction calculated from ¹H-NMR. Data summarized in Table S24.

2.4 Intensity Screening

The intensity of the LED used for irradiation can influence the polymerization, since it has an influence on the efficiency of the release of base from the PBG. Therefore, the intensity of the LED was varied and the effect on the conversion of monomers as well as on the chain length of the produced polymers was investigated.

Formulations contained PGE/MHHPA 1/1 (fg%/fg%) + 2.5 mol% WPBG 300 + 0.25 mol% ITX. Samples were cured using the photo-DSC at 100 °C by irradiating twice for 300 s with varying light intensities, and the cured samples were analyzed using qNMR measurements to determine the conversion of monomers, and SEC measurements to determine the chain length of the produced polymers.

Figure 50 (Table S25) shows that a higher intensity of the LED during irradiation leads to higher conversion. There seems to be a linear trend between intensity and monomer conversion, giving 24% more monomer conversion per intensity increase of 1 mW cm^{-1}.
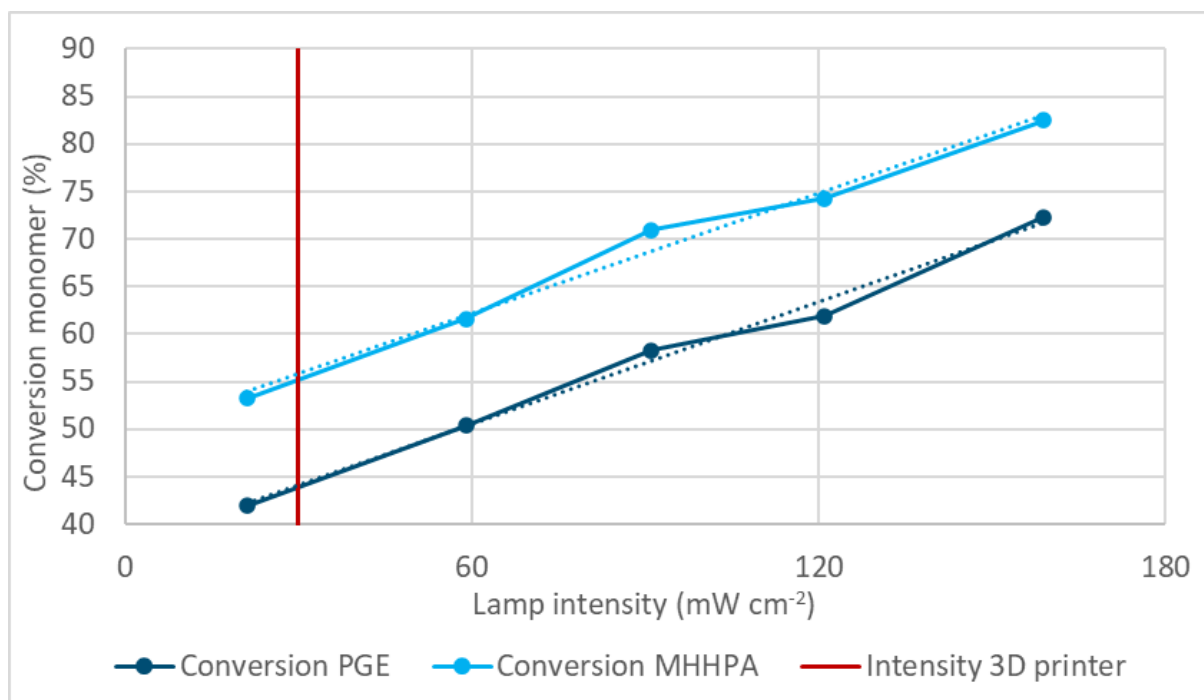
Figure 50. Conversion of PGE in correlation with LED intensity during irradiation. Red line marks the maximum available intensity on the sample surface for the 3D printer in question. Data summarized in Table S25.

Furthermore, SEC measurements show very similar chain lengths of the resulting polymers with a trend towards slightly higher molecular weights when using higher intensities (Figure 51, Table S26). However, these differences are very small and thus most likely within the margin of error.

* no flowrate marker found
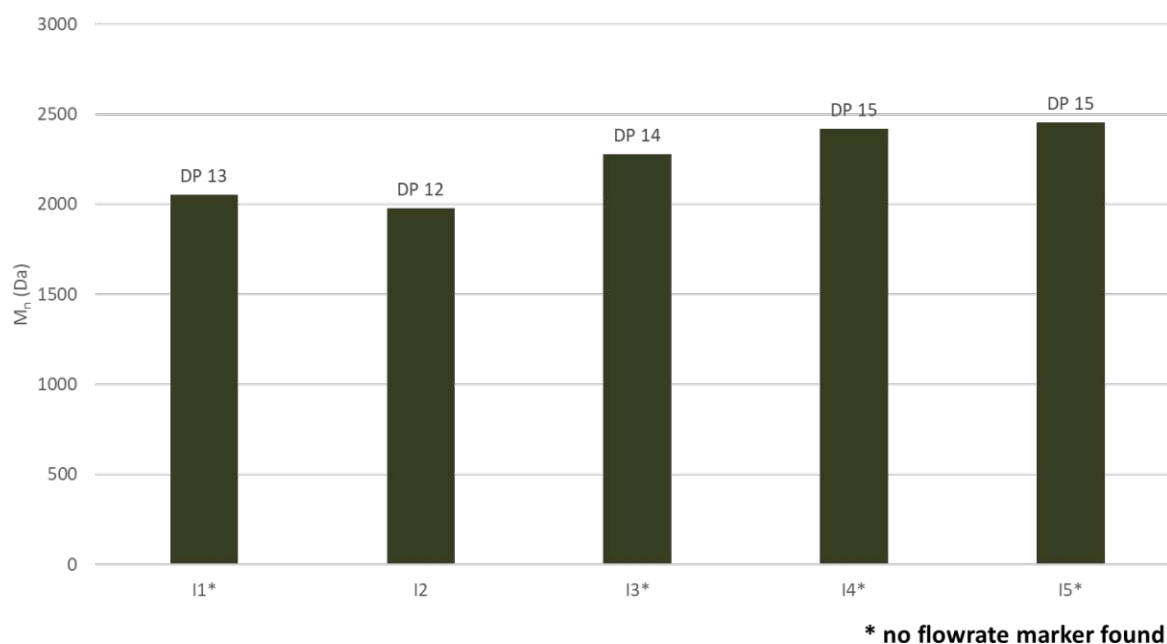
Figure 51. Highest M_n values and calculated average degree of polymerization (DP) determined by SEC measurements for different LED intensities. Data summarized in Table S26.

These results suggest that using the highest possible intensity is beneficial. However, other setups like the 3D printer might not able to provide such high intensities. Therefore, the process has to be adjusted to the instrument in question. In this case, the available 3D printer is only able to supply 30 mW cm^{-2} on the sample surface at maximum intensity, which corresponds to slightly below 45% conversion for the investigated model system. The experiments for the crosslinked system will have to focus on that intensity since it cannot be changed easily.

2.5 Anhydride Screening

A literature search revealed that even though there is a great number of multifunctional anhydrides available, none of those anhydrides have a melting point below 140 °C, which is the highest temperature possible for the 3D printing device that was used. Therefore, in order to obtain a liquid, homogenous formulation at the chosen temperature of 100 °C, no multifunctional anhydrides can be used.

Fortunately, several multifunctional epoxides with lower melting points are available, which can be copolymerized with one of the several possible monofunctional anhydrides. Therefore, screening monofunctional anhydrides is important since they will also be used in the crosslinked materials later, while it does not make sense for monofunctional epoxides since those will be replaced by multifunctional epoxides later in order to obtain crosslinked materials.

Three additional anhydrides besides MHHPA were chosen to determine if ring size and steric hindrance have an influence on the reactivity (Figure 52). Unfortunately, succinic anhydride, which would complete the anhydride series, has a melting point of 118-120 °C, and it was therefore impossible to get a homogenous formulation at 100 °C.
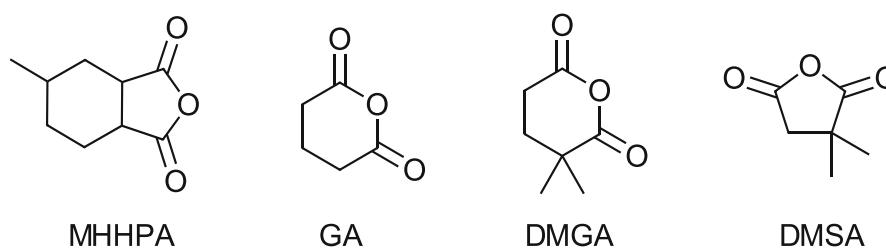
Figure 52. Anhydrides chosen for reactivity screening.

All monomers were analyzed using ^{1}H-NMR and, if the purity was not sufficient, purified beforehand. Since anhydrides are prone to hydrolyzation with moisture to the corresponding carboxylic acid, reverting this acid back to the anhydride was necessary in some cases.

All formulations contained PGE/anhydride 1/1 (fg%/fg%), 2.5 mol% WPBG 300 and 0.25 mol% ITX. Completely homogenous solutions were obtained at room temperature after using an ultrasonic bath

and a vortex mixer. The samples were then cured in the photo-DSC at 100 °C by irradiating twice for 300 s with 91 ± 1 mW cm^{-2}, and analyzed using qNMR and SEC measurements (Table 2, Table S27). In a few formulations, some sample signals overlapped with signals from CD$_3$CN in the quantitative ^{1}H-NMRs. However, for better comparability of the PGE signal in different formulations, the solvent was not changed.

Table 2. Monomer conversion, molecular weight of polymers (M_n) and average degree of polymerization (DP) using different anhydrides.

Anhydride	Conversion PGE (%)	M_n (Da)	DP
MHHPA	55	2290*	14
GA	23	1230	9
DMGA	19	1100	8
DMSA	21	1220	9

*no flowrate marker found

Ring size does not have a distinct impact on the reactivity since using either 2,2-dimethyl glutaric anhydride (DMGA) or 2,2-dimethyl succinic anhydride (DMSA) leads to similar results. Furthermore, the increased steric hindrance when introducing two methyl groups also resulted in very little change in reactivity, as seen when comparing DMGA to glutaric acid (GA). However, introducing a much larger group seems to be beneficial, since MHHPA shows both roughly twice as much conversion and twofold chain length. Therefore, this bulkier anhydride was chosen for all further experiments.

2.6 Summary

Taking into consideration all the experiments described above, the optimized linear model system consists of the monomers PGE and MHHPA in a ratio of 1/1 (fg%/fg%) with 2.5 mol% WPBG 300 and 0.25 mol% photosensitizer ITX. 2.5 mol% were chosen due to the high costs of PBG and high mass percentage in the produced polymers, even though using 5 mol% leads to better results.

This formulation should then be cured at 100 °C to enable the copolymerization reaction to happen, but at the same time avoid side reactions and economical and technical drawbacks at higher temperatures. Higher LED intensities are advantageous but not available at the 3D printer. Therefore, further experiments will utilize an irradiation intensity of 30 mW cm^{-2}, which is the highest possible intensity achievable on the 3D printer.

3 POST-CURING BEHAVIOR

Post-curing processes describe reactions that change a material after it has been cured. Since it was shown in the previous chapter that even after optimization of a linear model system, the conversion of monomers is not complete, post-curing might be ideal to achieve quantitative yields and thus influence the properties of the obtained materials.

In order to investigate if post-curing occurs, samples were cured using the optimized conditions determined in the last chapter (PGE/MHHPA 1/1 (fg%/fg%) + 2.5 mol% WPBG 300 + 0.25 mol% ITX, 100 °C, 2·5 min irradiation with 30 mW cm^{-2} intensity). After curing, one sample was quenched immediately, while the other samples were stored in the dark at room temperature (r.t.) and at 100 °C for 48 h before quenching and analyzing.

Table 3. Summary of qNMR and SEC results for analyzing the post-curing behavior at r.t. or 100 °C of the model system containing PGE/MHHPA 1/1 (fg%/fg%), 1 or 2.5 mol% WPBG 300 and 0.1 or 0.25 mol% ITX. No flowrate marker was found in all the SEC measurements.

Concentration PBG (mol%)	Time	PGE conversion (%)	M_n (Da)	DP
	immediate quench.	23	2070	13
1	48 h r.t.	45	2080	13
	48 h 100 °C	99	1790	11
	immediate quench.	58	2280	14
2.5	48 h r.t.	74	2320	15
	48 h 100 °C	99	2770	17

It is obvious that post curing processes occur, since the conversion of PGE increases (Table 3, Table S28). Apparently, post curing is slightly faster for systems in which more monomer is still available (1 mol% vs. 2.5 mol% PBG). Furthermore, temperature also benefits the post-curing processes, since quantitative conversions can be achieved when storing the samples at 100 °C for 48 h, while only a partial increase in conversion is seen at room temperature. However, this also shows that even though the reactivity at room temperature is reduced, it is still possible to post-cure at this temperature.

The SEC measurements show that the molecular weight does not change dramatically during the post-curing process, which confirms that the samples do not degrade (Table 3). There is even a slight tendency towards increased molecular weights, with the only exception of the formulation containing 1 mol% WPBG 300 that was stored at 100 °C for 48 h, which shows a slightly lower molecular weight

than before post-curing. It must be mentioned, however, that these differences are most likely within the margin of error.

Confirming that post-curing is possible is a great achievement, since only form-stable printed parts need to be obtained on the 3D printer that can be post-cured afterwards to achieve full conversion and reveal the full potential of the properties of those materials.

4 CROSSLINKED SYSTEMS

There are distinct differences between linear and crosslinked materials. In linear polymers, the monomers covalently bond to form a linear chain that is only linked to other chains through weaker forces such as Van der Waals forces. Therefore, those materials are classified as thermoplastics that can be molten and reshaped at higher temperatures. However, if covalent crosslinks are introduced, a material will remain in its original form after curing and will only soften slightly when heated. Those materials are called thermoset materials.[111] Increasing the crosslinking density of thermoset materials leads to high modulus, strength, hardness and chemical and heat resistance, while other properties such as elongation at break and toughness are reduced.[112]

4.1 Monomer Screening

In order to obtain crosslinked materials, multifunctional monomers are required. In this case, both the anhydride and the epoxide functional group are difunctional already since they react with two other functional groups each, thus forming linear polymers. However, for crosslinked materials, monomers with at least two functional groups have to be used. A literature search revealed that no molecules with more than one cyclic anhydride group and melting points below 140 °C are readily available. Since this is a prerequisite to obtain homogeneous, liquid formulations for the printing process, the crosslinks have to be introduced by using molecules with more than one epoxy group. Fortunately, there are several reported molecules with more than one epoxide group and low melting points. Some of those epoxides considered for this work are depicted in Figure 53. They include some very well-known commercial epoxides such as the ECC, as well as epoxides known for their good mechanical properties, for example PHTE, that are all liquid or have a melting point below 100 °C.
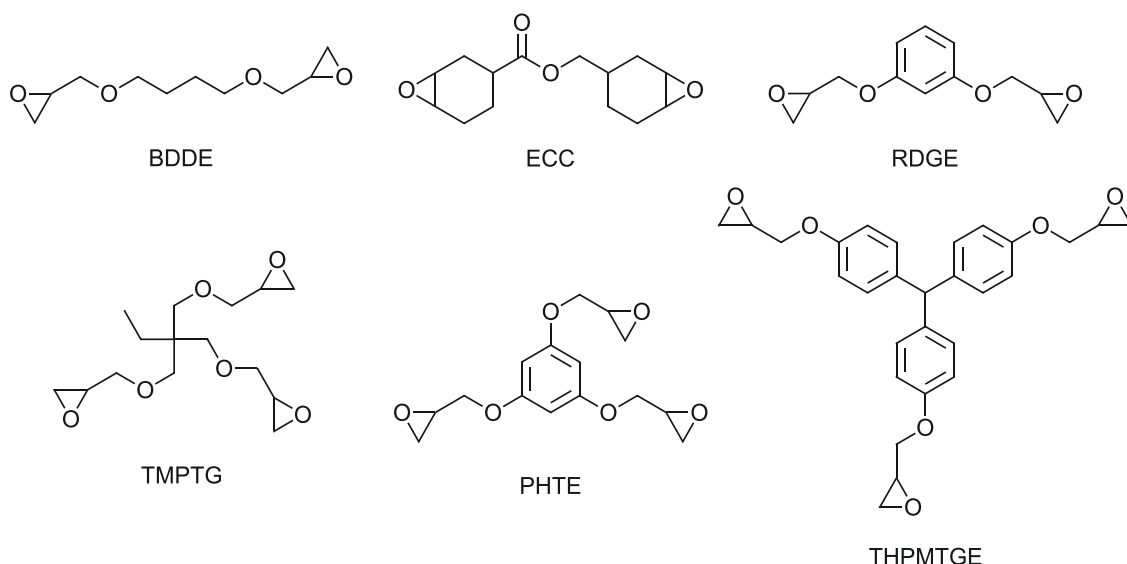
Figure 53. Multifunctional epoxides chosen as possible monomers for ROCOP with anhydrides to produce crosslinked polyesters.

Ideally, these monomers should be used in technical grade to avoid further purification steps and make the process more accessible for the industry. Even though ^{1}H-NMRs showed that the monomers are present, they also revealed impurities. HPLC and LC-MS measurements were performed to determine the purity, but unfortunately this analysis has proven quite complicated (results in Appendix - Monomer Screening for Crosslinked Systems). Therefore, since investigation and purification of the monomers is not a main goal of this thesis, no complete analysis of the monomers was performed.

Instead, the focus was put on only two monomers, ECC and THPMTGE. ECC was chosen as a representative with two epoxide groups that are highly strained and therefore should show good reactivity. Furthermore, it is also used regularly in industries. THPMTGE was chosen because it is commercially available and the technical monomer showed decent purity, and because it has three epoxide groups and should therefore give highly crosslinked materials. The technical THPMTGE was also purified using column chromatography to examine the effect of the impurities on the ROCOP.

4.2 Gelation Study

Since no exothermic behavior for neither linear nor crosslinked systems was observed when performing ROCOP between epoxides and anhydrides using photo-DSC, and SEC is not available for crosslinked structures, RT-FT-NIR photorheology was chosen as an alternative analysis method because it records both NIR data, which can be used to calculate the conversion, as well as rheological data for determining the time until gelation t_g. (Figure 54). This is an especially important characteristic since it shows how long it will take on the 3D printer to print one layer, and therefore how long the overall printing process will take.

60
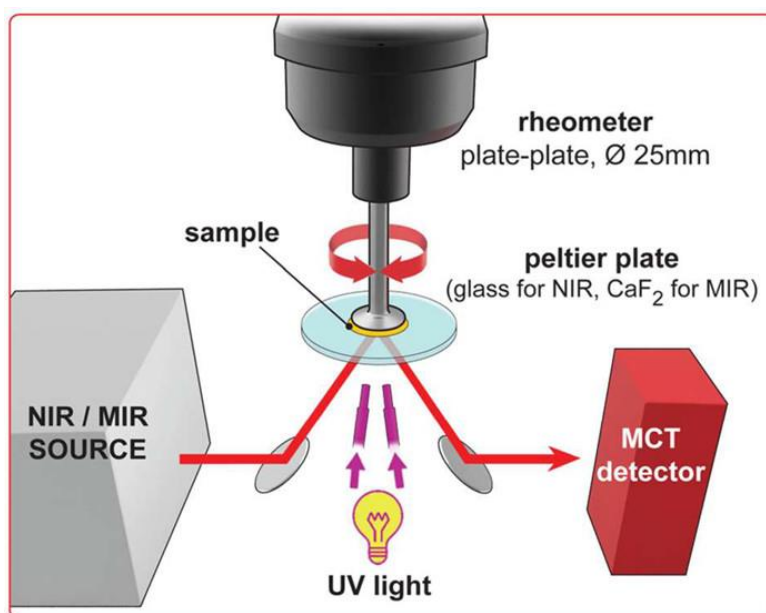
Figure 54. Schematic representation of RT-FT-NIR photorheology setup. Figure reproduced from ref[113] without changes. Copyright 2017 by ACS.

In order to allow for more comparability between the photo-DSC and the photorheology measurements, similar conditions were chosen. More specifically, the optimized conditions determined in chapter 2 were employed (epoxide/MHHPA 1/1 (fg%/fg%) + 2.5 mol% WPBG 300 + 0.25 mol% ITX, 100 °C, 2·5 min irradiation, 30 mW cm^{-2}).

Generally, all RT-FTIR-rheology measurements are performed using a PE tape to allow easy removal of the cured polymer sample, since some polymers tend to have high adhesion to the glass plate. It has been shown previously that a PE tape can be used without changing the results of the RT-FTIR-photorheology measurements.[113] Since normal PE-tapes are not applicable for temperatures over 80 °C because the glue starts to loosen at high temperatures, a special high-temperature PE tape was used for the measurements after tests showed that this tape was not changing the results as well (results in Appendix - Calibration of High-Temperature Polyethylene Tape for Photorheology).

First measurements revealed that a gap size of 50 nm was not sufficient because the sample thickness was too small for reproducible NIR data. Therefore, the gap size was increased to 200 nm, which resulted in thick enough samples for good absorption values and thus reproducible, evaluable NIR data.

This NIR data can be used to calculate the conversion by integrating a band peak of a monomer. In literature, terminal epoxides are reported to give signals at approximately 6060 cm^{-1} (first overtone of fundamental C-H stretching vibration) or 4532 cm^{-1} (combination of C-H stretching and CH$_2$ deformation fundamental).[114-116] Indeed, the signal at 4530 cm^{-1} has been used previously in

RT-FT-NIR-photorheology for determining the conversion when producing an epoxy resin,[117] and will therefore also be utilized for this system.

Another problem discovered during the first measurements was that 15 min is often not long enough for gelation to happen. Therefore, many measurements have to be conducted over the cause of one hour instead.

Lastly, it was discovered that the first measurement after turning on the photorheometer was always slightly faster. One possible explanation is that the tape is applied at lower temperatures for this first measurement compared to the measurement temperature. However, even when applying the tape only after heating up to measuring temperature, this discrepancy still prevailed. The problem is furthermore not connected to a specific formulation, but was observed in every measurement series. No meaningful explanation for this phenomenon has been found, so the first measurement was always excluded as an outlier.

After solving the initial problems that occurred when introducing RT-FT-NIR-photorheology as the new measurement system for crosslinked materials, THPMTGE and ECC were chosen as commercially available di- and trifunctional epoxies for further investigation.

As already mentioned before, the time until gelation (t_g) is an especially important parameter for the 3D printing process. It can be identified from rheology data as the crossover of storage and loss modulus, and amounts to 570 ± 60 s when using ECC as epoxide, and 1640 ± 30 s when using THPMTGE (Figure 55).
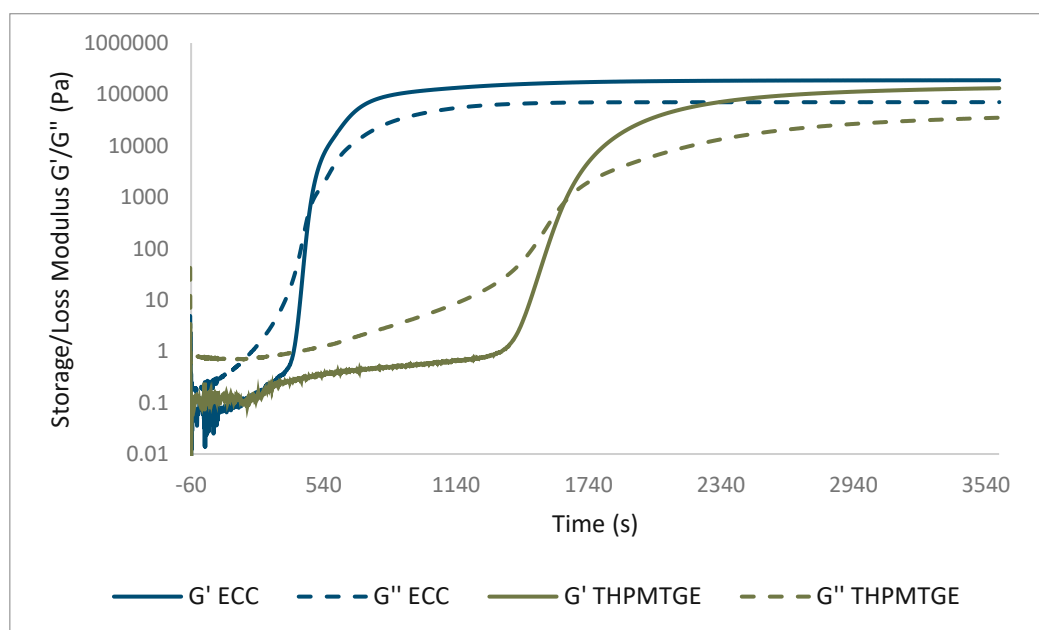
Figure 55. Comparison of storage modulus G' and loss modulus G'' of systems containing ECC or THPMTGE as epoxides (conditions: epoxide/MHHPA 1/1 (fg%/fg%) + 2.5 mol% WPBG300 + 0.25 mol% ITX, 100 °C, 30 mW cm^{-2}).

This has two very important implications: First of all, the two different epoxides differ enormously in reactivity. Even though ECC is only difunctional and thus results in a lower crosslinking density, it is much more reactive. One of the reasons for that is the additional ring strain of ECC due to the epoxide group being located on a hexyl ring, which results in higher thermodynamic driving force for ring-opening reactions.[118] The main reason, however, is that the THPMTGE contains glycidyl ether moieties. It has been reported in literature that those groups lead to lengthy induction periods in cationic polymerizations due to a metastable intramolecular hydrogen-bonded complex forming as intermediate. In this complex, the epoxide groups are stabilized through coordination of a proton in a supramolecular cage and thus much more unreactive (Figure 56).[118, 119] While the ring-opening copolymerization (ROCOP) is not a cationic polymerization, but instead catalyzed by a photobase generator (PBG), hydrogen bonding can still explain the reduced reactivity of THPMTGE.
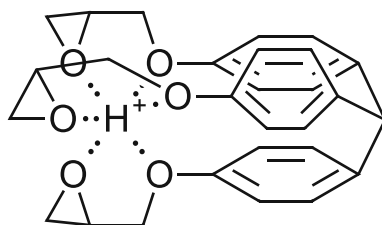
Figure 56. Proposed structure of metastable hydrogen-bonded complex formed by glycidyl ether groups of THPMTGE leading to reduced reactivity of this monomer.

Secondly, these t_gs also indicate a very slow system in general, which is problematic because the printing process would take extremely long. Even the significantly faster ECC system still takes around 10 min to harden. Therefore, several parameters, which had already been identified to be important in the optimization of the linear system, were investigated again in the new monomer system to improve the reactivity.

Influence of Temperature

It is known that temperature has a huge impact on the reaction rate – a rule of thumbs is that an increase in temperature of 10 °C leads to doubling of the reaction rate.[120] In the linear system, it was indeed shown that increasing the temperature led to higher monomer conversions, indicating higher reactivity. However, since it was also discovered that the system gets prone to unwanted homopolymerization when increasing the temperature towards 150 °C, the already used temperature of 100 °C was only increased by 20 °C to 120 °C to determine if the gelation time gets affected while still trying to avoid homopolymerization as best as possible.

Table 4. Influence of temperature on time until gelation (t_g), conversion at gel point (C_g) and final conversion (C_{final}) calculated from photorheology data. Formulations consisted of MHHPA/epoxide (techn. THPMTGE or techn. ECC) 1/1 (fg%/fg%) + 2.5 or 5 mol% WPBG 300 + 0.25 or 0.5 mol% ITX. Measurements were conducted at 100 or 120 °C using a broadband-Hg lamp (320-500 nm) with an intensity of 30 mW cm^{-2}.

Monomer	Temperature (°C)	PBG concentration (mol%)	t_g[a] (s)	C_g[b] (%)	C_{final}[c] (%)
THPMTGE	100	5	1050 ± 40	47 ± 6	69 ± 3
THPMTGE	120	5	500	59	88.6 ± 0.1
ECC	100	2.5	570 ± 60	100 ± 10	130 ± 4
ECC	120	2.5	350 ± 20	99 ± 1	123 ± 2
ECC	100	5	523 ± 7	72 ± 1	78 ± 1
ECC	120	5	299 ± 4	70 ± 1	77 ± 1

[a]time until gelation   [b]conversion at gel point   [c]final conversion

Indeed, increasing the temperature leads to distinct shortening of the t_g (Table 4). This is true using either of the multifunctional epoxides, and is also independent on the concentration of PBG used. However, the longer the t_g at 100 °C, the greater the reduction of this t_g with a temperature increase of 20 °C. For THPMTGE, the t_g gets halved, while the t_g of ECC is already way lower in general, and the temperature increase of 20 °C only results in reduction of a bit more than a third of the t_g.

The conversion of epoxide at the gel point C_g remains similar when changing the temperature, which was expected since the temperature change only affects how fast the monomers react with each other, and should not have a distinct influence on the produced polymers (Table 4). However, it is clear that THPMTGE with three epoxide groups has a lower C_g because of the higher crosslinking density than ECC with only two epoxide groups. Surprisingly, when using ECC as epoxide monomer, the final conversions C_{final} did also not change distinctly upon a temperature increase (Table 4). However, when using THPMTGE, the increase in temperature also resulted in a more complete reaction.

To sum up, the increase of temperature does indeed influence the t_g in a big way. However, since homopolymerization of epoxides also gets more likely, a temperature of 100 °C is still preferable, especially since it is also more economical to use lower temperatures in the 3D printing applications.

Influence of Irradiation Intensity

In the linear model system, it was shown that the irradiation intensity influences the reactivity of the ROCOP reaction since higher intensities lead to higher monomer conversions. While this influence might not be as pronounced as the influence of temperature, it is still a parameter worth considering. Unfortunately, limitations of the intensities of the currently available hot stereolithography devices strongly limit the possible intensity ranges. However, since these devices will surely be developed further in the future so that higher intensities become possible, an intensity increase from the currently highest possible intensity on the 3D printer, 30 mW cm^{-2}, to 40 mW cm^{-2} was investigated using the more reactive formulation containing ECC at 120 °C.

Table 5. Influence of irradiation intensity on time until gelation (t_g), conversion at gel point (C_g) and final conversion (C_{final}) calculated from photorheology data. Formulations consisted of MHHPA/ECC (techn.) 1/1 (fg%/fg%) + 5 mol% WPBG 300 + 0.5 mol% ITX. Measurements were conducted at 120 °C using a broadband-Hg lamp (320-500 nm) with an intensity of 30 mW cm^{-2} or 40 mW cm^{-2}.

Irradiation intensity (mW cm^{-2})	t_g[a] (s)	C_g[b] (%)	C_{final}[c] (%)
30	299 ± 4	70 ± 1	77 ± 1
40	267 ± 15	72 ± 4	77 ± 3

[a]time until gelation   [b]conversion at gel point   [c]final conversion

As expected, using higher intensities does indeed result in a reduced t_g (Table 5). However, the increase from 30 to 40 mW cm^{-2} only resulted in a relatively small reduction of around one-tenth of the t_g (30 s). As seen and discussed for temperature already, the C_g and C_{final} also barely change when changing the intensity (Table 5). Therefore, using other parameters to influence the reactivity seems to be a more promising approach.

Influence of PBG concentration

Changing the PBG concentration is another parameter that can be used to influence the reactivity of the system. As discovered in the linear model system, an increase of PBG concentration leads to higher monomer conversions which indicates higher reactivity. Therefore, the PBG concentration was increased from 2.5 to 5 mol%, and the effects were investigated using both THPMTGE and ECC as epoxide monomers.

Table 6. Influence of PBG concentration on time until gelation (t_g), conversion at gel point (C_g) and final conversion (C_{final}) calculated from photorheology data. Formulations consisted of MHHPA/epoxide (techn. THPMTGE or techn. ECC) 1/1 (fg%/fg%) + 2.5 or 5 mol% WPBG 300 + 0.25 or 0.5 mol% ITX. Measurements were conducted at 100 or 120 °C using a broadband-Hg lamp (320-500 nm) with an intensity of 30 mW cm^{-2}.

Monomer	Temperature (°C)	PBG concentration (mol%)	t_g[a] (s)	C_g[b] (%)	C_{final}[c] (%)
THPMTGE	100	2.5	1640 ± 30	42 ± 6	56 ± 4
THPMTGE	100	5	1050 ± 40	47 ± 6	69 ± 3
ECC	100	2.5	570 ± 60	100 ± 10	130 ± 4
ECC	100	5	523 ± 7	72 ± 1	78 ± 1
ECC	120	2.5	350 ± 20	99 ± 1	123 ± 2
ECC	120	5	299 ± 4	70 ± 1	77 ± 1

[a]time until gelation   [b]conversion at gel point   [c]final conversion

As expected, doubling the PBG concentration resulted in reduced t_gs (Table 6). Especially for THPMTGE, the t_g was reduced by a third from 1640 to 1050 s. For ECC, the effect was less pronounced but still clearly visible, with t_g reductions of a seventh to a tenth. Unfortunately, as discussed for the linear model system, increasing the PBG concentration is not the best way to improve the gelation time since it is a rather expensive component and remains in the polymer, thus possibly changing the material properties.

Influence of Monomer Purity

Finally, the effect of purity of the monomers was also investigated. This is important since using technical monomers is highly advantageous for the industry in order to avoid expensive purification steps, but might result in different polymerization behavior due to the impurities.

Therefore, THPMTGE was used in technical grade as well as in its purified form after column chromatography. Furthermore, since HPLC measurements suggested a purity of the technical monomer of 85%, the technical monomer was used in two different concentrations: One time, a purity of 85% was assumed, while a purity of 100% was assumed for the second measurement. Measurements were performed at 100 °C with an irradiation intensity of 30 mW cm^{-2}.

Table 7. Influence of monomer purity on time until gelation (t_g), conversion at gel point (C_g) and final conversion (C_{final}) calculated from photorheology data. Formulations consisted of MHHPA/THPMTGE (techn. 85% or 100%, purified) 1/1 (fg%/fg%) + 2.5 WPBG 300 + 0.25 ITX. Measurements were conducted at 100 using a broadband-Hg lamp (320-500 nm) with an intensity of 30 mW cm^{-2}.

Monomer	t_g[a] (s)	C_g[b] (%)	C_{final}[c] (%)
THPMTGE techn. 85%	1710 ± 20	49 ± 2	61 ± 1
THPMTGE techn. 100%	1640 ± 30	42 ± 6	56 ± 4
THPMTGE purified	1740 ± 30	42 ± 2	58 ± 1

[a]time until gelation [b]conversion at gel point [c]final conversion

Interestingly, while the effect of the purity of THPMTGE was not very pronounced, it is still clearly visible that the t_g improved when using technical THPMTGE compared to the purified THPMTGE (Table 7). This could be explained by the nature of the impurities being already dimerized or oligomerized monomers. Therefore, during polymerization, these oligomers lead to higher crosslinking density at lower conversion and thus faster gelation. Furthermore, using the technical THPMTGE with an assumed purity of 100% works better than using it with an assumed purity of 85%. This shows that an increase of epoxides in the formulation is disadvantageous for the t_g, which is surprising since the ring-opening and addition of epoxides to the propagating polymer chain is described as the rate-determining step in literature.[20]

However, when looking at the final conversion of monomers, while the differences are not huge, it still seems like using THPMTGE with an assumed purity of 100% leads to less conversion than using THPMTGE with an assumed purity of 85%. This might be because the ratio of epoxide and anhydride groups is not perfect when assuming 100% purity in a technical monomer.

To sum up, using technical THPMTGE does not result in problems regarding the reactivity of the system and is therefore highly advantageous since tedious purification steps can be avoided.

In conclusion, increasing the temperature, irradiation intensity and PBG concentration leads to reduced gelation times. However, changing the temperature is the easiest approach and also causes the most prominent effect. Furthermore, it was shown that technical monomers can be employed without negative effects on the polymerization process.

5 MATERIAL CHARACTERIZATION AND PROCESSING

5.1 Thermomechanical Properties

The glass transition temperature T_g is an important material property. It describes the reversible transition of a hard, brittle "glassy" material into a viscous rubber state.[111] The T_g can be determined by dynamic mechanical thermal analysis (DMTA) measurements, where the sample is slowly heated from -100 °C to 200 °C while being subjected to torsion strain. The storage modulus G' and the loss modulus G'' are recorded and can be used to determine the loss factor tanδ = G'/G''. The T_g was defined as the temperature at the maximum of the loss factor curve.

Polyester test specimens were cured in a hot-mold setup using 100 °C and 10 min irradiation with 365 nm and 290 mW cm^{-2}, yielding slightly yellow samples. The formulation contained ECC/MHHPA 1/1 (fg%/fg%) + 2.5 mol% WPBG300 + 0.25 mol% ITX.

As reference, a formulation containing only ECC with 1 wt% Irgacure 290 was used to produce pure polyether materials. However, this system is much more reactive. Brown, inhomogeneous samples with bubbles were obtained when using the hot mold setup, which probably indicates a frontal polymerization mechanism that occurs if temperatures get too high (Figure 57a). Therefore, instead of hot molding, a UV/Vis oven was used to cure the samples. Even then, obtaining the yellow, more flexible test specimens was not always possible since the conditions in the oven were fluctuating a lot and it was therefore very hard to control the curing behavior (Figure 57b).

Test specimens were measured immediately without post-curing, or after post-curing at 100 °C for 48 h. During post-curing, the polyether samples turned from yellow to brown (Figure 57c).
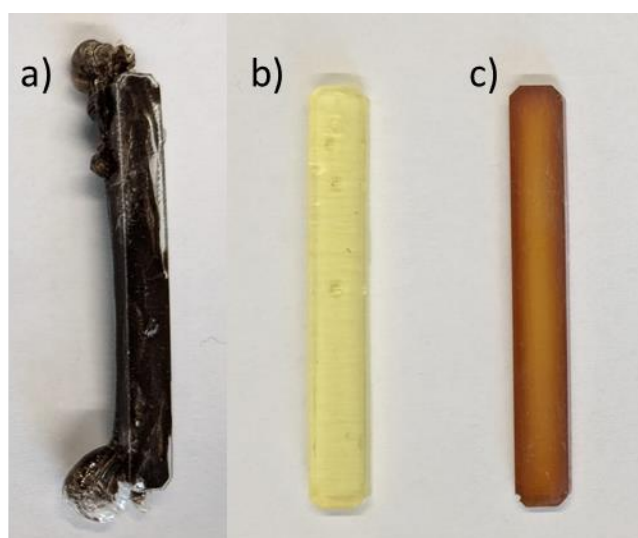
Figure 57. Reference samples of pure ECC polyether. a) Brown, inhomogeneous test specimen with bubbles obtained when curing in the hot mold. b) Yellow test specimen obtained after curing in the UV/Vis oven. c) Brown test specimen after post-curing at 100 °C for 48 h.

DMTA measurements were performed in torsion mode from -100 to 200 °C. The recorded storage modulus G' and the loss factor tanδ are depicted in Figure 58.

It is clearly visible that the polyester has a higher T_g of approximately 187 °C compared to the pure polyether system (Table 8). Furthermore, the tanδ forms a rather sharp peak. When comparing the polyester before and after post-curing, the T_g stays the same, but there is a slight shoulder in the tanδ curve of the sample that was not post-cured. This indicates that some processes still occur at higher temperatures during the measurement if no post-curing was applied beforehand. It also has to be noted that the samples changed color during the measurement from a light yellow to a dark yellow/orange, which is probably due to degradation processes of the PBG.

The reference polyether system containing only ECC shows a lower T_g of 172 °C. Interestingly, while the T_g did not change much with post-curing for the polyester system, there is a distinct difference in the polyether samples without and with post-curing. Before post-curing, there are clearly two different T_gs at 58 and 169 °C, and the test specimen undergoes a color change from yellow to brown during the measurement. This indicates major changes during the measurement, since the post-cured sample only shows the higher T_g of 172 °C.
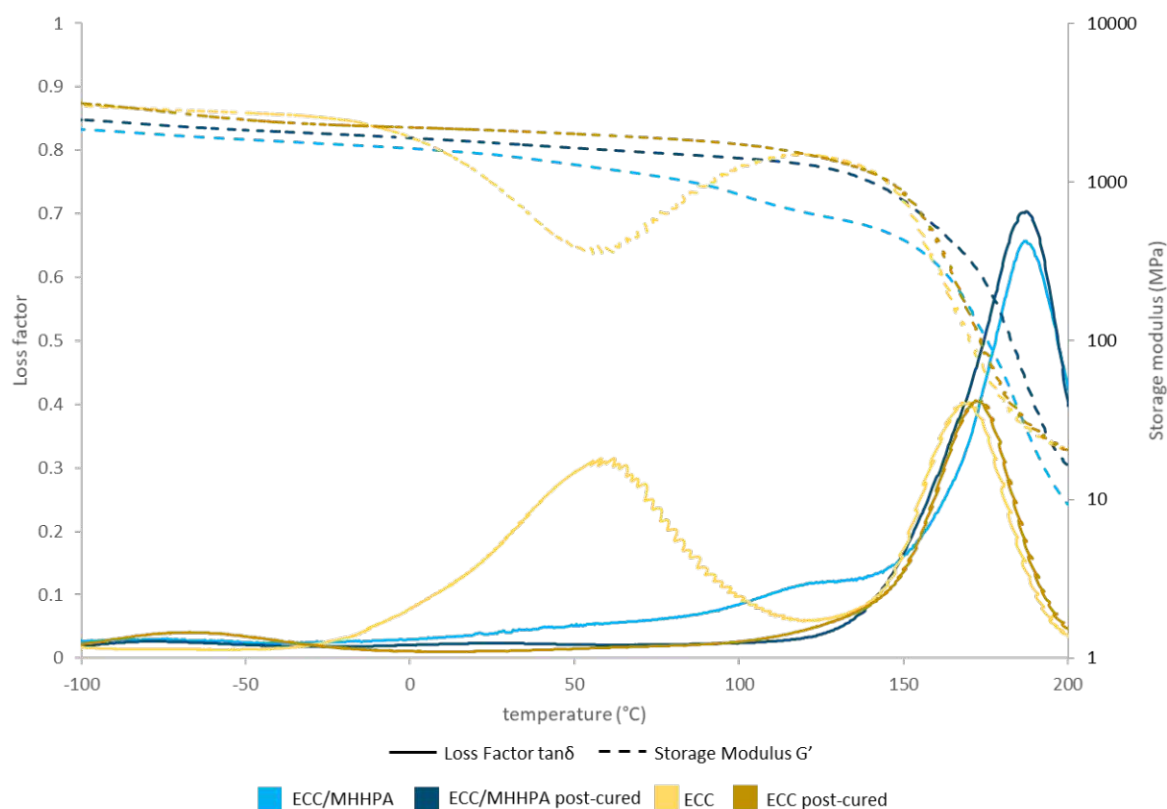
Figure 58. Storage modulus G' and loss factor tanδ over temperature for ECC/MHHPA polyester and reference ECC polyether system without and with post-curing.

69

Besides DMTA measurements, tensile tests can be performed to investigate the mechanical performance in general and tensile toughness of a material specifically. For this, test specimens are subjected to slow uniaxial deformation until the material fails. Thermosets are usually defined by a high modulus but also by high brittleness (Figure 59).[121]
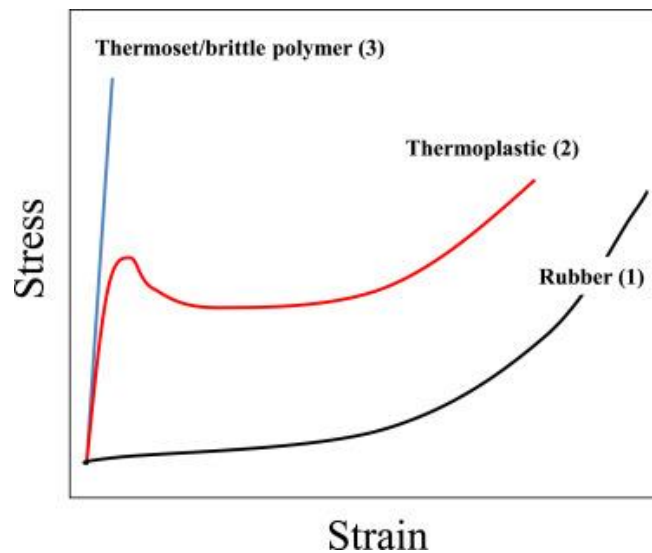
Figure 59. Schematic presentation of typical stress-strain behavior of different polymers. Figure reproduced from ref[121] without changes. Copyright 2022 by Elsevier Ltd.

Test specimens were cured as described before for the DMTA measurements, using the hot-mold setup at 100 °C for the ECC/MHHPA polyester samples, and the UV/Vis oven for the reference ECC polyether samples.

Both the polyester and the polyether showed properties typical for thermosets (Figure 60, Table 8). The post-cured polyester material has a high modulus of 62 ± 2 MPa, but low strain of only 3.8 ± 0.5%, while the post-cured polyether reached even slightly higher values of 80 ± 23 MPa stress and 4.5 ± 1.6% strain. However, the polyether material shows a high variation of properties in different samples, indicating low reproducibility. This might be attributed to the easily varying curing behavior depending on the curing conditions that was discovered for this system.

Furthermore, it is very interesting that unlike in the DMTA measurements, the properties of the polyester vary distinctly if post-curing is applied or not. The polyester exhibits much worse properties of only 17 ± 6 MPa stress and 0.9 ± 0.3% strain when not post-cured, showing that post-curing is indeed an important step to obtaining the full potential of the materials. However, it is also interesting to note that the slope, which corresponds to the stiffness of the material, is similar for the polyester with and without post-curing, which indicates that the crosslinking density is already quite high even without post-curing.
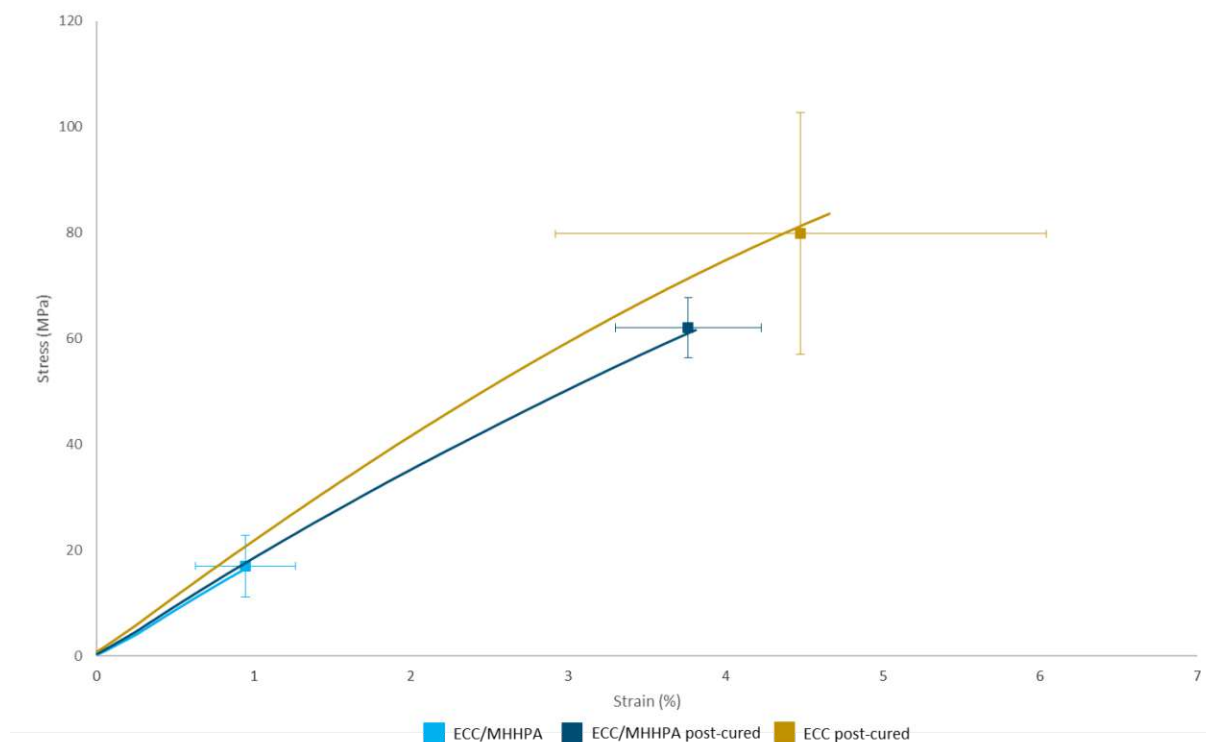
Figure 60. Strain-stress behavior of ECC/MHHPA and reference ECC materials without and with post-curing.

To sum up, the obtained materials show typical properties of thermosets: materials of high strength and with a high T_g, but also high brittleness were obtained after post-curing (Table 8). The stress-strain behavior was quite similar, with the polyether slightly outperforming the polyester. However, the polyester curing was much easier and more reproducible than the polyether curing, and the obtained polyester had a higher T_g.

Table 8. Summary of T_g, stress and strain of ECC/MHHPA and reference ECC materials determined using DMTA measurements and tensile tests.

sample	T_g (°C)	Stress (MPa)	Strain (%)
ECC/MHHPA	187	17 ± 6	0.9 ± 0.3
ECC/MHHPA post-cured	187	62 ± 2	3.8 ± 0.5
ECC	58 & 169	/	/
ECC post-cured	172	80 ± 23	4.5 ± 1.6

5.2 3D Printing

Finally, the developed system was evaluated for its suitability to print. A 3D printer with a top-down DLP setup was utilized to print the developed material. The most reactive formulation ECC/MHHPA 1/1 (fg%/fg%) + 2.5 mol% WPBG300 + 0.25 mol% ITX was chosen for the printing experiments. A

71

wavelength of 385 nm was used for irradiation. Temperatures between 70-120 °C were used, and the intensity was varied between 35-75 mW cm^{-2} (entered on the printer, intensity on the sample is far less).

First irradiation tests revealed that the system hardens much faster than expected from photorheology results. At 100 °C, the formulation was already cured completely after 120 s, while it took 570 s on the photorheometer. This could have several explanations: While the temperature can be modified on the photorheometer, the actual temperature on the sample might be lower due to the sensor being located outside the measurement spot. Another possible explanation could be that during photorheology measurements, frictions are caused due to the oscillation of the stamp and hinder the gelation process.

Since the hardening worked really well, the next step was to try and print a chip designed to test the resolution of the printing process (Figure 61). However, during the printing process, not only the irradiated parts of the sample hardened, but the entire formulation polymerized. Even though the first few layers were printed correctly and stuck to the building platform, somewhere during the printing process everything else hardened as well, making the printing of further layers impossible. This effect could be reduced by reducing the temperature and intensity as well as irradiation time during the printing process. However, even at the optimized conditions using 70 °C, 45 mW cm^{-2} and 45 s irradiation per layer, the formulation on the bottom of the vat still polymerized over the whole area even in the dark parts, but at least the formulation further up was still liquid.

Figure 61. Layout of the chip used as model for 3D printing.

There are three possible explanations for this overpolymerization. First of all, this could be a general stability problem of the formulation. Even though the stability of the linear system did not suggest such behavior, the stability of this new formulation was tested at both 70 and 100 °C analogously to the method described in chapter 1.4. Indeed, introducing multifunctional epoxides distinctly reduces the stability of the formulation (Figure 62). While the formulation remains stable for at least one hour at 70 °C, the same is unfortunately not true when using 100 °C. However, even at 100 °C, the formulation was still liquid after one hour. Therefore, this cannot explain the complete hardening of formulation after just 30 min of printing.
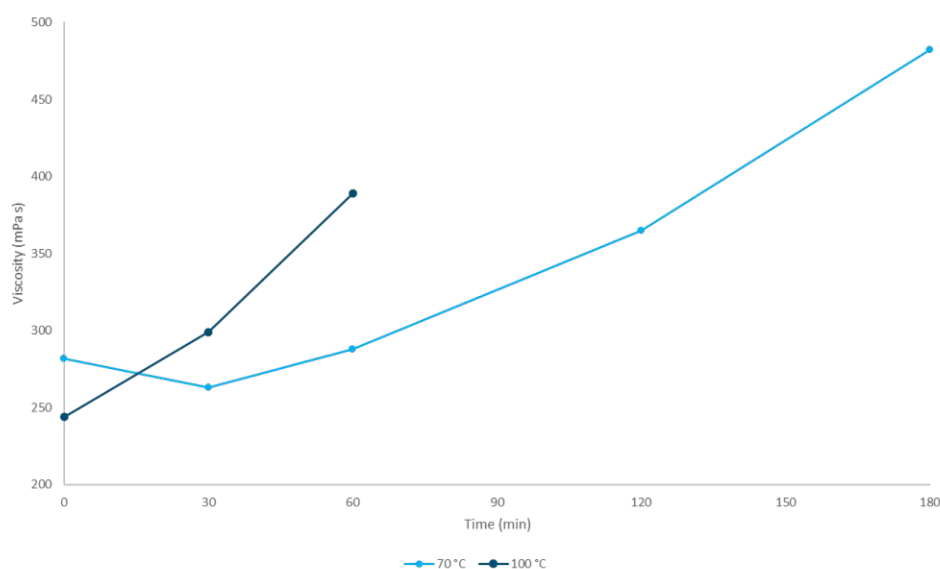
Figure 62. Stability of formulation containing ECC/MHHPA 1/1 (fg%/fg%) + 2.5 mol% WPBG300 + 0.25 mol% ITX at 70 and 100 °C determined by rheology measurements.

A second possibility is overpolymerization due to diffusion of the base, which is the active catalyst, in not-irradiated regions (Figure 63). This process is well-known for cationic photopolymerizations, since the small proton can relatively easily diffuse through the formulation. However, such behavior is much more unlikely for photobase-utilizing photopolymerizations since the active base is much larger than a proton and therefore cannot diffuse that easily. Indeed, this overpolymerization was not observed in PBG-catalyzed photopolymerizations before. However, since this reaction is still rather new, this possibility cannot be ruled out entirely.

In cationic photopolymerization, diffusion-based overpolymerization can be suppressed by adding small amounts of base to the formulation. This results in the quenching of protons in the unexposed areas, while only a slight reduction of reactivity is caused in the irradiated areas. Therefore, applying the same method by adding an acid could possibly help to reduce the undesired effect in PBG-catalyzed systems. Since it was shown before that strong acids can be used to catalyze both the copolymerization of epoxides and anhydrides and the homopolymerization of epoxides, only weak

acids can be utilized. Ketoprofen has a pK$_a$ value of 4.4[122] and is thus considered a weak acid. Furthermore, if it gets exposed to light, decarboxylation takes place, which deactivates the acidic behavior of ketoprofen in the irradiated parts. Therefore, adding ketoprofen should not reduce the reactivity in the irradiated parts because it gets destroyed there, but should be able to quench any bases that might diffuse outside of the irradiation area (Figure 63).
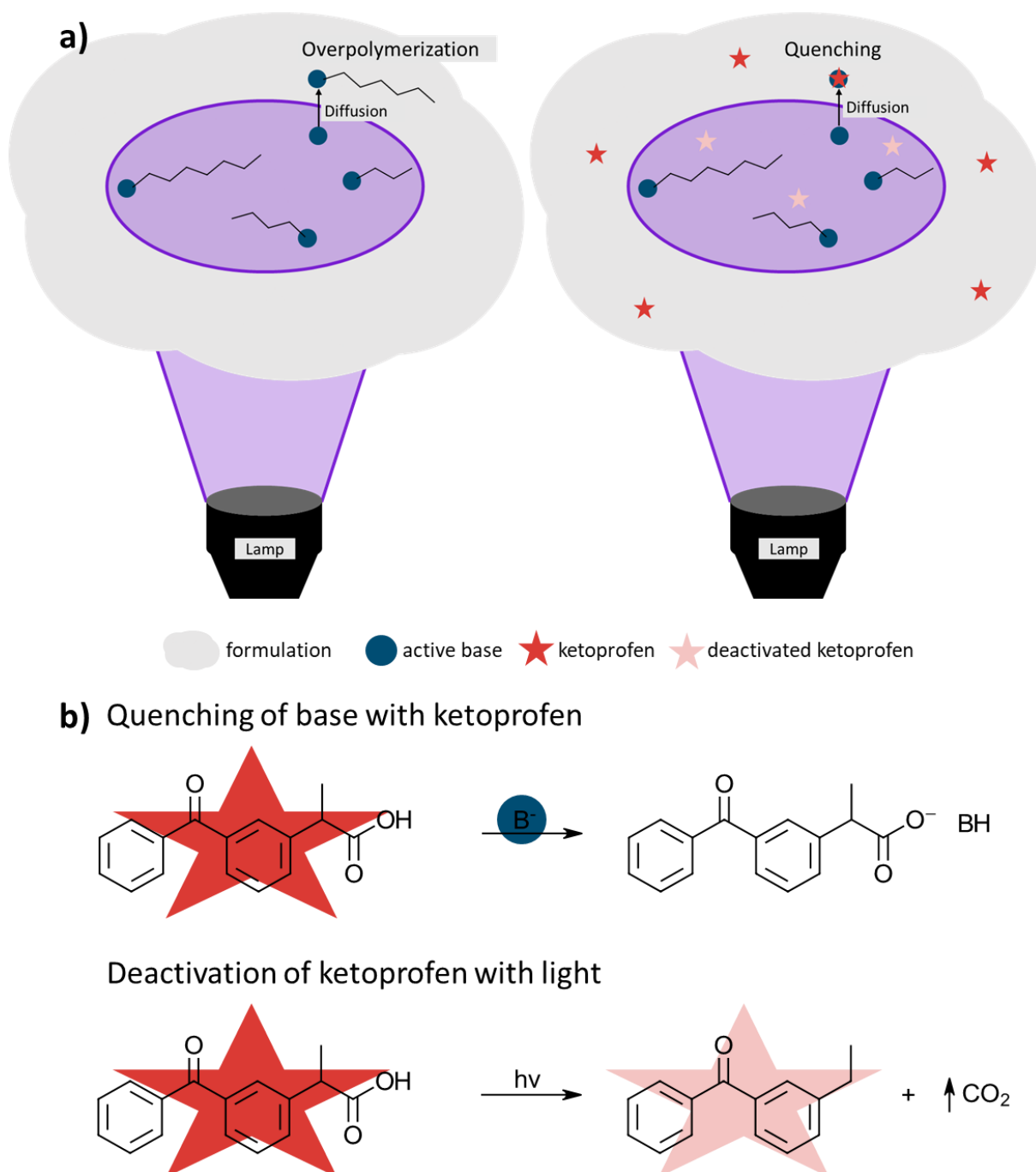
Figure 63. a) Concept of diffusion-based overpolymerization (left) and how to suppress it in PBG-catalyzed polymerization reactions using ketoprofen (right). b) Reactions of ketoprofen with base and light.

To further investigate if the effect observed can indeed be explained by the concept of diffusion-based overpolymerization, a special setup was developed to investigate the overpolymerization behavior. A silicon form with defined channels was affixed to the 3D printer (Figure 64), and the printer was programmed so that only half of the silicon form would be irradiated. After marking the separation line, the channels were filled with formulations containing different amounts of ketoprofen (0, 0.25, 0.5 and 2.5 mol%).
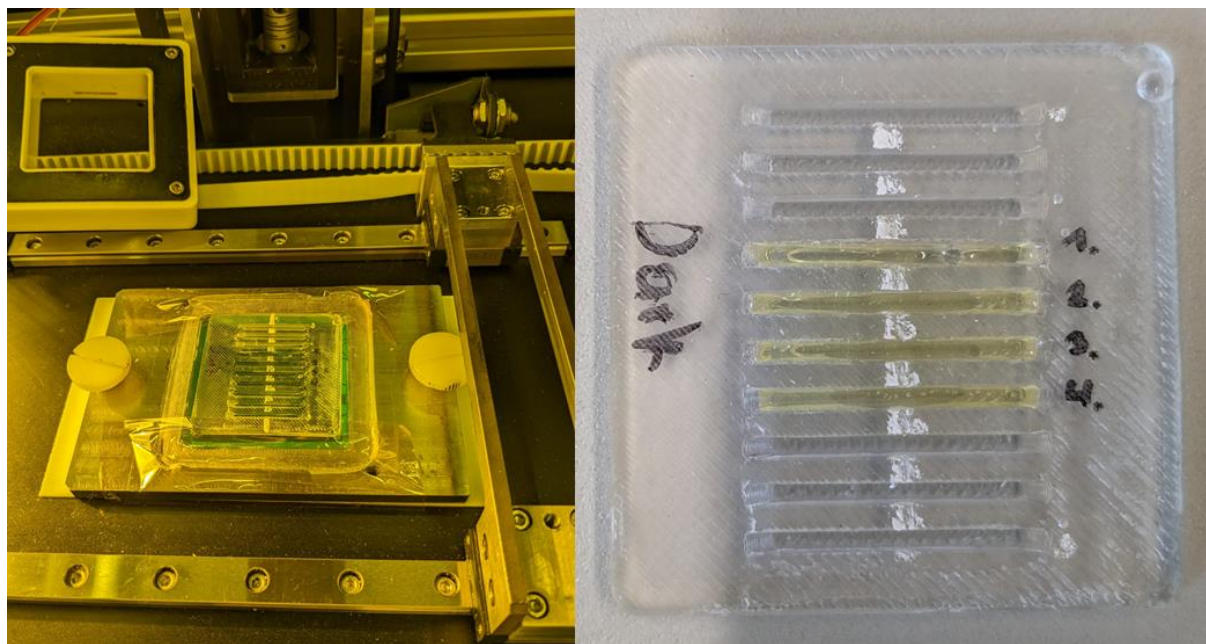
Figure 64. Setup for investigating the overpolymerization of formulations on the 3D printer.

After ten irradiation cycles, only the irradiated areas were polymerized, and no overpolymerization was visible in any of the channels. However, after irradiating for 50 cycles, all of the formulation was again polymerized. This shows that diffusion of the PBG does not cause the overpolymerization, since this would already result in some overpolymerization after ten irradiation cycles. Furthermore, there were no differences observed when adding ketoprofen, and usually this kind of overpolymerization only results in a few mm of additionally hardened sample and not complete polymerization of all the formulation.

Therefore, the last possibility is that some light gets to the dark areas. Since DLP is used, it is possible that some light shines even through the closed mirrors and causes this polymerization. Therefore, using a laser might solve this problem.

5.3 Degradation Behavior

The produced materials are polyesters and as such should be degradable. Therefore, preliminary tests were conducted using the very thin samples obtained from RT-FT-NIR-photorheology measurements of formulations containing THPMTGE/MHHPA 1/1 (fg%/fg%). The samples were put into vials containing three different alkaline solutions (1 M aqueous NaOH solution, 1 M methanolic KOH solution, 0.2 M methanolic KOtBu) and then stirred at room temperature.

The samples in the 1M alkaline solutions were fully dissolved after just 24 h indicating that ROCOP into degradable polyester prevailed over homopolymerization into nondegradable polyether. However, while the methanolic solution led to a homogenous solution, the degradation products were not soluble in water. The samples in 0.2 M KOtBu methanolic solutions degraded much slower.

With this information in hand, a degradation study with thicker samples containing post-cured ECC/MHHPA was prepared. The samples were put into 1 M NaOH and pure water and stored at room temperature. The pH was monitored, and swelling as well as dry weight were determined after certain time spans.

The degradation happened surprisingly slowly (Figure 65). Within the first three weeks, no change was observed at all, therefore the temperature was increased to 80 °C to accelerate the degradation. This indeed resulted in some degradation of the samples stored in 1M NaOH over the next few weeks, which was also clearly visible since the degradation products are not soluble in water and thus a white suspension was formed. However, within seven weeks, under 4% degradation was achieved for the samples stored in alkaline solution, and the aqueous solution did not show any degradation yet.
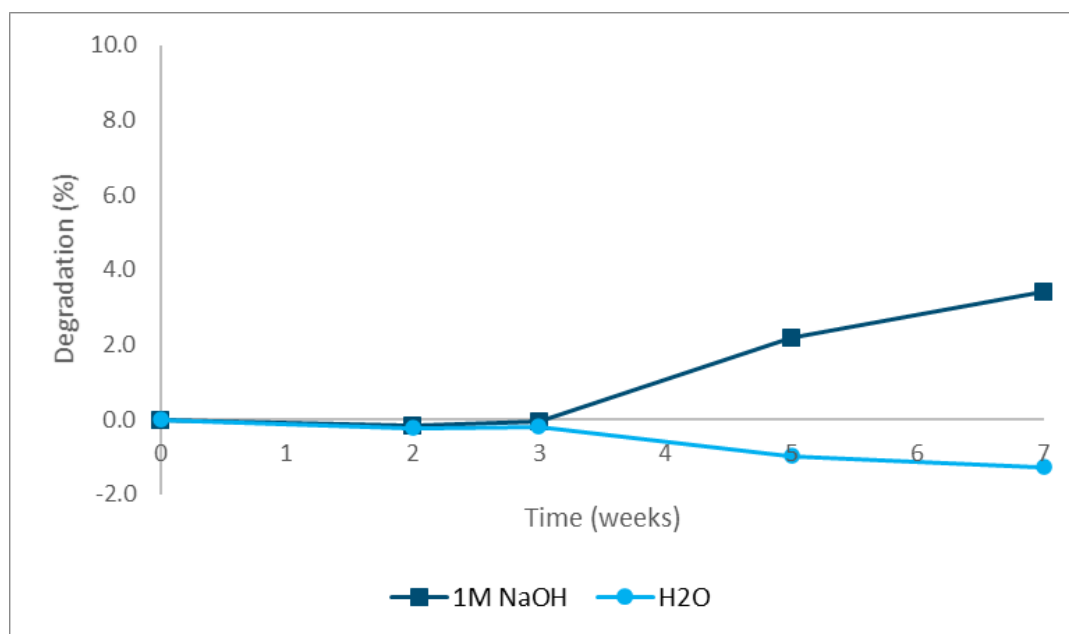
Figure 65. Degradation of post-cured ECC/MHHPA samples in 1M NaOH and water.

This much slower degradation compared to the preliminary study can have several possible explanations. First of all, the samples were much thicker, exposing less surface for the solvent to attack. Secondly, the samples were post-cured, which results in more thoroughly crosslinked materials. And finally, the monomer was also changed from THPMTGE to ECC, which can strongly influence the degradation behavior.

While this study revealed only slow degradation of the produced polyesters, full degradation should still be possible when given enough time.

MATERIALS AND METHODS

1 MATERIALS

All not synthesized chemicals were purchased from respective suppliers and used as received unless otherwise noted. Solvents and reagents were purchased in a quality common for organic synthesis and purified according to common organic procedures if necessary. Commercial grade tetrahydrofuran (THF, Donau Chemie) was dried with a PureSolvsystem (Inert, Amesbury, MA).

chemical	supplier
1,1,1-Trimethylolpropane triglycidyl ether	Sigma Aldrich
1,3-dicyclohexylurea	BLD pharm
1,4-Butanediol diglycidyl ether	Bodo Möller Chemie
2,2-Dimethyl glutaric anhydride	Sigma Aldrich
2,2-Dimethyl succinic anhydride	BLD pharm
3,4-Epoxycyclohexylmethyl 3,4-epoxycyclohexanecarboxylate	Bodo Möller Chemie
4-Methyl-1,2-cyclohexanedicarboxylic anhydride	TCI
Acetic acid anhydride	Alfa Aesar
Acetonitrile	VWR Chemicals
Acetonitrile-d_3	Eurisotop
BP2T	Synthesized by Klaus Ableidinger
Butylhydroxytoluol	Sigma Aldrich
Chloroform-d_3	Eurisotop
Ethyl acetate	Sigma Aldrich
Ethylene carbonate	TCI
Glutaric anhydride	Sigma Aldrich
Isopropylthioxanthone	Lambson
Irgacure 290	BASF
Ketoprofen	TCI
KP2T	Synthesized by Klaus Ableidinger
PDBN	Synthesized by Klaus Ableidinger
Petrol ether	Sigma Aldrich
Phenylglycidylether	TCI
Phloroglucinol triepoxide	Synthesized by Antonella Fantoni

Pyridine	Sigma Aldrich
Resorcinol diglycidyl ether	NAGASE
Sodium hydroxide	Merck
Tris(4-hydroxyphenyl)methane triglycidyl ether	Sigma Aldrich
WPBG 266	Fujifilm
WPBG 300	Fujifilm

2 METHODS

Preparation of Formulations for Copolymerization Reactions

The formulations contained the epoxide and the anhydride in a molar ratio of 1/1 (fg%/fg%), where fg% stands for functional groups in each monomer, and each functional group was treated as difunctional. Unless noted otherwise, 2.5 mol% PAG or 2.5 mol% PBG and 0.25 mol% ITX as photosensitizer were added. Formulations were prepared in the orange light lab to avoid light of all wavelengths below 480 nm. Homogeneous formulations were obtained by using a vortex mixer and/or an ultrasonic bath. For the crosslinked systems, the PBG and the photosensitizer were first dissolved in the anhydride before adding the epoxide, which had to be heated up to 60 °C in some cases.

Photo-Differential Scanning Calorimetry

Photo-differential scanning calorimetry (photo-DSC) was chosen as a reliable and easy-to-handle system for the copolymerization process, even though no exothermic behavior was observed for the ROCOP reaction.

Photo-DSC measurements were conducted with a DSC 204 F1 Phoenix device with an autosampler from the company Netzsch. The DSC-device was connected with Omnicure 2000 as the light source in combination with a double core lightguide (3 mm fiber diameter). The Omnicure was equipped with a broadband Hg-lamp and a spectral range of 320-500 nm was set with a filter. Calibration of the Omnicure was performed with an Omnicure R2000 radiometer before every measurement.

7-14 mg of the prepared formulation were weighed into aluminum crucibles and closed with a glass lid. The crucibles were then transported into the measuring chamber, which was kept inert by a continuous nitrogen flow (20 mL min^{-1}), *via* the auto sampler. Temperatures were varied between 50 and 150 °C, and light intensity on the sample surface was varied between 20 and 160 mW cm^{-2}. Before

irradiation, each sample was conditioned to the set temperature in a four-minute isothermal phase. Then, the samples were irradiated twice for 300 s.

(Quantitative) ^{1}H-NMR Analysis

^{1}H- and ^{13}C-NMR spectra were recorded on a Bruker Avance DRX-400 FT-NMR spectrometer at 400 MHz. Deuterated acetonitrile (CD_3CN) was used as solvent and internal standard to reference the chemical shifts unless otherwise noted. For samples cured with PAG, 0.3 wt% pyridine were added to the solvent in order to quench excess acid. Cured samples were immediately quenched with solvent after the curing process to suppress further polymerization reactions. The software MestReNova v14.3.0 was used for analysis.

Quantitative ^{1}H-NMR was performed by adding an exact amount of ethylene carbonate as internal standard after curing of the samples just before adding CD_3CN. The percentage of analyte was calculated from Equation 1.

$$X_A = \frac{I_A}{I_{iS}} \cdot \frac{N_{iS}}{N_A} \cdot \frac{M_A}{M_{iS}} \cdot \frac{m_{iS}}{m_P} \cdot 100 \qquad (1)$$

X_A .... percentage of analyte in sample (wt %)   Subscripts:

I .... integral   A .... analyte

N .... number of protons   iS .... internal Standard

M .... molecular weight (g/mol)   P .... sample

m .... mass (mg)
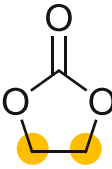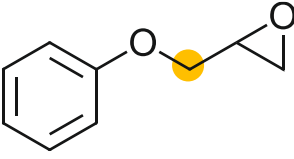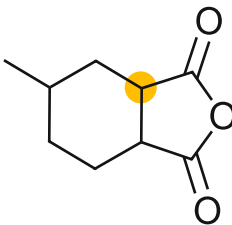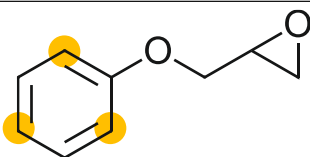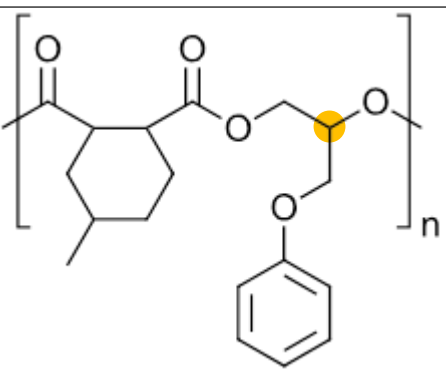
The conversion of monomers was calculated from (quantitative) ^{1}H-NMRs by integrating one signal of each monomer as well as from the internal standard ethylene carbonate. The signals used and their integration areas are summarized in Table 9.

Table 9. Summary of peak signals and their corresponding peak integral boundaries used for the determination of the conversion.

Substance	ppm-Range for integration	Signal
EC	4.500-4.410	
PGE	PAG: 4.328-4.280 PBG: 3.850-3.790	
MHHPA	3.445-3.320	
PGE constant	7.000-6.820	
Polyester	PAG: 5.400-5.050 PBG: 5.450-5.050 or 5.400-5.130	

Size Exclusion Chromatography

Size exclusion chromatography (SEC) was performed on a Malvern VISCOTEK TDA system fitted with three detectors (ViscotekTDA 305-021 RI + Viscodetector, UV Detector Module 2550 for TDA 305, VISCOTEK SEC-MALS 9 light scattering detector). For the separation, three columns (PSS SDC columns with particle sizes of 100 Å, 1000 Å and 100 000 Å) were connected in series, and dry THF (stabilized with BHT) was used as eluent at a flow rate of 0.8 mL min^{-1} under isothermal conditions at 35 °C.

Samples were dissolved in THF with $0.5\ \text{mg mL}^{-1}$ BHT as flowrate marker in concentrations of $0.3\text{-}0.5\ \text{mg mL}^{-1}$ and filtered. The samples were either measured immediately or otherwise stored at -20 °C in the freezer until measurement.

Conventional calibration with ten polystyrene standards of $375 - 177{,}000\ \text{Da}$ was performed. OmniSEC 5.12 from Malvern was used for data analysis. Approximate average degrees of polymerization were calculated from the obtained M_n values using Equation 3.

$$DP = \frac{M_n}{\overline{M_{monomer}}}$$

(3)

DP .... average degree of polymerization

M_n .... number average molecular weight of the polymer

$\overline{M_{monomer}}$ .... average molecular weight of the monomers

In several measurements, the flowrate marker was not found due to peaks overlapping, which causes results to be more error-prone.

Attenuated Total Reflectance-Fourier Transform Infrared Spectroscopy

Attenuated total reflectance-fourier transform infrared spectroscopy (ATR-FTIR) was performed on a PerkinElmer Spectrum 65 FT-IR Spectrometer equipped with a Specac MKII Golden Gate Single Reflection ATR System at room temperature. The IR spectrum of the specimens was measured in the range of 4000 to $600\ \text{cm}^{-1}$ with a resolution of $1\ \text{cm}^{-1}$ and eight scans per spectrum. Perkin Elmer Spectrum v10.4.1 was used as analysis software.

Rheology Measurements

Rheology was measured on an Anton Paar MCR 300 rheometer with a Peltier PTD 150 system and a CP-25 measuring system. Approximately 80 µL sample were measured at room temperature using a constant shear rate of $100\ \text{s}^{-1}$. The gap size between stamp and plate was set to 48 µm. The software used for evaluation was RheoPlus v3.40.

Thin Layer Chromatography

Thin layer chromatography (TLC) was carried out using aluminum TLC plates coated with silica gel (60 F245) from Merck.

Medium Pressure Liquid Chromatography

Medium pressure liquid chromatography (MPLC) was performed with a Büchi MPLC-system equipped with the control unit C-620, fraction collector C-660, RI detector and UV-photometer C-635. As stationary phase, Merck silica gel 60 (0.040-0.063 mm) was used, while PE/EtOAc was used as eluent with a flowrate of $120\ \text{mL min}^1$ (max. 10 bar).

High Performance Liquid Chromatography

Samples were analyzed on a reversed-phase HP-1100 Chemstation HPLC system with a diode array detector and a Inertsil ODS 3V C18 column, using a flow rate of 1 mL min^{-1} at a column temperature of 40 °C. Measurements were performed using a solvent ratio of 40/60 MeOH/H_2O for 50 s, then using a gradient to get to pure MeOH over 14 min, and measuring another 10 min using pure MeOH. An Agilent G4218A LT-ELSD and an Agilent 1100/1200 diode array detector were used continuously during the measurement.

High performance liquid chromatography (HPLC) samples were prepared by dissolving an exact amount of sample (around 15 mg) in 1 mL acetonitrile and filtering through a 0.2 μm filter.

Liquid Chromatography – Mass Spectrometry

Liquid chromatography – mass spectrometry (LC-MS) analysis was performed on a Nexera X2® UHPLC system (Shimadzu®) comprised of LC-30AD pumps, SIL-30AC autosampler, CTO-20AC column oven and DGU-20A5/3 degasser module. Detection was done using an SPD-M20A photo diode array, an RF-20Axs fluorescence detector, and ELS-2041 evaporative light scattering detector (JASCO®) and an LC-MS-2020 mass spectrometer (ESI/APCI).

Sample preparation consists of dissolving an exact amount of sample (around 1 mg) in 2 mL acetonitrile and then adding 0.2 mL water. The solution was then filtered through a 0.2 μm filter into an LC-MS vial.

Real Time-Fourier-Transformed-Near Infrared Photorheology

Real time-fourier-transformed-near infrared (RT-FT-NIR) photorheology measurements were conducted on an Anton Paar MCR 302 WESP. As a measuring system, a PP25 plate-plate arrangement and a P-PTD 200/GL Peltier glass plate were used. Polyethylene tape (SPT5A from tape providers, 5 mm thickness, acrylic adhesive, up to 150 °C) was used to cover the glass plate for easy removal of the photopolymerized samples. 150 μL formulation were applied to the glass disk and the gap between the measuring system and the plate was set to 0.2 mm unless stated otherwise. A broadband-Hg lamp (320-500 nm, light intensity of 30 mW cm^{-2} at the surface of the PE tape) was used for UV curing. The light intensity was measured by an Ocean Optics USB 2000+ spectrometer. An oscillatory sheer with an angular strain of 1% and a frequency of 1 Hz was applied to the sample. The formulation was irradiated for 10 min after an equilibration period of 60 s, and the measurement was then continued for another 50 min unless noted otherwise. For the guidance of the IR beam through the sample during the rheology measurements, an FTIR spectrometer (Bruker Vertex 80) with external mirrors was coupled with the rheometer and the reflected beam was detected by a mercury cadmium telluride (MCT)-detector. More details about the setup and the measurements can be found in

literature.[113] The measurements were performed at 100 °C unless stated otherwise. The conversion can be calculated over time because NIR spectra are measured simultaneously during irradiation. Hence, the peak area of the epoxide at about 4500 cm^{-1} wavenumbers was integrated, which reduces with increasing polymerization progress.

The photorheology measurements were analyzed with Rheoplus V3.62 from Anton Paar and the IR spectra with Opus 7.0 from Bruker.

Hot Molding

Silicon molds containing 20 wt% aluminum were used for producing tensile, DMTA and degradation test specimens. Those molds were then put into a hot-mold setup that was heated to 100 °C. A UVET lamp with 365 nm was used in an intensity of 290 mW cm^{-2} to irradiate the samples for 10 min.

UV/Vis Oven

The formulations were filled into silicon molds of the desired shape and cured in the UV/Vis oven "Uvitron International INTELLIRAY 600 UV-oven" (320-500 nm Hg broadband UV lamp; 600 W; UV-A: 125 mW cm^{-2}; Vis: 125 mW cm^{-2}) for 20-60 s with intensities between 50 and 60%.

Tensile Testing

Tensile tests were conducted on a Zwick Z050 tensile machine with a maximum test force of 50 kN and a speed of 5 mm min^{-1}. The test specimens were produced from a hot mold (ECC/MHHPA) or cured in the UV/Vis oven (pure ECC) in specimen shape ISO 527 test specimen 5B (total length of 35 mm^2 and a parallel region dimension of $2 \times 2 \times 12$ mm^3) and polished and their dimensions determined using a caliper. The software TextXpert II was used to record the stress-strain curve and analyze the results.

Dynamic Mechanical Thermal Analysis

Dynamic mechanical thermal analysis (DMTA) measurements were performed with an Anton Paar MCR 301 device, equipped with a CTD 450 oven. Test specimens were polished and their dimensions were determined using a caliper. Then, they were subjected to a torsion strain of 0.1% and 1 Hz. The temperature was scanned from -100 to 200 °C with a heating rate of 2 °C min^{-1}. The data was recorded and processed with the RheoCompass 1.24 software by Anton Paar. The glass transition temperature T_g was determined as the temperature at the maximum loss factor (tanδ).

Hot Lithography 3D Printing

Hot Lithography 3D printing was conducted on a BP10 (Blue Printer 10 of TU Wien) with a digital light processing (DLP) system using a transparent, rotatable, and heated material vat. The liquid resin was dispensed on this material vat, which was heated to different temperatures. The three-dimensional

matrix was created with a digital mirror device (DMD) projected UV light (385 nm, intensity between 3.8 and 75 mW cm^{-2}). The building process was performed in a top-down layer-by-layer approach. The In-Vision Ikarus 2 was used as a DLP light engine, and the pixel pitch was 50 µm. The building platform was 42 × 38 mm. The three-dimensional model was created out of a Common Layer Interface (CLI) file, which was transformed into 500 PNG files to provide the light exposure information of each image.

Degradation Procedure

The weight of the post-cured test specimens was determined. The pH of the solvents was determined with a pH electrode (WTW pH meter 330i), and then 15 mL solvent was added to each sample. The samples were stored at room temperature first, but the temperature was increased to 80 °C after three weeks for accelerated degradation. After certain time frames, the pH of the solutions was determined before they were decanted off. The remaining samples were then dispersed in 15 mL fresh water three times for 30 min each to leach any remaining salts out. The swelling weight was determined after taking off excess liquid with a tissue, and the dry weight was determined after drying at 100 °C until weight consistency was reached (overnight).

EXPERIMENTAL

1 ELUCIDATION OF POLYMERIZATION BEHAVIOR

1.1 Polymerization Process

Since the ^{1}H-NMRs of the monomers showed some impurities, they were purified by distillation before use. The NMR of the purified MHHPA, however, still contained more signals then expected, which was contributed to different stereoisomers (Figure 66). Some older MHHPA that was mainly hydrolyzed to the corresponding acid was resynthesized by adding acetic acid anhydride and refluxing for two hours before distillation to get rid of excess acetic acid anhydride and formed acetic acid and obtain the purified MHHPA.

Figure 66. Stereoisomers of MHHPA.

The formulations were produced according to the general procedure described in the Methods section. Formulations contained PGE/MHHPA 1/1 (fg%/fg%) with 2.5 mol% Irgacure 290 or 2.5 mol% WPBG 266 + 0.25 mol% ITX. For the control experiments, formulations containing PGE and 2.5 mol% Irgacure 290 or 2.5 mol% WPBG 266 + 0.25 mol% ITX were produced. The exact compositions are summarized in Table 10. The samples were cured using the standard photo-DSC setup at 50, 100 and 150 °C and an intensity of 91 ± 1 mW cm^{-2}. The samples were analyzed using ^{1}H-NMR, ATR-FTIR and SEC measurements according to the general procedure described in the Methods section.

Table 10. Composition of formulations used for the determination of polymerization behavior via ^{1}H-NMR analysis.

Substance	Eq.[a]	Theoretical m (mg)	Weighed-in m (mg)
PGE	1	90.11	92.44
MHHPA	1	100.91	113.47
Irgacure 290	0.05[b]	41.79	41.76
PGE	1	180.22	181.99
Irgacure 290	0.05[b]	83.58	83.53
PGE	1	90.11	90.06
MHHPA	1	100.91	101.74
WPBG 266	0.05[b]	14.87	15.14
ITX	0.005	0.76	0.80
PGE	1	180.22	182.14
WPBG 266	0.05[b]	29.74	30.11
ITX	0.005	1.53	1.52

[a]corresponds to the molecular molar equivalents irrespective of their functional group content

[b]corresponds to 2.5 mol% in regard to functional groups

To determine the ratio of copolymerization to homopolymerization, qNMR was established as analysis method. The same photo-DSC experiment as described before was used to produce another set of cured polymers. The exact composition of the formulations is summarized in Table 11. Then, qNMR analysis was performed as described in the Methods (Table S9).

Table 11. Composition of formulations used for the determination of the ratio of copolymerization to homopolymerization using qNMR.

Substance	Eq.[a]	Theoretical m (mg)	Weighed-in m (mg)
PGE	1	30.04	30.70
MHHPA	1	33.64	33.74
Irgacure 290	0.05[b]	13.93	13.96
PGE	1	30.04	30.16
MHHPA	1	33.64	34.57
WPBG 266	0.05[b]	4.96	4.98
ITX	0.005	0.25	0.25

[a]corresponds to the molecular molar equivalents irrespective of their functional group content

[b]corresponds to 2.5 mol% in regard to functional groups

1.2   Conversion of Monomers

The conversion of monomers was calculated from (quantitative) ^{1}H-NMRs as described in the Methods sections with the integration areas summarized in Table 9 (p.82). Equation 2 was used to calculate the conversion using only NMR (Table S10). Thereby, the integral of the aromatic signal, which should remain constant before and after polymerization, was utilized as reference signal.

$$X_A = \frac{I_A}{I_{cs}} \cdot \frac{N_{cs}}{N_A} \cdot 100 \qquad (2)$$

X$_A$ ....percentage of analyte in sample (wt %)

I...........Integral

N ....Number of protons

Subscripts:

A..........analyte (changing signal)

cs.........constant signal

1.3   Chain Length of Polymers

The chain length of the produced polymers was determined by performing SEC measurements as described in Methods (Table S12).

1.4   Stability of Formulation

For the preliminary reactivity study at 90 °C, the formulation was produced according to the general procedure described in the Methods section. Formulations contained PGE/MHHPA 1/1 (fg%/fg%) with 2.5 mol% WPBG 266 + 0.25 mol% ITX. The exact composition is summarized in Table 12.

Table 12. Composition of formulation containing WPBG 266 as PBG for the preliminary determination of the stability of this formulation at 90 °C.

Substance	Eq.[a]	Theoretical m (mg)	Weighed-in m (mg)
PGE	1	180.22	182.98
MHHPA	1	201.83	203.37
WPBG 266	0.05[b]	29.74	29.74
ITX	0.005	1.53	1.52

[a]corresponds to the molecular molar equivalents irrespective of their functional group content

[b]corresponds to 2.5 mol% in regard to functional groups

The formulation for the stability study at 100 °C was produced according to the general procedure described in the Methods section. Formulations contained PGE/MHHPA 1/1 (fg%/fg%) with 1 mol% WPBG 266 + 0.1 mol% ITX. The exact composition is summarized in Table 13.

Table 13. Composition of formulation containing WPBG 266 as PBG for the determination of the stability of this formulation at 100 °C.

Substance	Eq.[a]	Theoretical m (mg)	Weighed-in m (mg)
PGE	1	420.50	422.94
MHHPA	1	470.93	473.30
WPBG 266	0.02[b]	27.76	27.82
ITX	0.002	1.42	1.46

[a]corresponds to the molecular molar equivalents irrespective of their functional group content

[b]corresponds to 1 mol% in regard to functional groups

For determining the stability, the formulations were stored in brown glass vials at 100 °C in the oven. qNMR measurements as described in Materials were conducted after exact time periods to determine the conversion of monomers and thus the stability of the formulation (Table S15).

Furthermore, rheology was measured according to the general procedure described in the Methods section. After exact time periods of storage at 100 °C, approximately 80 µL sample were measured at room temperature, measuring five points to determine statistical parameters (Table S16).

2   OPTIMIZING THE LINEAR MODEL SYSTEM

2.1   PBG Screening

2.1.1   Reactivity Study

Formulations were produced according to the general procedure described in the Methods section. Formulations contained PGE/MHHPA 1/1 (fg%/fg%) with 1 mol% of one of the PBG (WPBG 266, WPBG 300, PDBN, KP2T, BP2T) + 0.1 mol% ITX (Table 14). The samples were cured using the standard photo-DSC setup at 100 °C and an intensity of 91 ± 1 mW cm^{-2}. The samples were analyzed using quantitative ^{1}H-NMR (Table S14) and SEC measurements (Table 1) as described in Methods.

Table 14. Composition of formulations with different PBGs for determining the effect of these different PBGs on the polymerization process.

Substance	Eq.[a]	Theoretical m (mg)	Weighed-in m (mg)
PGE	1	45.05	46.22
MHHPA	1	50.46	50.63
WPBG 266	0.02[b]	2.97	3.01
ITX	0.002	0.15	0.19
PGE	1	45.05	45.79
MHHPA	1	50.46	50.55
WPBG 300	0.02[b]	3.73	3.72
ITX	0.002	0.15	0.20
PGE	1	45.05	45.08
MHHPA	1	50.46	50.82
PDBN	0.02[b]	1.65	1.71
ITX	0.002	0.15	0.22
PGE	1	75.09	75.38
MHHPA	1	84.10	86.01
KP2T	0.02[b]	6.22	6.33
ITX	0.002	0.25	0.23
PGE	1	75.09	76.62
MHHPA	1	84.10	85.33
BP2T	0.02[b]	6.88	6.88
ITX	0.002	0.25	0.26

[a]corresponds to the molecular molar equivalents irrespective of their functional group content

[b]corresponds to 1 mol% in regard to functional groups

2.1.2 Stability Study
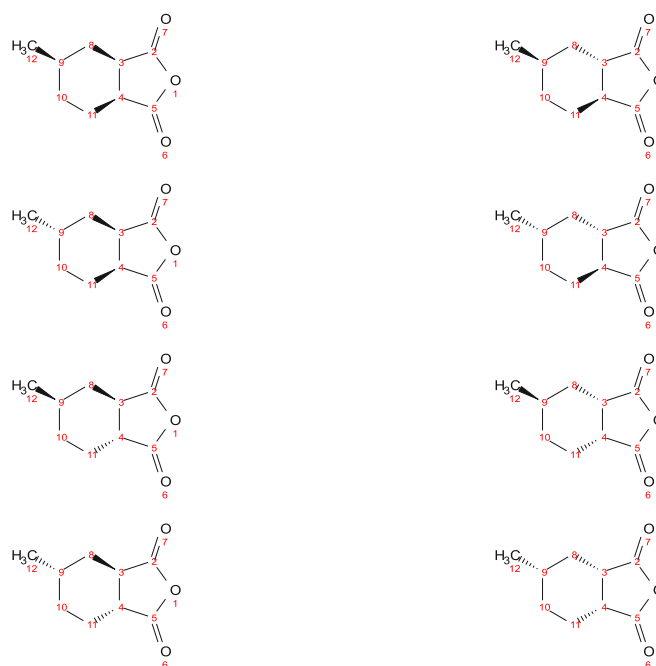
The formulations were produced according to the general procedure described in the Methods section. Formulations contained PGE/MHHPA 1/1 (fg%/fg%) with 1 mol% of different PBGs + 0.1 mol% ITX. The exact composition is summarized in Table 15.

For determining the stability, the formulations were stored in brown glass vials at 100 °C in the oven. qNMR measurements as described in Materials were conducted after exact time periods to determine the conversion of monomers and thus the stability of the formulation (Table S15).

Furthermore, rheology was measured according to the general procedure described in the Methods section. After exact time periods of storage at 100 °C, approximately 80 μL sample were measured at room temperature, measuring five points to determine statistical parameters (Table S16).

Table 15. Composition of formulations with different PBGs used for the determination of the stability of these formulations at 100 °C.

Substance	Eq.[a]	Theoretical m (mg)	Weighed-in m (mg)
PGE	1	420.50	422.94
MHHPA	1	470.93	473.30
WPBG 266	0.02[b]	27.76	27.82
ITX	0.002	1.42	1.46
PGE	1	420.50	421.48
MHHPA	1	470.93	470.88
WPBG 300	0.02[b]	34.82	34.88
ITX	0.002	1.42	1.40
PGE	1	420.50	420.67
MHHPA	1	470.93	471.12
PDBN	0.02[b]	15.36	15.35
ITX	0.002	1.42	1.41
PGE	1	420.50	426.25
MHHPA	1	470.93	470.91
KP2T	0.02[b]	34.82	34.97
ITX	0.002	1.42	1.41
PGE	1	420.50	423.58
MHHPA	1	470.93	470.85
BP2T	0.02[b]	38.51	38.45
ITX	0.002	1.42	1.46

[a]corresponds to the molecular molar equivalents irrespective of their functional group content

[b]corresponds to 1 mol% in regard to functional groups

2.2 Concentration of PBG

Formulations were produced according to the general procedure described in the Methods section. Formulations contained PGE/MHHPA 1/1 (fg%/fg%) with 0.5, 1 or 2.5 mol% WPBG 266 or WPBG 300 + 0.05, 0.1 or 0.25 mol% ITX (Table 16). The samples were cured using the standard photo-DSC setup at 100 °C and an intensity of 91 ± 1 mW cm^{-2}. The samples were analyzed using quantitative ^{1}H-NMR (Table S17 and Table S18) and SEC measurements (Table S19) as described in Methods.

Table 16. Composition of formulations with different concentrations of PBGs for determining the effect of these different PBG concentrations on the polymerization process.

Substance	Eq.[a]	Theoretical m (mg)	Weighed-in m (mg)
PGE	1	45.05	47.34
MHHPA	1	50.46	52.82
WPBG 266	0.01[b]	1.49	1.55
ITX	0.001	0.08	0.11
PGE	1	45.05	46.22
MHHPA	1	50.46	50.63
WPBG 266	0.02[c]	2.97	3.01
ITX	0.002	0.15	0.19
PGE	1	120.14	120.91
MHHPA	1	134.55	135.98
WPBG 266	0.05[d]	19.83	19.91
ITX	0.005	1.02	1.07
PGE	1	45.05	45.83
MHHPA	1	50.46	51.72
WPBG 300	0.01[b]	1.87	1.91
ITX	0.001	0.08	0.17
PGE	1	45.05	45.79
MHHPA	1	50.46	50.55
WPBG 300	0.02[c]	3.73	3.72
ITX	0.002	0.15	0.20
PGE	1	75.09	75.08
MHHPA	1	84.10	86.16
WPBG 300	0.05[d]	15.54	15.66
ITX	0.005	0.64	0.65

[a]corresponds to the molecular molar equivalents irrespective of their functional group content

[b]corresponds to 0.5 mol% in regard to functional groups

[c]corresponds to 1 mol% in regard to functional groups

[d]corresponds to 2.5 mol% in regard to functional groups

2.3 Temperature Screening

Formulations were produced according to the general procedure described in the Methods section. Formulations contained PGE/MHHPA 1/1 (fg%/fg%) with 2.5 mol% WPBG 266 + 0.25 mol% ITX (Table 17). The samples were cured using the standard photo-DSC setup at different temperatures (50, 60, 70, 80, 90, 100 °C) and an intensity of 91 ± 1 mW cm^{-2}. The samples were analyzed using quantitative ^{1}H-NMR (Table S20) and SEC measurements (Table S21) as described in Methods.

Table 17. Composition of formulations for determining the effect of different curing temperatures on the polymerization process.

Substance	Eq.[a]	Theoretical m (mg)	Weighed-in m (mg)
PGE	1	120.14	120.91
MHHPA	1	134.55	135.98
WPBG 266	0.05[b]	19.83	19.91
ITX	0.005	1.02	1.07

[a]corresponds to the molecular molar equivalents irrespective of their functional group content

[b]corresponds to 2.5 mol% in regard to functional groups

A second temperature screening was performed similarly using again the standard photo-DSC setup with a light intensity of 91 ± 1 mW cm^{-2} at higher temperatures of 120, 130 and 140 °C. The formulations now contained PGE/MHHPA 1/1 (fg%/fg%) with 2.5 mol% WPBG 300 (instead of WPBG 266) + 0.25 mol% ITX (Table 18). Furthermore, a control experiment using only PGE with 2.5 mol% WPBG 300 + 0.25 mol% ITX was also performed (Table 18). The samples were analyzed using quantitative ^{1}H-NMR (Table S22) and SEC measurements (Table S23).

Table 18. Composition of formulations for determining the effect of different higher curing temperatures on the polymerization process.

Substance	Eq.[a]	Theoretical m (mg)	Weighed-in m (mg)
PGE	1	105.13	106.79
MHHPA	1	117.73	117.91
WPBG 300	0.05[b]	21.76	21.83
ITX	0.005	0.89	0.99
PGE	1	150.18	150.84
WPBG 300	0.05[b]	31.09	31.14
ITX	0.005	1.27	1.38

[a]corresponds to the molecular molar equivalents irrespective of their functional group content

[b]corresponds to 2.5 mol% in regard to functional groups

2.4   Intensity Screening

Formulations were produced according to the general procedure described in the Methods section. Formulations contained PGE/MHHPA 1/1 (fg%/fg%) with 2.5 mol% WPBG 300 + 0.25 mol% ITX (Table 19). The samples were cured using the standard photo-DSC setup at 100 °C. Different intensities between 20 and 160 mW cm^{-2} were used. Analysis was performed using qNMR (Table S25) and SEC measurements (Table S26) as described in the Materials section.

Table 19. Composition of formulations for determining the effect of different irradiation intensities on the polymerization process.

Substance	Eq.[a]	Theoretical m (mg)	Weighed-in m (mg)
PGE	1	180.22	186.72
MHHPA	1	201.83	208.73
WPBG 300	0.05[b]	37.31	37.32
ITX	0.005	1.53	1.54

[a]corresponds to the molecular molar equivalents irrespective of their functional group content

[b]corresponds to 1 mol% in regard to functional groups

2.5   Anhydride Screening

The purity of the anhydrides (4-methyl-1,2-cyclohexanedicarboxylic anhydride MHHPA, 2,2-dimethyl succinic anhydride DMSA, glutaric anhydride GA, 2,2-dimethyl glutaric anhydride DMGA) was checked using ^{1}H-NMR. DMGA was pure enough and therefore used without further purification. GA was slightly contaminated, most likely with the hydrolyzed product glutaric acid. Recrystallization in ethyl acetate/hexane 5/3 unfortunately did not result in purification, therefore Kugelrohr ball-tube distillation was used to obtain the pure GA. DMSA was completely hydrolyzed to the acid and therefore resynthesized by adding acetic acid anhydride and refluxing for 3 h. Distillation was used for separation and purification of the DMSA. To get rid of all acetic acid anhydride, the product had to be dried under high vacuum.

Formulations were produced according to the general procedure described in the Methods section. Formulations contained one of the epoxides/PGE 1/1 (fg%/fg%) with 2.5 mol% WPBG 300 + 0.25 mol% ITX (Table 20). The samples were cured using the standard photo-DSC setup at 100 °C and an intensity of 91 ± 1 mW cm^{-2}. The samples were analyzed using quantitative ^{1}H-NMR (Table S27) and SEC measurements (Table 2) as described in the Materials section.

Table 20. Composition of formulations with different anhydrides for determining the effect of these different anhydrides on the polymerization process.

Substance	Eq.[a]	Theoretical m (mg)	Weighed-in m (mg)
PGE	1	30.04	29.90
MHHPA	1	33.64	33.93
WPBG 300	0.05[b]	6.22	6.31
ITX	0.005	0.25	0.31
PGE	1	30.04	31.28
GA	1	22.82	22.80
WPBG 300	0.05[b]	6.22	6.24
ITX	0.005	0.25	0.25
PGE	1	75.09	76.85
DMGA	1	71.08	72.48
WPBG 300	0.05[b]	15.54	15.86
ITX	0.005	0.64	0.67
PGE	1	30.04	30.98
DMSA	1	25.63	25.68
WPBG 300	0.05[b]	6.22	6.28
ITX	0.005	0.25	0.23

[a]corresponds to the molecular molar equivalents irrespective of their functional group content

[b]corresponds to 2.5 mol% in regard to functional groups

3   POST-CURING BEHAVIOR

For the investigation of the post curing behavior of the model system consisting of PGE/MHHPA 1/1 (fg%/fg%) with either 1 or 2.5 mol% WPBG 300 (exact formulations Table 21) and 0.1 or 0.25 mol% ITX, the formulations were prepared and cured on the photo-DSC as described above in the Methods section using 100 °C and 91 ± 1 mW cm^{-2}. One of the samples was quenched immediately after the curing process for both qNMR and SEC measurements, while further samples were stored in brown glass vials after curing at room temperature in the orange lab or at 100 °C in an oven. These stored samples were quenched 48 h later, and qNMR (Table S28) and SEC measurements (Table 3) of all samples were conducted following the general procedure described in the Methods section.

Table 21. Composition of formulations for determining the post-curing behavior of samples catalyzed with different PBG concentrations.

	Substance	Eq.[a]	Theoretical m (mg)	Weighed-in m (mg)
1 mol% WPBG 300	**PGE**	1	90.11	92.22
	MHHPA	1	100.91	100.72
	WPBG 300	0.02[b]	7.46	7.59
	ITX	0.002	0.31	0.32
2.5 mol% WPBG 300	**PGE**	1	180.22	186.72
	GA	1	201.83	208.73
	WPBG 300	0.05[c]	37.31	37.32
	ITX	0.005	1.53	1.54

[a]corresponds to the molecular molar equivalents irrespective of their functional group content

[b]corresponds to 1 mol% in regard to functional groups

[c]corresponds to 2.5 mol% in regard to functional groups

4 CROSSLINKED SYSTEMS

4.1 Monomer Screening

Technical THPMTGE was purified using column chromatography. A column was packed with 213 g silica and equilibrated with mobile phase (PE/EtOAc 1/1). The mobile phase was first optimized using TLC (Figure S14).

Approximately 5 g technical THPMTGE were dissolved in as little EtOAc as possible. Since solubility is not great, prolonged dissolution times, a vortex mixer and an ultrasonic bath had to be employed. Furthermore, solvent was gradually added to a total volume of 5 mL. A liquid addition onto the column was performed. However, a septum blocked during addition, therefore some of the sample was lost and some was not added at all. The separation was tracked with the UV detector and TLC for determining the fractions containing sample. Two different fractions were collected, with the main fraction yielding 1.91 g white purified product, which however still contained EtOAc. Since the product is very viscous, removal of the EtOAc took several days on the high vacuum pump.

4.2 Gelation Study

Several RT-FT-NIR-photorheology measurements were conducted using different conditions and formulations. These formulations were always prepared according to the general procedure described in the Methods section and contain multifunctional epoxide/PGE 1/1 (fg%/fg%) + 2.5 mol% WPBG 300 and 0.25 mol% ITX. The exact compositions are summarized in Table 22.

Table 22. Composition of formulations used in RT-FTIR-NIR-photorheology measurements for determining the effect of different compositions of the formulation as well as different reaction conditions on the polymerization process.

	Substance	Eq.[a]	Theoretical m (mg)	Weighed-in m (mg)
THPMTGE techn. 85%	THPMTGE	1	433.44	435.31
	MHHPA	1	403.66	406.86
	WPBG 300	0.05[b]	74.61	74.64
	ITX	0.005	3.05	3.08
THPMTGE techn. 100%	THPMTGE	1	460.53	461.57
	MHHPA	1	504.57	505.14
	WPBG 300	0.05[b]	93.26	94.99
	ITX	0.005	3.82	3.81
THPMTGE purified	THPMTGE	1	460.53	460.80
	MHHPA	1	504.57	504.59
	WPBG 300	0.05[b]	93.26	93.23
	ITX	0.005	3.82	3.82
THPMTGE techn. 100%	THPMTGE	1	460.53	462.86
	MHHPA	1	504.57	504.55
	WPBG 300	0.1[c]	186.53	186.60
	ITX	0.01	7.63	7.68
ECC techn.	ECCE	1	524.81	526.06
	MHHPA	1	437.29	437.25
	WPBG 300	0.05[b]	80.83	80.97
	ITX	0.005	3.31	3.38
ECC techn.	ECC	1	1049.62	1052.44
	MHHPA	1	874.59	875.39
	WPBG 300	0.1[c]	323.31	323.38
	ITX	0.01	13.23	13.21

[a]corresponds to the molecular molar equivalents irrespective of their functional group content

[b]corresponds to 2.5 mol% in regard to functional groups

[c]corresponds to 5 mol% in regard to functional groups

5   MATERIAL CHARACTERIZATION AND PROCESSING

5.1   Thermomechanical Properties

Test specimens were produced following the general procedure described in the Methods chapter. Formulations containing ECC/MHHPA 1/1 (fg%/fg%) + 2.5 mol% WPBG 300 + 0.25 mol% ITX were filled in silicon forms containing aluminum, and air bubbles were removed with a syringe (Table 23). The formulation was then cured in the hot-mold setup at 100 °C by irradiating for 10 min with 290 mW cm^{-2} at 365 nm. The test specimens were sanded to afford smooth surfaces, and their exact dimensions were determined using a caliper. Half of the specimens were measured immediately, while the other half was post-cured at 100 °C for 48 h before measurement.

Table 23. Composition of formulations for the production of ECC/MHHPA tensile test and DMTA test specimens.

Substance	Eq.[a]	Theoretical m (mg)	Weighed-in m (mg)
ECC	1	4238.85	4238.94
MHHPA	1	3531.99	3532.31
WPBG 300	0.05[b]	652.84	652.83
ITX	0.005	26.71	26.81

[a]corresponds to the molecular molar equivalents irrespective of their functional group content

[b]corresponds to 2.5 mol% in regard to functional groups

Reference samples containing only ECC and 0.1 wt% Irgacure 290 were cured in the UV/Vis oven as described in the Materials section. (Table 24).

Table 24. Composition of formulations for the production of tensile test and DMTA test specimens.

Substance	Eq.[a]	Theoretical m (mg)	Weighed-in m (mg)
ECC	1	14936.90	14939.37
Irgacure 290	0.01	149.37	149.44

[a]corresponds to weight percent

[b]corresponds to ≈ 0.3 mol% in regard to functional groups

DMTA and tensile tests were performed according to the general procedure described in the Methods section.

5.2   3D Printing

Formulations for the 3D printing process were mixed according to the general procedure described in the Methods section (Table 25).

Table 25. Composition of formulations used for different irradiation, 3D printing and overpolymerization tests.

	Substance	Eq.[a]	m (mg)	Weighed-in m (mg)
Irradiation tests	ECC	1	262.41	262.63
	MHHPA	1	218.65	218.89
	WPBG 300	0.05[b]	40.41	40.47
	ITX	0.005	1.65	1.70
3D printing	ECC	1	2099.24	2103.52
	MHHPA	1	1749.18	1752.33
	WPBG 300	0.05[b]	323.31	323.34
	ITX	0.005	13.23	13.21
Overpolymerization tests	ECC	1	40.37	41.15
	MHHPA	1	33.64	33.62
	WPBG 300	0.05[b]	6.22	6.29
	ITX	0.005	0.25	0.25
	ECC	1	40.37	40.61
	MHHPA	1	33.64	34.18
	WPBG 300	0.05[b]	6.22	6.19
	ITX	0.005	0.25	0.24
	Ketoprofen	0.005	0.25	0.27
	ECC	1	40.37	41.48
	MHHPA	1	33.64	34.50
	WPBG 300	0.05[b]	6.22	6.25
	ITX	0.005	0.25	0.27
	Ketoprofen	0.01	0.51	0.49
	ECC	1	40.37	40.50
	MHHPA	1	33.64	33.97
	WPBG 300	0.05[b]	6.22	6.23
	ITX	0.005	0.25	0.25
	Ketoprofen	0.05	2.54	2.51

[a]corresponds to the molecular molar equivalents irrespective of their functional group content

[b]corresponds to 2.5 mol% in regard to functional groups

Several different conditions were tried during the irradiation and printing tests and are summarized in Table 26.

Table 26. Conditions used for different irradiation, 3D printing and overpolymerization tests.

	Temp. (°C)	Intensity[1] (mW cm^{-2})	Time/layer (s)	Results
Irradiation tests	120	75	10x400	Hardening in fraction of time
	100	75	3x40	hardening
	100	50	60	No hardening
	100	40	65	hardening
	100	65	2x40	hardening
3D printing	100/100/60	75/65	70	Complete polymerization of the whole formulation
	80/80/55	40/35	60	Slightly better compared to 1st print, but still complete polymerization
	75/70/55	50/45	45	Only slight overpolymerization (at the bottom)
	70/70/55	65	45	More overpolymerization again (thicker, harder layer on bottom)
Overpolym. Test	80	45	10x45	No overpolymerization observed
	80	45	50x45	Complete polymerization of the whole formulation

[1]corresponds to intensity on computer, intensity on sample is significantly lower

5.3 Degradation Behavior

For the preliminary degradation studies, samples containing purified THPMTGE and MHHPA were weighed after curing by photorheology (Table 27) and then put into vials with 5 mL solvent. Three different solvents (5 wt% KOH methanolic solution, 1 M NaOH solution or 0.2 M KOtBu methanolic solution) were used. The samples were stirred at room temperature. After 24 h, the sample in the KOH solution was already completely dissolved. The sample in the NaOH solution was also already quite dissolved. However, it was hard to see if complete degradation was achieved since the aqueous environment does not dissolve the small degradation products and thus no clear solution but rather a dispersion was obtained. The sample in the KOtBu solution was still quite intact but slowly degraded over the course of the next few days.

Table 27. Exact sample mass of the photorheology samples used for the preliminary degradation studies.

5 wt% KOH methanolic solution	1 M NaOH solution	0.2 M KOtBu methanolic solution
126.5 mg	134.7 mg	180.2 mg

For the final degradation study, test specimens containing ECC/MHHPA 1/1 (fg%/fg%) + 2.5 mol% WPBG 300 + 0.25 mol% ITX (Table 28) were prepared and cured at 100 °C using the hot mold setup according to the general procedure described in the Methods section. The test specimens were then post-cured at 100 °C for 48 h.

Table 28. Composition of formulation used for the production of degradation specimens.

Substance	Eq.[a]	Theoretical m (mg)	Weighed-in m (mg)
ECC	1	1816.65	1818.25
MHHPA	1	1513.71	1514.99
WPBG 300	0.05[b]	279.79	279.89
ITX	0.005	11.45	11.42

[a]corresponds to the molecular molar equivalents irrespective of their functional group

[b]corresponds to 2.5 mol% in regard to functional groups

Distilled water and 1M aqueous NaOH solution were chosen as solvents. Each sample was dispersed in 15 mL solvent and left to degrade at room temperature for three weeks, then the temperature was increased to 80 °C. At certain time points, sample triplicates were measured. First, the pH of the solvent was determined, then it was decanted off. The remaining samples were then dispersed in 15 mL fresh water for 30 min three times to leach any remaining salts. The swelling weight was determined after drying superficially with a tissue, and the dry weight was determined after drying at 100 °C until weight consistency (overnight).

CONCLUSION AND OUTLOOK

This work focuses on the novel approach of using photo-triggered ring-opening copolymerization (ROCOP) between epoxides and anhydrides for the production on polyester networks. This approach allows for the production of these polyesters using hot stereolithography, and the polyesters show degradability and possible recyclability due to the hydrolysable ester bonds.

Firstly, it was shown that the copolymerization between an anhydride and an epoxide occurs when using either a photoacid generator (PAG) or a photobase generator (PBG) as catalyst (Figure 67). However, using PAG leads to strong homopolymerization of the epoxide into polyether. Therefore, PAGs are not suitable candidates for the photoinitiated ROCOP of epoxides and anhydrides. It might be possible to improve the rate of copolymerization to homopolymerization if less reactive epoxides or oxetanes are used, but this method was not explored in this work since no homopolymerization of epoxide was observed using temperatures of 100 °C or below when initiating with PBG. However, major stability problems and very low molecular weights of the produced copolymers required further optimization.
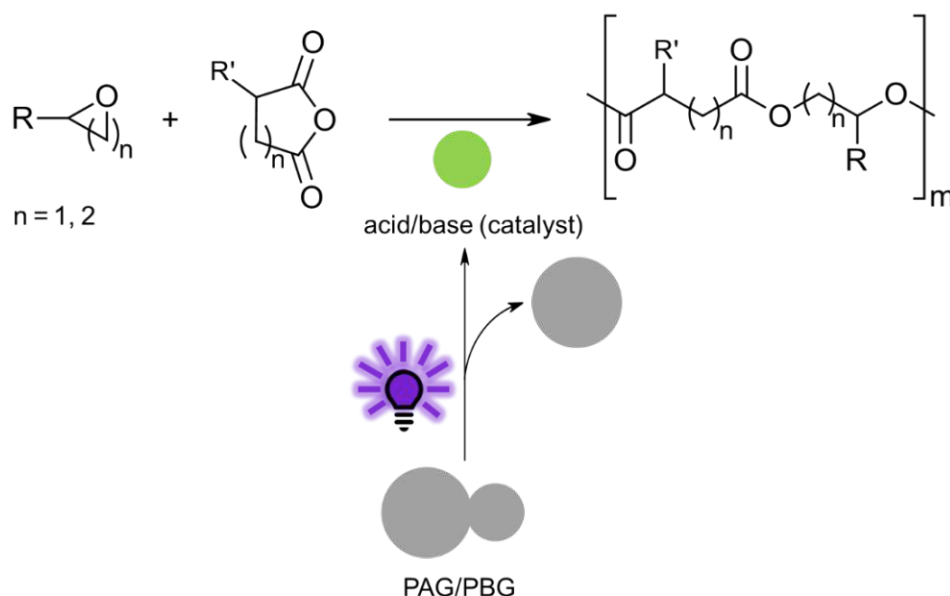
Figure 67. Ring-opening copolymerization reaction (ROCOP) between epoxides and anhydrides using photoacid generators (PAGs) or photobase generators (PBGs) as photocatalysts.

Optimization was performed for a linear model system using PGE and MHHPA as monomers (Figure 68). Different types and concentration of PBGs, temperatures, intensities and anhydrides were screened. Screening different PBGs surprisingly resulted in very different behavior, especially regarding the stability. It was discovered that a bisguanidine base with a borate counterion,

WPBG 300, resulted in good stability of the formulation at 100 °C as well as good conversion of monomers and relatively long polymer chains. As expected, increasing the PBG concentration leads to higher conversion. However, it was also surprising to discover that the molecular weight is also increasing with increased PBG concentration, since more chain starters usually result in lower molecular weight products. This could be due to the fact that full conversion is not achieved anyways, therefore enough monomer is still available to form chains of similar length. Temperature screening revealed that at least 80-90 °C are needed for the copolymerization process to happen, while high temperatures of 150 °C have to be avoided since they facilitate unwanted side reactions. It has been shown that higher temperatures lead to higher conversions and slightly higher molecular weight of the copolymer. A similar trend can be seen changing the intensity of the light source used to irradiate the sample: the higher the intensity, the higher the conversion and the molecular weight of the copolymer. Regarding anhydrides, the biggest, bulkiest anhydride MHHPA performed best, resulting both in good conversion and arguably longer polymer chains than the other tested anhydrides. In summary, the optimized linear system uses a mixture of monomers PGE/MHHPA 1/1 (fg%/fg%), 2.5 mol% WPBG 300 and 0.25 mol% ITX at 100 °C curing temperature.
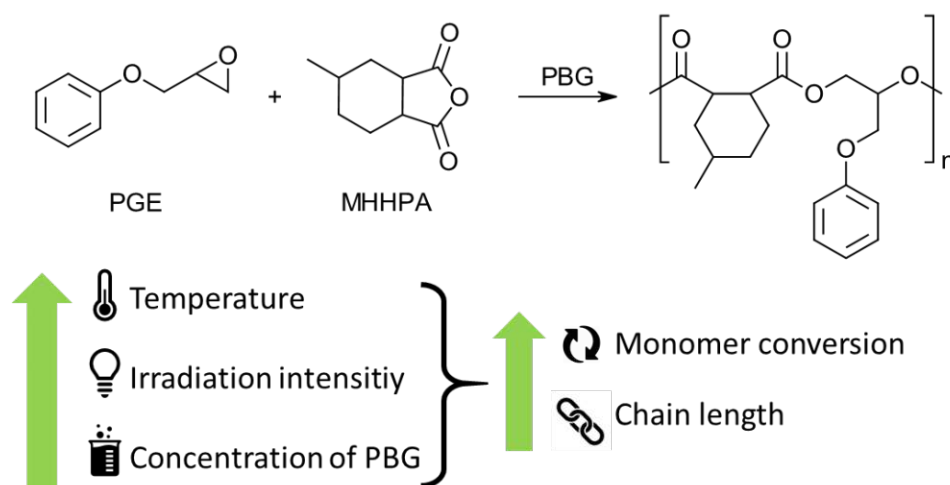
Figure 68. Model reaction for the ring-opening copolymerization between PGE and MHHPA and different parameters that influence the polymerization process.

Even though the optimal parameters for the reaction were found, other factors also have to be taken into consideration. For example, the 3D printer might not be able to handle such high intensities or temperatures, and it might also be economically disadvantageous since it requires more energy. In this case, the 3D printer available can only supply intensities of around 30 mW cm^{-2} on the sample surface.

Even when using optimized conditions, the reaction was not complete after the irradiation. Thus, it was very important to investigate the post-curing behavior of the system. Luckily, experiments

showed post-curing behavior of the system even at room temperature. When using 100 °C storage temperature, quantitative yields could be achieved within 48 h.

After the optimization of the linear model system, the focus was shifted towards crosslinked materials. In this regard, several multifunctional epoxides were identified as possible candidates, and THPMTGE and ECC were chosen for further investigations. THPMTGE contains three glycidyl ether moieties for more crosslinking and is readily available, while likewise commercially available ECC contains only two epoxide groups (Figure 69).

Since the linear systems showed no exothermic behavior using photo-DSC and SEC is not available for crosslinked materials, RT-FT-NIR-photorheology was introduced as a new measurement system to simultaneously give information about both conversion and time until gelation.
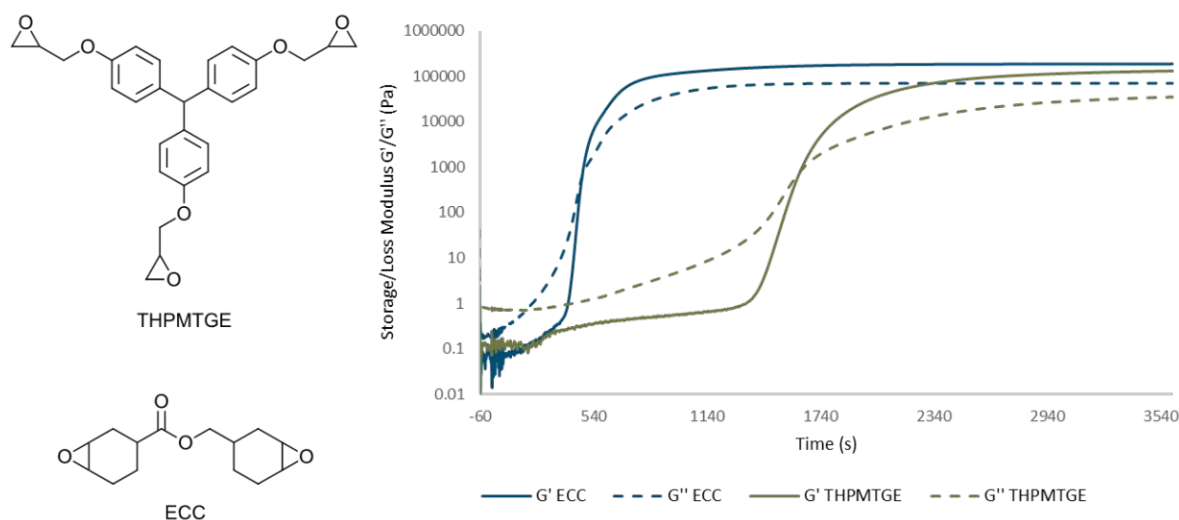
Figure 69. Multifunctional epoxides THPMTGE and ECC used in RT-FT-NIR photorheology measurements and the measured storage and loss modulus over time showing huge differences in gelation time.

Reactivity studies revealed very slow gelation overall, and a huge reactivity difference between the two investigated epoxides THPMTGE and ECC (Figure 69). Glycidyl ether groups seem to stabilize intermediates during polymerization and thus lead to reduced reactivity. Furthermore, the same trends already discovered for the linear system also applied: higher temperature, higher light intensity and higher PBG concentration resulted in faster gelation. Finally, it was also discovered that using technical monomers rather than purified ones was actually beneficial since it reduced the t_g. This is probably due to the fact that most of the impurities are di- or oligomerized monomers that can still partake in the polymerization reaction and actually reduce the gelation time since introducing higher molecular weight monomers results in gelation at lower conversion.

Material characterization of the copolymer obtained from ECC/MHHPA revealed typical tensile behavior of thermosets including high modulus, high brittleness and a high T_g of 187 °C. It was also

shown that post-curing is required to obtain the final properties of the material, since materials performed much worse without post-curing. In the future, tougher behavior could be reached by reducing the crosslinking density via partial substitution of the difunctional epoxide with monofunctional epoxide.

The 3D printing of the material surprisingly revealed very different behavior than expected from the characterization via photorheometry. In fact, much milder conditions and shorter gelation times could be used for the printing process. Unfortunately, full polymerization and hardening of the vat occurred, which could not be fully explained up to now. Though stability of the formulation is not ideal, it was found to be sufficient and was ruled out for such extreme loss of spatiotemporal control over the polymerization process. Diffusion-based overpolymerization could also be ruled out through a uniquely designed experiment where the partial formulation illumination on the 3D printer was aided by a mask. Therefore, the only possible explanation remaining is that some stray light is getting to the dark areas of the formulation and causes polymerization there. This could be overcome in the future by translating the 3D printing process from DLP-based to a laser-based curing.

A degradation study revealed that the produced polymers could indeed be degraded and thus possibly recycled, although the degradation is slow. Retrieval of the monomers is in principle possible and should be attempted in the future, for the formulation composition that can be printed successfully.

Overall, this work has successfully demonstrated light-triggered ring-opening copolymerization of epoxides and anhydrides for the first time. The system displays suitable gelation behavior for 3D printing in the future and has been shown to be degradable.

Literature

1. Sangermano, M., M. Bergoglio, and S. Schögl, *Biobased Vitrimeric Epoxy Networks.* Macromolecular Materials and Engineering, 2023. **n/a**(n/a): p. 2300371.

2. Klee, P.S., et al., *Designing Sustainable Polymers: Lactate Esters for 3D Printing and Upcycling.* ACS Applied Polymer Materials, 2024. **6**(1): p. 935-942.

3. Anastas, P. and N. Eghbali, *Green Chemistry: Principles and Practice.* Chemical Society Reviews, 2010. **39**(1): p. 301-312.

4. *Sustainable Polymers for Improved Chemical Circularity*. [cited 2024 07.02.]; Available from: https://faculty.engineering.asu.edu/jin/research/sustainable-polymers/.

5. Speight, J.G., *Chapter 14 - Monomers, polymers, and plastics*, in *Handbook of Industrial Hydrocarbon Processes (Second Edition)*, J.G. Speight, Editor. 2020, Gulf Professional Publishing: Boston. p. 597-649.

6. Wang, Y., et al., *Production and waste treatment of polyesters: application of bioresources and biotechniques.* Critical Reviews in Biotechnology, 2023. **43**(4): p. 503-520.

7. Schneiderman, D.K. and M.A. Hillmyer, *50th Anniversary Perspective: There Is a Great Future in Sustainable Polymers.* Macromolecules, 2017. **50**(10): p. 3733-3749.

8. Kaushal, J., M. Khatri, and S.K. Arya, *Recent insight into enzymatic degradation of plastics prevalent in the environment: A mini - review.* Cleaner Engineering and Technology, 2021. **2**: p. 100083.

9. Christoff-Tempesta, T., R.M. O'Dea, and T.H. Epps, III, *Unlocking Circularity Through the Chemical Recycling and Upcycling of Lignin-Derivable Polymethacrylates.* Macromolecules, 2023. **56**(23): p. 9796-9803.

10. Zhang, C., *Biodegradable Polyesters: Synthesis, Properties, Applications*, in *Biodegradable Polyesters*. 2015. p. 1-24.

11. Kausar, A., *Review of fundamentals and applications of polyester nanocomposites filled with carbonaceous nanofillers.* Journal of Plastic Film & Sheeting, 2018. **35**(1): p. 22-44.

12. *Step Polymerization*, in *Principles of Polymerization*. 2004. p. 39-197.

13. Lin, L., et al., *Fully alternating sustainable polyesters from epoxides and cyclic anhydrides: economical and metal-free dual catalysis.* Green Chemistry, 2019. **21**(9): p. 2469-2477.

14. Li, H., et al., *Well-Defined and Structurally Diverse Aromatic Alternating Polyesters Synthesized by Simple Phosphazene Catalysis.* Macromolecules, 2018. **51**(6): p. 2247-2257.

15. Hirschmann, M., F. Andriani, and T. Fuoco, *Functional and degradable copolyesters by ring-opening copolymerization of epoxides and anhydrides.* European Polymer Journal, 2023. **183**: p. 111766.

16. Dubois, P.Q.P., *Handbook of ring-opening polymerization*. 2009, Weinheim: Weinheim : Wiley-VCH. XVIII, 408 S., Ill., graph. Darst., 25 cm.

17. Hošťálek, Z., et al., *Alternating copolymerization of epoxides with anhydrides initiated by organic bases.* European Polymer Journal, 2017. **88**: p. 433-447.

18. Lidston, C.A.L., et al., *Multifunctional Catalysts for Ring-Opening Copolymerizations.* ACS Catalysis, 2022. **12**(18): p. 11037-11070.

19. Longo, J.M., M.J. Sanford, and G.W. Coates, *Ring-Opening Copolymerization of Epoxides and Cyclic Anhydrides with Discrete Metal Complexes: Structure–Property Relationships.* Chemical Reviews, 2016. **116**(24): p. 15167-15197.

20. Kummari, A., S. Pappuru, and D. Chakraborty, *Fully alternating and regioselective ring-opening copolymerization of phthalic anhydride with epoxides using highly active metal-free Lewis pairs as a catalyst.* Polymer Chemistry, 2018. **9**(29): p. 4052-4062.

21. Liang, X., F. Tan, and Y. Zhu, *Recent Developments in Ring-Opening Copolymerization of Epoxides With CO2 and Cyclic Anhydrides for Biomedical Applications.* Frontiers in Chemistry, 2021. **9**.

22.   Hu, L.-F., et al., *Highly Active Organic Lewis Pairs for the Copolymerization of Epoxides with Cyclic Anhydrides: Metal-Free Access to Well-Defined Aliphatic Polyesters.* Macromolecules, 2018. **51**(8): p. 3126-3134.

23.   Pappuru, S. and D. Chakraborty, *Progress in metal-free cooperative catalysis for the ring-opening copolymerization of cyclic anhydrides and epoxides.* European Polymer Journal, 2019. **121**: p. 109276.

24.   Nurhan Onar, C., *Introductory Chapter: Introduction to "Polyester – Production, Characterization and Innovative Applications"*, in *Polyester*, C. Nurhan Onar, Editor. 2018, IntechOpen: Rijeka. p. Ch. 1.

25.   Bharat, D., *Unsaturated Polyester Resin for Specialty Applications*, in *Polyester*, M.S. Hosam El-Din, Editor. 2012, IntechOpen: Rijeka. p. Ch. 7.

26.   Burelo, M., et al. *Recent Developments in Synthesis, Properties, Applications and Recycling of Bio-Based Elastomers*. Molecules, 2024. **29**, DOI: 10.3390/molecules29020387.

27.   Ligon, S.C., et al., *Polymers for 3D Printing and Customized Additive Manufacturing.* Chemical Reviews, 2017. **117**(15): p. 10212-10290.

28.   Raos, P., I. Klapan, and T. Galeta, *Additive Manufacturing of Medical Models--Applications in Rhinology.* Coll Antropol, 2015. **39**(3): p. 667-73.

29.   Medelli´n-Castillo, H.I. and J.E. Pedraza Torres, *Rapid Prototyping and Manufacturing: A Review of Current Technologies*. 2009. p. 609-621.

30.   Srivatsan, T.S. and T.S. Sudarshan, *Additive Manufacturing of Materials: Viable Techniques, Metals, Advances, Advantages, and Applications*, T.S. Srivatsan and T.S. Sudarshan, Editors. 2016, United Kingdom: CRC Press: United Kingdom. p. 64.

31.   Black, H.T., M.C. Celina, and J.R. McElhanon, *Additive Manufacturing of Polymers: Materials Opportunities and Emerging Applications*. 2016: United States.

32.   CustomPartNet. *Fused Deposition Modeling (FDM)*. 2024 [cited 2024 07/02]; Available from: https://www.custompartnet.com/wu/fused-deposition-modeling.

33.   Appuhamillage, G.A., et al., *110th Anniversary: Vat Photopolymerization-Based Additive Manufacturing: Current Trends and Future Directions in Materials Design.* Industrial & Engineering Chemistry Research, 2019. **58**(33): p. 15109-15118.

34.   Fouassier, J.-P.Q.J.-P., *Photoinitiation, photopolymerization, and photocuring : fundamentals and applications*. 1995, Munich Vienna [u.a.]: Munich : Vienna [u.a.] : Hanser [u.a.]. XII, 375 S., Ill., graph. Darst., 23 cm.

35.   Voet, V.S.D., J. Guit, and K. Loos, *Sustainable Photopolymers in 3D Printing: A Review on Biobased, Biodegradable, and Recyclable Alternatives.* Macromolecular Rapid Communications, 2021. **42**(3): p. 2000475.

36.   Pfaffinger, M., *Hot Lithography – New Possibilities in Polymer 3D Printing.* Laser Technik Journal, 2018. **15**(4): p. 45-47.

37.   Dall'Argine, C., et al., *Hot-Lithography SLA-3D Printing of Epoxy Resin.* Macromolecular Materials and Engineering, 2020. **305**(10): p. 2000325.

38.   Jin, F.-L., X. Li, and S.-J. Park, *Synthesis and application of epoxy resins: A review.* Journal of Industrial and Engineering Chemistry, 2015. **29**: p. 1-11.

39.   Vidil, T., et al., *Control of reactions and network structures of epoxy thermosets.* Progress in Polymer Science, 2016. **62**: p. 126-179.

40.   Sangermano, M., *Advances in cationic photopolymerization.* 2012. **84**(10): p. 2089-2101.

41.   Ligon-Auer, S.C., et al., *Toughening of photo-curable polymer networks: a review.* Polymer Chemistry, 2016. **7**(2): p. 257-286.

42.   Fouassier, J.-P., *Photoinitiation, photopolymerization, and photocuring : fundamentals and applications*. 1995, Munich Vienna [u.a.]: Hanser/Gardner Publications, Inc. XII, 375 S., Ill., graph. Darst., 23 cm.

43.   Gruber, H.F., *Photoinitiators for free radical polymerization.* Progress in Polymer Science, 1992. **17**(6): p. 953-1044.

44. Mitterbauer, M.Q.M., *Tin-based long wavelength photoinitiators for dental composites*. Zinn basierte Photoinitiatoren für Dentalmaterialien. 2019, Wien: Wien. 213 Seiten, Illustrationen, Diagramme.

45. Suyama, K. and M. Shirai, *Photobase generators: Recent progress and application trend in polymer systems.* Progress in Polymer Science, 2009. **34**(2): p. 194-209.

46. Zivic, N., et al., *Recent Advances and Challenges in the Design of Organic Photoacid and Photobase Generators for Polymerizations.* Angewandte Chemie International Edition, 2019. **58**(31): p. 10410-10422.

47. Sangermano, M., I. Roppolo, and A. Chiappone *New Horizons in Cationic Photopolymerization*. Polymers, 2018. **10**, DOI: 10.3390/polym10020136.

48. Dadashi-Silab, S., S. Doran, and Y. Yagci, *Photoinduced Electron Transfer Reactions for Macromolecular Syntheses.* Chemical Reviews, 2016. **116**(17): p. 10212-10275.

49. Crivello, J.V. and E. Reichmanis, *Photopolymer Materials and Processes for Advanced Technologies.* Chemistry of Materials, 2014. **26**(1): p. 533-548.

50. Crivello, J.V. and J.H.W. Lam, *Diaryliodonium Salts. A New Class of Photoinitiators for Cationic Polymerization.* Macromolecules, 1977. **10**(6): p. 1307-1315.

51. Crivello, J.V., *The discovery and development of onium salt cationic photoinitiators.* Journal of Polymer Science Part A: Polymer Chemistry, 1999. **37**(23): p. 4241-4254.

52. Green, W.A., *Industrial photoinitiators : a technical guide*. 2010, CRC Press Boca Raton: Boca Raton.

53. Martin, C.J., et al., *Recent progress in development of photoacid generators.* Journal of Photochemistry and Photobiology C: Photochemistry Reviews, 2018. **34**: p. 41-51.

54. Sipani, V. and A.B. Scranton, *Dark-cure studies of cationic photopolymerizations of epoxides: Characterization of the active center lifetime and kinetic rate constants.* Journal of Polymer Science Part A: Polymer Chemistry, 2003. **41**(13): p. 2064-2072.

55. Cameron, J.F. and J.M.J. Frechet, *Base catalysis in imaging materials. 1. Design and synthesis of novel light-sensitive urethanes as photoprecursors of amines.* The Journal of Organic Chemistry, 1990. **55**(23): p. 5919-5922.

56. Xi, W., et al., *Spatial and Temporal Control of Thiol-Michael Addition via Photocaged Superbase in Photopatterning and Two-Stage Polymer Networks Formation.* Macromolecules, 2014. **47**(18): p. 6159-6165.

57. Denissen, W., J.M. Winne, and F.E. Du Prez, *Vitrimers: permanent organic networks with glass-like fluidity.* Chemical Science, 2016. **7**(1): p. 30-38.

58. Kloxin, C.J. and C.N. Bowman, *Covalent adaptable networks: smart, reconfigurable and responsive network systems.* Chemical Society Reviews, 2013. **42**(17): p. 7161-7173.

59. Bijalwan, V., et al., *3D Printing of Covalent Adaptable Networks: Overview, Applications and Future Prospects.* Polymer Reviews, 2024. **64**(1): p. 36-79.

60. Hayashi, M. *Implantation of Recyclability and Healability into Cross-Linked Commercial Polymers by Applying the Vitrimer Concept*. Polymers, 2020. **12**, DOI: 10.3390/polym12061322.

61. Zhu, G., et al., *Recyclable and reprintable biobased photopolymers for digital light processing 3D printing.* Chemical Engineering Journal, 2023. **452**: p. 139401.

62. Zhu, G., et al., *Reprintable Polymers for Digital Light Processing 3D Printing.* Advanced Functional Materials, 2021. **31**(9): p. 2007173.

63. Coates, G.W. and Y.D.Y.L. Getzler, *Chemical recycling to monomer for an ideal, circular polymer economy.* Nature Reviews Materials, 2020. **5**(7): p. 501-516.

64. Hong, M. and E.Y.X. Chen, *Completely recyclable biopolymers with linear and cyclic topologies via ring-opening polymerization of γ-butyrolactone.* Nature Chemistry, 2016. **8**(1): p. 42-49.

65. García, J.M., et al., *Recyclable, Strong Thermosets and Organogels via Paraformaldehyde Condensation with Diamines.* Science, 2014. **344**(6185): p. 732-735.

66. Christensen, P.R., et al., *Closed-loop recycling of plastics enabled by dynamic covalent diketoenamine bonds.* Nature Chemistry, 2019. **11**(5): p. 442-448.

67. Barker, C.M., et al., *Solvent-free vat photopolymerization of unsaturated polyesters: Structure-property relationships for depolymerization.* MRS Communications, 2023.

68. Song, Y., et al., *Measurements of the mechanical response of unidirectional 3D-printed PLA.* Materials & Design, 2017. **123**: p. 154-164.

69. Costanzo, A., D. Cavallo, and C. McIlroy, *High-performance co-polyesters for material-extrusion 3D printing: A molecular perspective of weld properties.* Additive Manufacturing, 2022. **49**: p. 102474.

70. Chiulan, I., et al., *Recent Advances in 3D Printing of Aliphatic Polyesters.* Bioengineering (Basel), 2017. **5**(1).

71. Invernizzi, M., et al., *4D printed thermally activated self-healing and shape memory polycaprolactone-based polymers.* European Polymer Journal, 2018. **101**: p. 169-176.

72. Elomaa, L., et al., *Porous 3D modeled scaffolds of bioactive glass and photocrosslinkable poly(ε-caprolactone) by stereolithography.* Composites Science and Technology, 2013. **74**: p. 99-106.

73. Seppälä, J., et al., *Photocrosslinkable Polyesters and Poly(ester anhydride)s for Biomedical Applications.* Macromolecular Bioscience, 2011. **11**(12): p. 1647-1652.

74. Thompson, J.R., et al., *Two-photon polymerized poly(caprolactone) retinal cell delivery scaffolds and their systemic and retinal biocompatibility.* Acta Biomaterialia, 2019. **94**: p. 204-218.

75. Lammel-Lindemann, J., et al., *Photocrosslinking-based 3D printing of unsaturated polyesters from isosorbide: A new material for resorbable medical devices.* Bioprinting, 2020. **18**: p. e00062.

76. Mete, Y., et al., *Cationic photopolymerization of cyclic esters at elevated temperatures and their application in hot lithography.* Polymer International, 2022. **71**(9): p. 1062-1071.

77. Kojic, D., et al., *Stereolithographic 3D printing of pure poly(ether–ester) networks from spirocyclic monomers via cationic ring-opening photopolymerization at high temperatures.* Polymer Chemistry, 2023. **14**(42): p. 4809-4818.

78. Xie, R., et al., *A direct comparison between ring-opening copolymerization and polycondensation to produce polyesters using poly(ethylene succinate) as an example.* Polymer Chemistry, 2024.

79. Ryzhakov, D., et al., *Organo-catalyzed/initiated ring opening co-polymerization of cyclic anhydrides and epoxides: an emerging story.* Polymer Chemistry, 2021. **12**(20): p. 2932-2946.

80. Stühler, M.R., et al., *Ring-opening terpolymerisation of phthalic thioanhydride with carbon dioxide and epoxides.* Polymer Chemistry, 2023. **14**(42): p. 4848-4855.

81. Fischer, R.F., *Polyesters from expoxides and anhydrides.* Journal of Polymer Science, 1960. **44**(143): p. 155-172.

82. Paul, S., et al., *Ring-opening copolymerization (ROCOP): synthesis and properties of polyesters and polycarbonates.* Chemical Communications, 2015. **51**(30): p. 6459-6479.

83. Jeske, R.C., A.M. DiCiccio, and G.W. Coates, *Alternating Copolymerization of Epoxides and Cyclic Anhydrides: An Improved Route to Aliphatic Polyesters.* Journal of the American Chemical Society, 2007. **129**(37): p. 11330-11331.

84. Merckle, D. and A.C. Weems, *Organocatalysis in ring opening copolymerization as a means of tailoring molecular weight dispersity and the subsequent impact on physical properties in 4D printable photopolymers.* Polymer Chemistry, 2023. **14**(31): p. 3587-3599.

85. Niknam, F., et al., *Dinuclear chromium complexes with [OSSO]-type ligands in the copolymerization of epoxides with CO2 and phthalic anhydride.* Catalysis Science & Technology, 2023. **13**(16): p. 4684-4692.

86.   Lin, M.-L. and C.-Y. Tsai, *High-Activity and High-Selectivity Air-Stable Nickel and Copper Complexes for Copolymerization of Epoxides with Anhydrides.* Inorganic Chemistry, 2023. **62**(31): p. 12298-12307.

87.   Mauri, A.N., et al., *Kinetic Model for Gelation in the Diepoxide–Cyclic Anhydride Copolymerization Initiated by Tertiary Amines.* Macromolecules, 1997. **30**(6): p. 1616-1620.

88.   Fernàndez-Francos, X., X. Ramis, and À. Serra, *From curing kinetics to network structure: A novel approach to the modeling of the network buildup of epoxy–anhydride thermosets.* Journal of Polymer Science Part A: Polymer Chemistry, 2014. **52**(1): p. 61-75.

89.   Ikeda, I., Y. Simazaki, and K. Suzuki, *Synthesis of graft polyesters by ring-opening copolymerization of epoxy-terminated poly(ethylene glycol) with acid anhydrides.* Journal of Applied Polymer Science, 1991. **42**(11): p. 2871-2877.

90.   Han, B., et al., *Controllable Synthesis of Stereoregular Polyesters by Organocatalytic Alternating Copolymerizations of Cyclohexene Oxide and Norbornene Anhydrides.* Macromolecules, 2015. **48**(11): p. 3431-3437.

91.   Lustoň, J. and Z. Maňásek, *Ammonium salt catalyzed copolymerization of 2-hydroxy-4-(2,3-epoxypropoxy)benzophenone with phthalic anhydride.* Die Makromolekulare Chemie, 1980. **181**(3): p. 545-555.

92.   Li, H., J. Zhao, and G. Zhang, *Self-Buffering Organocatalysis Tailoring Alternating Polyester.* ACS Macro Letters, 2017. **6**(10): p. 1094-1098.

93.   Zhang, D., et al., *Metal-Free Alternating Copolymerization of CO2 with Epoxides: Fulfilling "Green" Synthesis and Activity.* Journal of the American Chemical Society, 2016. **138**(35): p. 11117-11120.

94.   Ji, H.-Y., et al., *Lewis pairs for ring-opening alternating copolymerization of cyclic anhydrides and epoxides.* Green Chemistry, 2018. **20**(3): p. 641-648.

95.   Liang, X., et al., *Self-switchable polymerization catalysis with monomer mixtures: using a metal-free commercial thiourea catalyst to deliver block polyesters.* Polymer Chemistry, 2023. **14**(43): p. 4918-4926.

96.   Brooks, S., D. Merckle, and A.C. Weems, *4D Photopolymers Derived From Ring-Opening Copolymerization of Cyclic Anhydrides and Limonene Oxide.* ACS Sustainable Chemistry & Engineering, 2023. **11**(28): p. 10252-10263.

97.   Peña Carrodeguas, L., C. Martín, and A.W. Kleij, *Semiaromatic Polyesters Derived from Renewable Terpene Oxides with High Glass Transitions.* Macromolecules, 2017. **50**(14): p. 5337-5345.

98.   Brandolese, A., et al., *Catalytic Ring-Opening Copolymerization of Fatty Acid Epoxides: Access to Functional Biopolyesters.* Macromolecules, 2022. **55**(7): p. 2566-2573.

99.   Yang, J., et al., *Phase Transition and Crystallization of Bio-based Comb-like Polymers Based on Renewable Castor Oil-Derived Epoxides and CO2.* Macromolecules, 2021. **54**(18): p. 8503-8511.

100.   Zheng, L., et al., *Organocatalytic synthesis of sugar-derived polyesters via ring-opening alternating copolymerization of anhydrosugar oxetane and anhydrides.* Journal of Polymer Science, 2023. **61**(14): p. 1430-1438.

101.   Kameyama, A., et al., *The First Synthesis of Alternating Copolymers of Oxetanes with Cyclic Carboxylic Anhydrides Using Quaternary Onium Salts.* Macromolecules, 2002. **35**(10): p. 3792-3794.

102.   Jian, Y., et al., *Thiol–epoxy/thiol–acrylate hybrid materials synthesized by photopolymerization.* Journal of Materials Chemistry C, 2013. **1**(29): p. 4481-4489.

103.   Shin, J., et al., *Thiol−Isocyanate−Ene Ternary Networks by Sequential and Simultaneous Thiol Click Reactions.* Chemistry of Materials, 2010. **22**(8): p. 2616-2625.

104.   Tsang, E.M.W. and S. Holdcroft, *10.35 - Alternative Proton Exchange Membranes by Chain-Growth Polymerization*, in *Polymer Science: A Comprehensive Reference*, K. Matyjaszewski and M. Möller, Editors. 2012, Elsevier: Amsterdam. p. 651-689.

105. Shimomura, O., et al., *DABCO- and DBU-intercalated α-zirconium phosphate as latent thermal catalysts in the copolymerization of glycidyl phenyl ether (GPE) and hexahydro-4-methylphthalic anhydride (MHHPA).* Journal of Molecular Catalysis A: Chemical, 2016. **411**: p. 230-238.

106. Sigma-Aldrich, *Quantitative NMR _ Technical Details and TraceCERT (Certified Reference Materials)*. 2017.

107. *IR-Spektrum: Tabelle & Schema*. 2023 [cited 2023 10/08/2023]; Available from: https://www.sigmaaldrich.com/AT/de/technical-documents/technical-article/analytical-chemistry/photometry-and-reflectometry/ir-spectrum-table.

108. Lemaire, C.F., et al., *Fast Production of Highly Reactive No-Carrier-Added [18F]Fluoride for the Labeling of Radiopharmaceuticals.* Angewandte Chemie International Edition, 2010. **49**(18): p. 3161-3164.

109. Glasovac, Z., et al., *Gas phase basicity of biguanides – Comparison of the equilibrium and the kinetic methods.* International Journal of Mass Spectrometry, 2019. **435**: p. 61-68.

110. Schwesinger, R., et al., *Extremely Strong, Uncharged Auxiliary Bases; Monomeric and Polymer-Supported Polyaminophosphazenes (P2–P5).* Liebigs Annalen, 1996. **1996**(7): p. 1055-1081.

111. Strong, A.B., *Plastics: Materials and Processing*. 2006: Pearson Prentice Hall.

112. An, J., *Chapter 6 - Polymer materials for additive manufacturing*, in *Digital Manufacturing*, C.D. Patel and C.-H. Chen, Editors. 2022, Elsevier. p. 221-245.

113. Gorsche, C., et al., *Real Time-NIR/MIR-Photorheology: A Versatile Tool for the in Situ Characterization of Photopolymerization Reactions.* Analytical Chemistry, 2017. **89**(9): p. 4958-4968.

114. Peck, M.C.P., R.O. Carter Iii, and S.B.A. Qaderi, *Near infrared measurements of terminal epoxides in polymer resin systems. I. Analytical considerations.* Journal of Applied Polymer Science, 1987. **33**(1): p. 77-86.

115. Goddu, R.F. and D.A. Delker, *Determination of Terminal Epoxides by Near-Infrared Spectrophotometry.* Analytical Chemistry, 1958. **30**(12): p. 2013-2016.

116. Lachenal, G., A. Pierre, and N. Poisson, *FT-NIR spectroscopy: Trends and application to the kinetic study of epoxy/triamine system (comparison with DSC and SEC results).* Micron, 1996. **27**(5): p. 329-334.

117. Pezzana, L., et al., *Hot-lithography 3D printing of biobased epoxy resins.* Polymer, 2022. **254**: p. 125097.

118. Park, S., et al., *Molecular Origin of the Induction Period in Photoinitiated Cationic Polymerization of Epoxies and Oxetanes.* Macromolecules, 2019. **52**(3): p. 1158-1165.

119. Bulut, U. and J.V. Crivello, *Investigation of the Reactivity of Epoxide Monomers in Photoinitiated Cationic Polymerization.* Macromolecules, 2005. **38**(9): p. 3584-3595.

120. Wiberg, N., *Lehrbuch der Anorganischen Chemie*. 2008: De Gruyter.

121. Adhikari, R., et al., *4 - Mechanical properties of conjugated polymers*, in *Conjugated Polymers for Next-Generation Applications*, V. Kumar, et al., Editors. 2022, Woodhead Publishing. p. 113-146.

122. Zgoła-Grześkowiak, A., *Application of DLLME to Isolation and Concentration of Non-Steroidal Anti-Inflammatory Drugs in Environmental Water Samples.* Chromatographia, 2010. **72**(7): p. 671-678.

123. Klikovits, N., *Thermally promoted cationic photopolymerization of ring-opening monomers for Hot Lithography*. 2020, Wien.

APPENDIX

ABBREVIATIONS

AMT	Additive manufacturing technology
ATR-FTIR	Attenuated total reflectance-fourier transform infrared spectroscopy
BAPO	phenylbis(2,4,6-trimethylbenzoyl) phosphine oxide
BDDE	1,4-Butanediol diglycidyl ether
BDI	β-diiminate
BHT	Butylhydroxytoluol
BP2T	1-tert-butyl-2,2,4,4,4-pentakis(dimethylamino)-2λ^5,4λ^5-catenadi(phosphazene) tetraphenylborate
CAN	covalent adaptable network
CHO	Cyclohexene oxide
DBU	1,8-Diazabicyclo(5.4.0)undec-7-ene
DLP-SL	digital light processing-based stereolithography
DMAP	4-(dimethylamino)pyridine
DMGA	2,2-dimethyl glutaric anhydride
DMSA	2,2-dimethyl succinic anhydride
DSC	Dynamic scanning calorimetry
EC	Ethylene carbonate
ECC	3,4-epoxycyclohexylmethyl 3,4-epoxycyclohexanecarboxylate
ELSD	Evaporative light scattering detector
EO	Ethylene oxide
EtOAc	Ethyl acetate
FDM	Fused deposition modeling
GA	Glutaric anhydride
HPLC	High performance liquid chromatography
HTT	High-temperature PE tape
HU	1,3-dicyclohexylurea
ITX	isopropylthioxanthone
KP2T	1-tert-butyl-2,2,4,4,4-pentakis(dimethylamino)-2λ^5,4λ^5-catenadi(phosphazene) 2-(3-benzoylphenyl)propionate

LA	Lewis acid
L-AMT	lithography-based additive manufacturing technology
LB	Lewis base
LC-MS	Liquid chromatography – mass spectrometry
L-SL	laser-stereolithography
MA	Maleic anhydride
MHHPA	4-Methyl-1,2-cyclohexanedicarboxylic anhydride
MPLC	Medium pressure liquid chromatography
NMR	Nuclear magnetic resonance
PA	Phthalic anhydride
PAG	photoacid generator
PBG	photobase generator
PCL	poly(caprolactone)
PDBN	4-(hexahydro-pyrrolo[1,2-a]pyrimidin-1-ylmethaneyl)-benzoic acid methyl ester
PE	polyethylene
PE	Petrol ether
PET	Poly(ethylene terephthalate)
PGE	Phenylglycidylether
PHTE	phloroglucinol triepoxide
PI	photoinitiator
PLA	poly(lactic acid)
PO	Propylene oxide
qNMR	Quantitative nuclear magnetic resonance
RDGE	Resorcinol diglycidyl ether
ROCOP	ring-opening copolymerization
r.t.	Room temperature
RT-FT-NIR-photorheology	Real Time-Fourier-Transformed-Near Infrared photorheology
SEC	Size exclusion chromatography
TEB	Triethyl borane
THF	Tetrahydrofuran
THPMTGE	Tris(4-hydroxyphenyl)methane triglycidyl ether
TLC	Thin layer chromatography

TMPTG	1,1,1-trimethylolpropane triglycidyl ether
TOF	Turnover frequency
TON	Turnover number
TPO-L	2,4,6-trimethylbenzoyl-diphenyl-phosphinoxide
UPE	Unsaturated polyester
UPy	2-ureido-4[1H]-pyrimidinone
WPBG 266	1,2-Diisopropyl-3-[bis(dimethylamino)methylene]guanidium 2-(3-benzoylphenyl)propionate
WPBG 300	1,2-Dicyclohexyl-4,4,5,5-tetramethylbiguanidium n-butyltriphenylborate

MONOMER SCREENING FOR CROSSLINKED SYSTEMS

Six different monomers containing two or three epoxide groups each were identified as possible crosslinking monomers for the ROCOP reaction (Figure S1). ^{1}H-NMR showed that those monomers were indeed present in the technical products, but also revealed some impurities. Therefore, HPLC and LC-MS measurements were performed to further analyze the technical monomers and determine the amount and type of impurities.
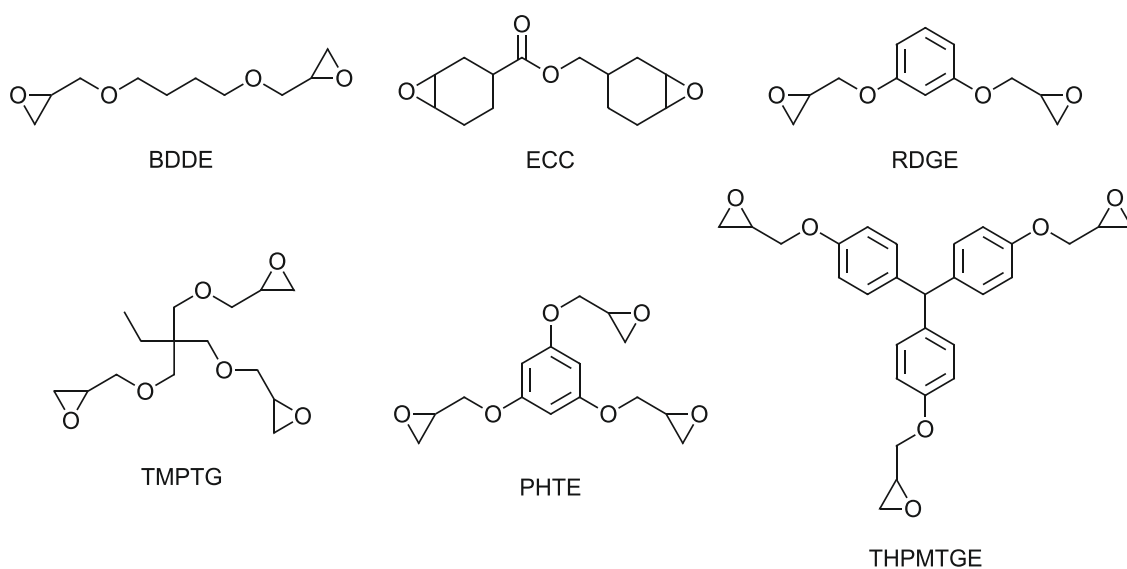
Figure S1. Multifunctional epoxides chosen as possible monomers for ROCOP with anhydrides to produce crosslinked polyesters.

115

HPLC Measurements

HPLC measurements were performed to quantify the purity of the monomers. For this, an exact amount of technical monomer was dissolved in 1 mL acetonitrile and filtered through a 0.2 µm filter (Table S1). Unfortunately, PHTE was not soluble in small amounts of acetonitrile. Solubility tests also did not reveal a proper solvent for dissolving PHTE in just small amounts of any other solvent. Therefore, PHTE could not be measured.

Table S1. Exact concentrations of the HPLC samples of the multifunctional epoxides.

RDGE	BDDE	ECC	TMPTG	THPMTGE
15.40 mg mL^{-1}	15.70 mg mL^{-1}	14.28 mg mL^{-1}	14.82 mg mL^{-1}	14.76 mg mL^{-1}

However, the other epoxides were analyzed and their fractions quantified using an evaporative light scattering detector ELSD and software for analysis (Table S2, Figure S2).
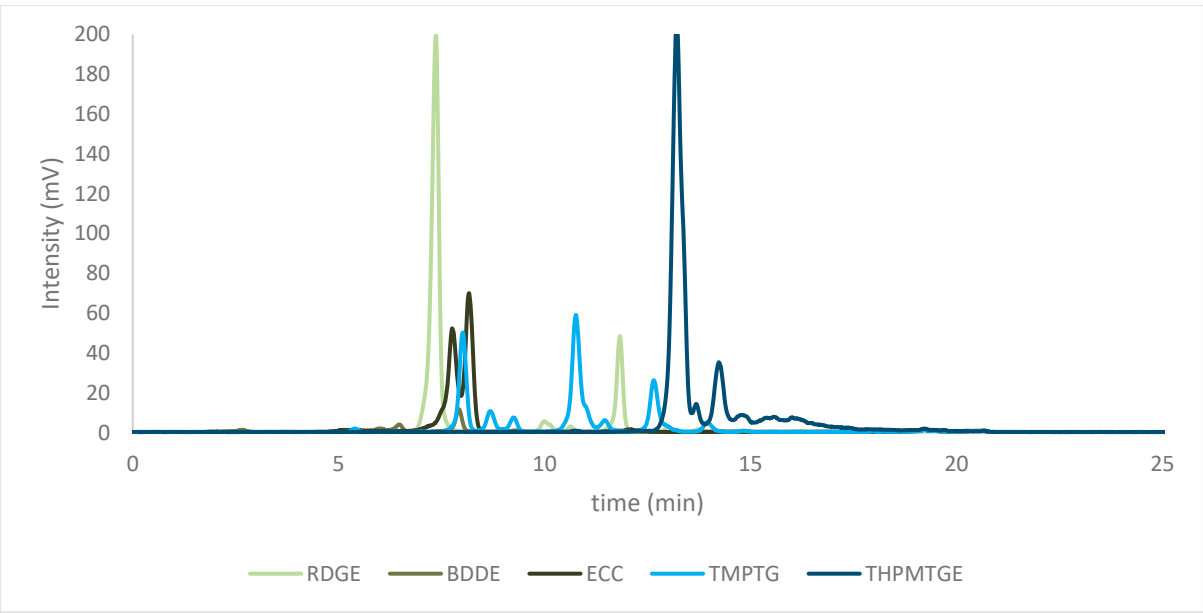
Figure S2. ELSD data obtained from HPLC measurements of the multifunctional epoxides RDGE, BDDE, ECC, TMPTG and THPMTGE.

Table S2. Results of HPLC measurements for quantification of multifunctional epoxide monomer purities.

Epoxide	Purity
RDGE	80%
BDDE	Bad recovery rate
ECC	2 peaks 50:50
PHTE	Not soluble
TMPTG	Many peaks
THPMTGE	85%

116

Unfortunately, the results were not very satisfying and further optimization of the measurement conditions would be required. However, since HPLC only gives quantitative information without certainty if the main peak is actually the monomer expected, LC-MS was chosen as an alternative analysis method.

LC-MS Measurements

LC-MS measurements of the possible multifunctional epoxide monomers were chosen since both quantitative information *via* the ELSD detector and qualitative information using the MS detector is obtained.

An exact amount of the five chosen, soluble, multifunctional epoxide monomers (RDGE, BDDE, ECC, TMPTG, THPMTGE) was dissolved in 2 mL acetonitrile and 0.2 mL water, and filtered through a 0.2 μm filter (Table S3).

Table S3. Exact concentrations of the LC-MS samples of the multifunctional epoxides.

RDGE	BDDE	ECC	TMPTG	THPMTGE
0.45 mg mL^{-1}	0.45 mg mL^{-1}	0.44 mg mL^{-1}	0.45 mg mL^{-1}	0.45 mg mL^{-1}

The main detected masses are summarized in Table S4, and the ELSD data is depicted in Figure S3. This ELSD data shows that optimization steps are required, because the baseline is shifting a lot, and the peaks are often not distinctly separated from the noise. Therefore, the concentration of the samples on the column needs to be increased for better results. However, if the concentration becomes too high, the MS detector gets overloaded. Another problem is that some peaks are not clearly separated from each other. For example, in the measurement of THPMTGE some of the peaks overlap slightly. This can be improved by changing the gradient of the mobile phase.

Table S4. MS data assigned to fractions of multifunctional epoxides with certain retention times.

	Retention time (min)	m/z
RDGE	1.757	296.10, 279.10, **223.05** (+ H)
	1.990	**332.05**, 315.05
	2.167	**462.15** (Dimer + H_2O), 445.15
	2.389	**684.25** (Trimer + H_2O)
BDDE	1.363	244.15, **220.15**
	1.508	**350.15**
	1.723	**422.20**
ECC	1.743	294.15, **253.10** (+ H)
	2.119	**582.30**
	2.434	**296.25**
TMPTG	1.463	264.15, **247.10**
	1.773	**320.20** (+ H_2O)
	2.060	**412.15**
	2.280	**504.15**
	2.447	**596.20**, 296.25
THPMTGE	0.945	**478.25** (+H_2O), 311.00
	1.064	502.35, **478.20** (+H_2O)
	1.230	**478.25** (+H_2O)
	1.870	323.20, **282.20**
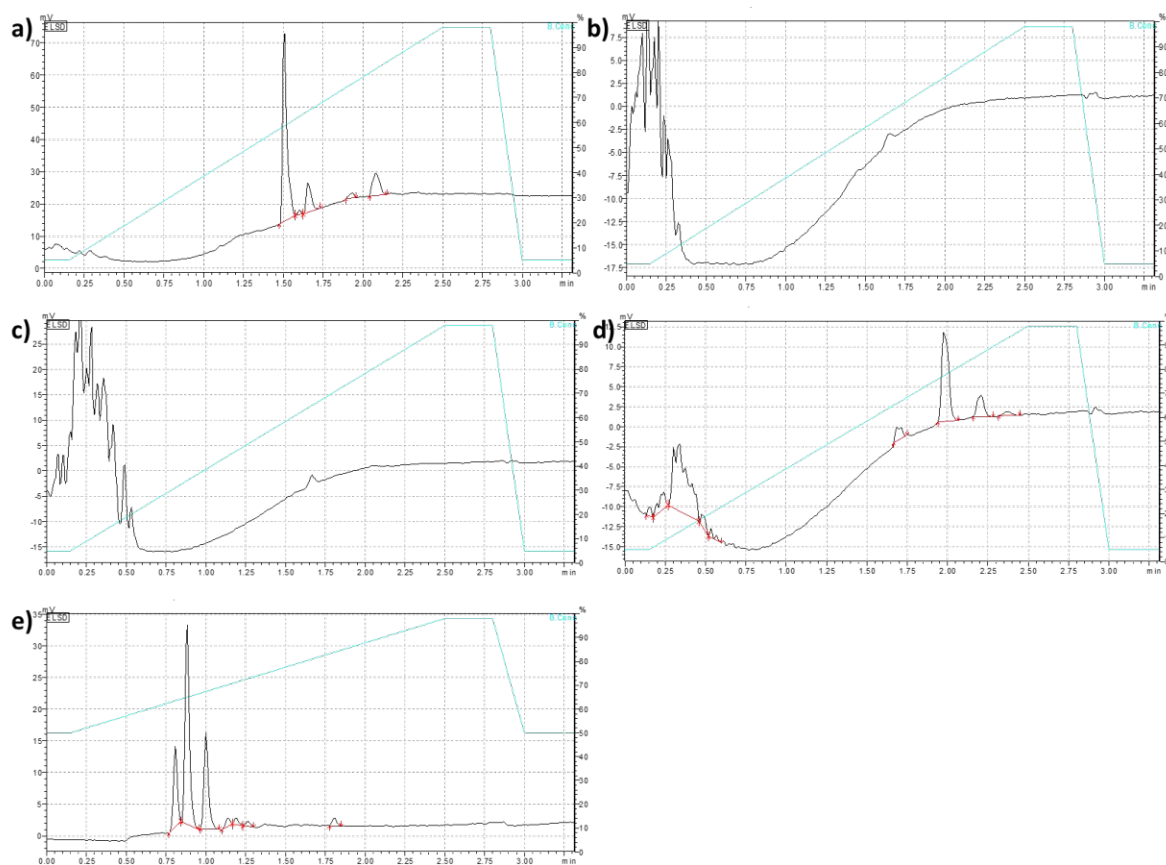
Figure S3. ELSD data obtained from LC-MS measurements of a) RDGE, b) BDDE, c) ECC, d) TMPTG, e) THPMTGE. The blue line indicates the solvent gradient used.

Since optimization of the analysis method is quite time-intensive, the focus was put on THPMTGE. The solvent gradient was optimized experimentally to get clearly separated peaks. Then, different injection volumes were tested to determine the best outcome for the ELSD without overloading the MS detector. Figure S4 shows the ELSD data for injection volumes of 0.5, 1 and 2 µL. The results for 0.5 µL are still without optimization of the solvent gradient, and therefore the peaks are not separated very well. It becomes apparent that the baseline distinctly improves when increasing the injection volume. Even though 2 µL gives even slightly better results than 1 µL injection volume, the MS detector is already at its limits at this concentration, therefore making 1 µL the better option.
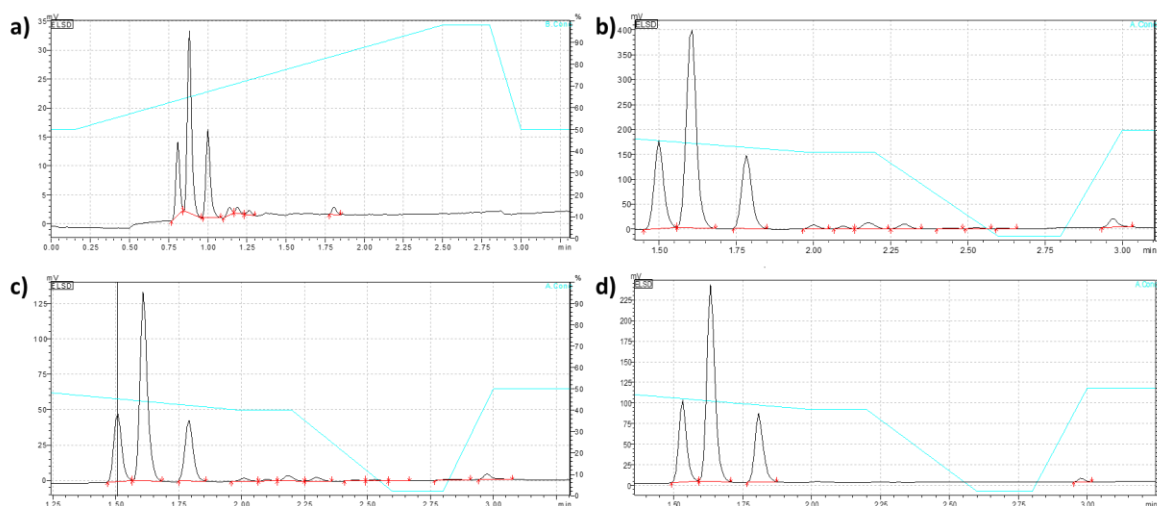
Figure S4. ELSD results from LC-MS measurement of techn. THPMTGE using a) 0.5 µL sample injection, b) 1 µL sample injection, c) 2 µL sample injection and d) of purified THPMTGE using 1 µL sample injection volume. The blue line indicates the solvent gradient used.

There are three main peaks visible from the ELSD data (Figure S4), which is quite unexpected. However, the main detected mass for all of those three peaks corresponds to the mass of [THPMTGE+H_2O] (Table S5). This could imply that one of the epoxides was hydrolyzed. However, it remains unclear if this really happened to the monomer or is just happening on the column during the measurement process, since the slightly acidic conditions would speed up hydrolysis.

Some of the smaller peaks at longer retention times are of higher mass, which points to impurities from oligomerization or other high-molecular weight impurities (Table S5).

Table S5. Major masses observed during LC-MS analysis of commercial THPMTGE

m/z	Difference	Fragment
478	+18	+ H_2O
311	-149	2* (epoxide-OH) + 3H^+
502	+42	+ ACN + H^+
788	+328	[a]
570	+110	[a]
769	+309	[a]

[a]unidentified

120

In order to get a better understanding of the results, THPMTGE was purified using column chromatography, and the purified product was measured again using LC-MS. Figure S4d shows the corresponding ELSD results. The three main peaks remain the same and still retain the same peak area ratio, while the peaks corresponding to higher molecular weight molecules disappeared. This emphasizes the theories that the three peaks either indicate stereochemical differences or hydrolysis products on the column, and not an impurity of the monomer.

However, since investigation and purification of the monomers is not a main goal of this thesis, no further experiments in this direction were conducted.

CALIBRATION OF HIGH-TEMPERATURE POLYETHYLENE TAPE FOR PHOTORHEOLOGY

In order to test if the high-temperature PE tape (HTT; SPT5A from tape providers, 5 mm thickness, acrylic adhesive, up to 150 °C) can be used in RT-FTIR-photorheology measurements without changing the results, a system that has been measured previously by Klikovits[123] consisting of BDDMA cured with Ivocerin (Figure S5) was chosen as reference. The reaction conditions were recreated closely (Table S6), and the same formulation was used (exact composition Table S7). Measurements were conducted in triplicates at 80 °C using both the normal PE tape as well as the high-temperature tape, and at 100 °C using the high-temperature tape.
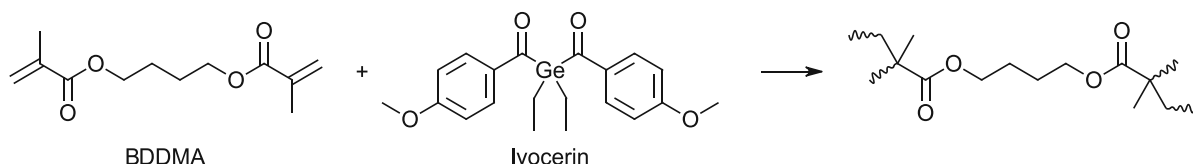
Figure S5. Reference system for testing of the high-temperature PE tape

Table S6. Summary of parameters for the testing of the high-temperature PE tape for RT-FTIR-photorheology measurements

	Dissertation Klikovits	**This work**
Formulation	BDDMA + 2 mol% Ivocerin	BDDMA + 2 mol% Ivocerin
Gap size	200 µm	200 µm
Sample size	150 µL	150 µL
Surface	PE tape	PE tape, high-temperature tape
Temperature	100 °C	80 °C, 100 °C
Conditioning	5 minutes	1 minute
Irradiation time	300 s	300 s
Light source	320 – 500 nm broadband Hg lamp	320 – 500 nm broadband Hg lamp
Light intensity	80 mW·cm^{-2}	75 mW·cm^{-2}
Strain, frequency	1%, 1 Hz	1%, 1Hz
Reproducibility	duplicates	triplicates

Table S7. Composition of formulation used for the testing of the high-temperature PE tape in RT-FTIR-photorheology measurements

Substance	Eq.	n(mmol)	M (g/mol)	Theoretical m (mg)	Weighed-in m (mg)
BDDMA	1	8.00	226.27	1810.16	1812.75
Ivocerin	0.04	0.32	401.00	128.32	128.42

Figure S6 shows a comparison of the measured storage modulus for different temperatures and tapes. The storage modulus obtained during measurements with the normal PE tape and with the HTT at 80 °C are very similar. The differences in the storage modulus of the HTT at 80 and 100 °C are marginal as well. Comparing the results using the HTT at 100 °C with the reported results from Klikovits,[123] a slightly reduced storage modulus was obtained, probably due to slightly different reaction conditions.
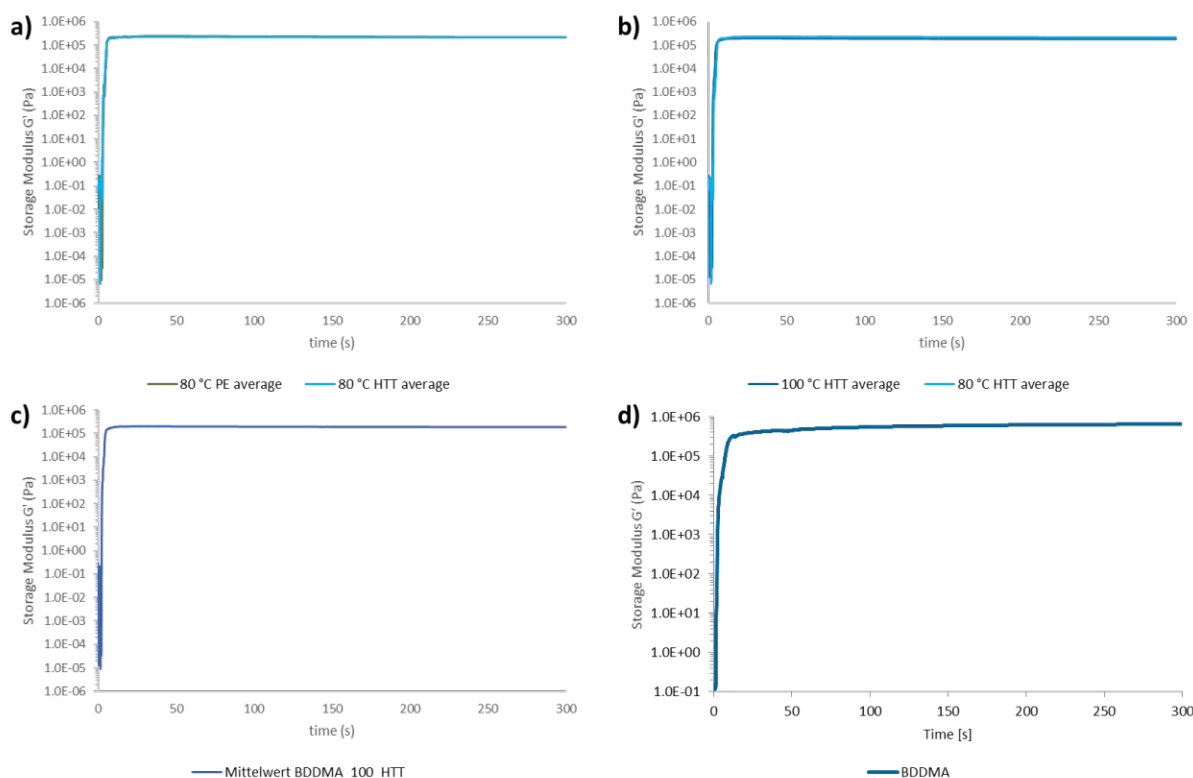
Figure S6. Comparison of storage modulus of BDDMA with Ivocerin a) using the PE tape vs using the HTT at 80 °C, b) using the HTT at 80 vs 100 °C, c) using the HTT at 100 °C, d) reference measurement at 100 °C from Klikovits.[123]

The gel point is reached in the crosssection of the storage modulus G' and the loss modulus G''. However, this crosssection is not easily determined since the results fluctuate a lot in this region as shown exemplarily in Figure S7a. Therefore, alternatively the intersection of lines where the normal force F_N is changing was used to determine the gel point, as shown exemplarily in Figure S7b for one of the measurements using the HTT at 100 °C.
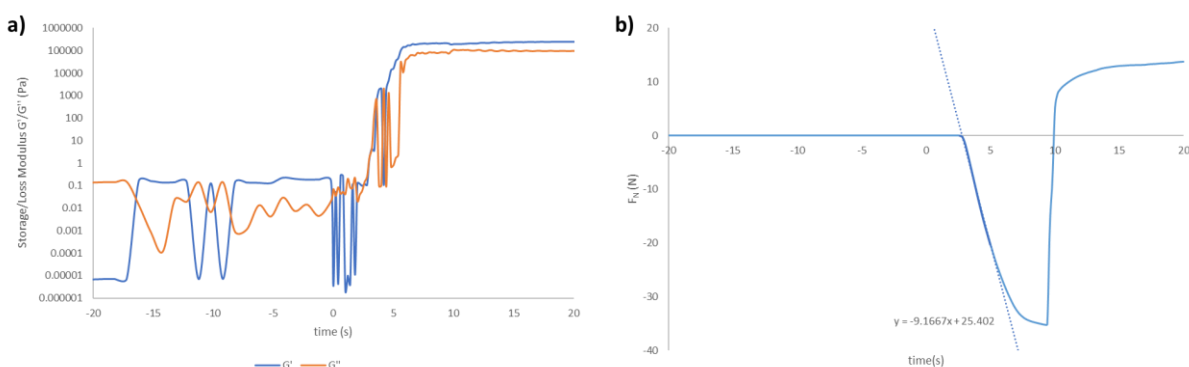
Figure S7. a) Zoom of intersection of storage modulus G' and loss modulus G'' for a RT-FT-NIR-photorheology measurement of BDDMA + 2 mol% Ivocerin at 100 °C using HTT. b) Zoom of gel point region of the normal force F_N for a RT-FT-NIR-photorheology measurement of BDDMA + 2 mol% Ivocerin at 100 °C using HTT.

123

The conversion was determined using the NIR data. A band at approximately 6160 cm^{-1} corresponds to the double bonds of BDDMA. The conversion was calculated using the ratio of this peak area at the start and after a certain irradiation period.

The time until gelation (t_g), the conversion at the gel point (C_g), and the final conversion (C_{final}) are representative parameters and can be calculated from the data above. These parameters are summarized in Table S8 and show that using the high-temperature tape does not distinctly change the results of the measurement at 80 °C. Furthermore, the results obtained at 100 °C are similar to the ones reported by Klikovits, though there are slight differences. However, these differences are likely due to slight differences in the reaction conditions, for example using slightly different monomers and slightly lower light intensity since the current Hg lamp cannot supply more than 75 mW cm^{-2} intensity on the sample surface. Therefore, it can be concluded that the high-temperature tape can be used for the measurements at high temperatures without changing the results.

Table S8. Results of the high-temperature tape testing used in RT-FTIR-photorheology measurements using BDDMA with 2 mol% Ivocerin.

	80 °C PE	80 °C HTT	100 °C HTT	100 °C reference[123]
C_{final}	90 %	91 %	91 %	87 %
t_g	2.6 ± 0.2 s	2.5 ± 0.2 s	1.9 ± 0.01 s	1.7 s
C_g	14 %	17 %	14 %	24 %

SUPPORTING DATA

NMRs
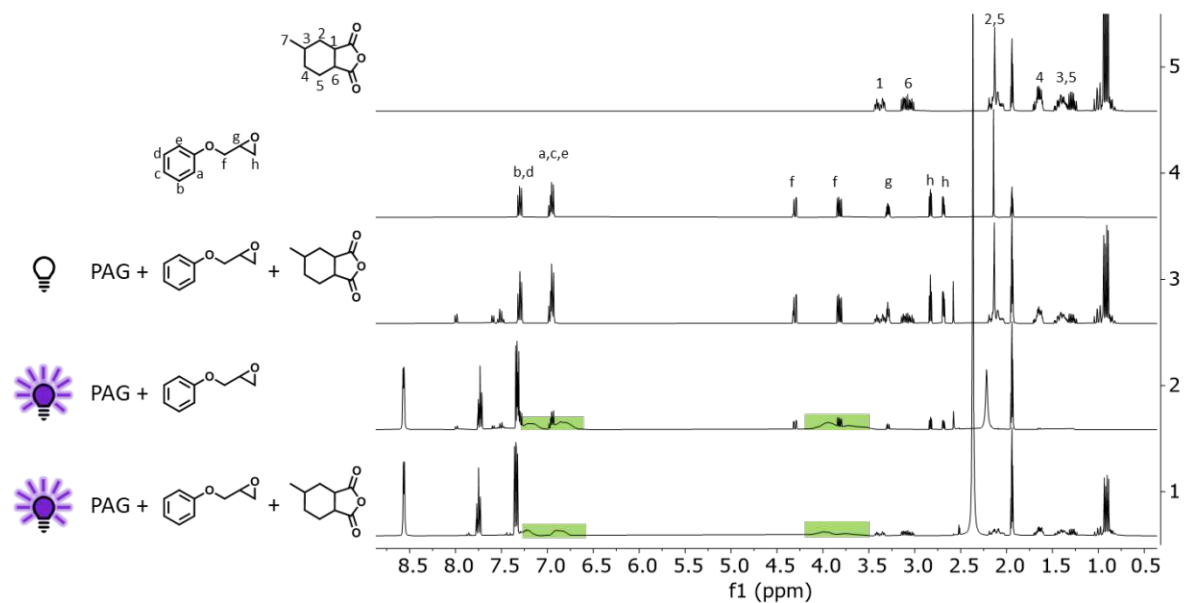
Figure S8. ^{1}H-NMR of PAG-catalyzed systems cured at 50 °C. 1) MHHPA, PGE + PAG cured at 50 °C. 2) PGE + PAG cured at 50 °C. 3) MHHPA, PGE + PAG formulation before irradiation. 4) PGE. 5) MHHPA.
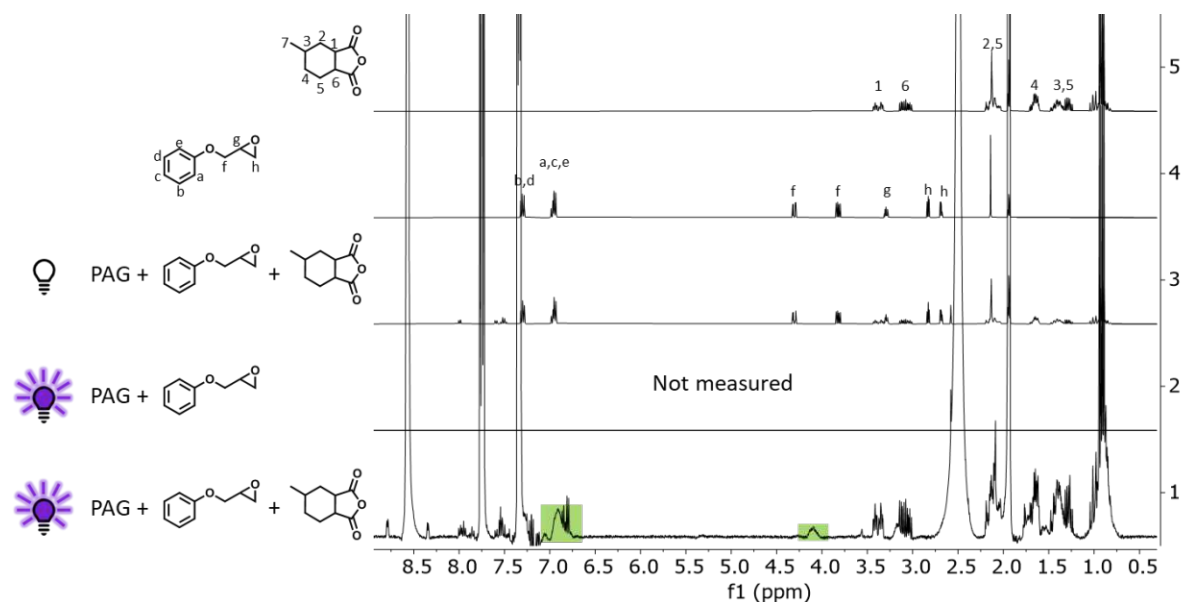
Figure S9. ^{1}H-NMR of PAG-catalyzed systems cured at 150 °C. 1) MHHPA, PGE + PAG cured at 50 °C. 2) control experiment not measured 3) MHHPA, PGE + PAG formulation before irradiation. 4) PGE. 5) MHHPA.
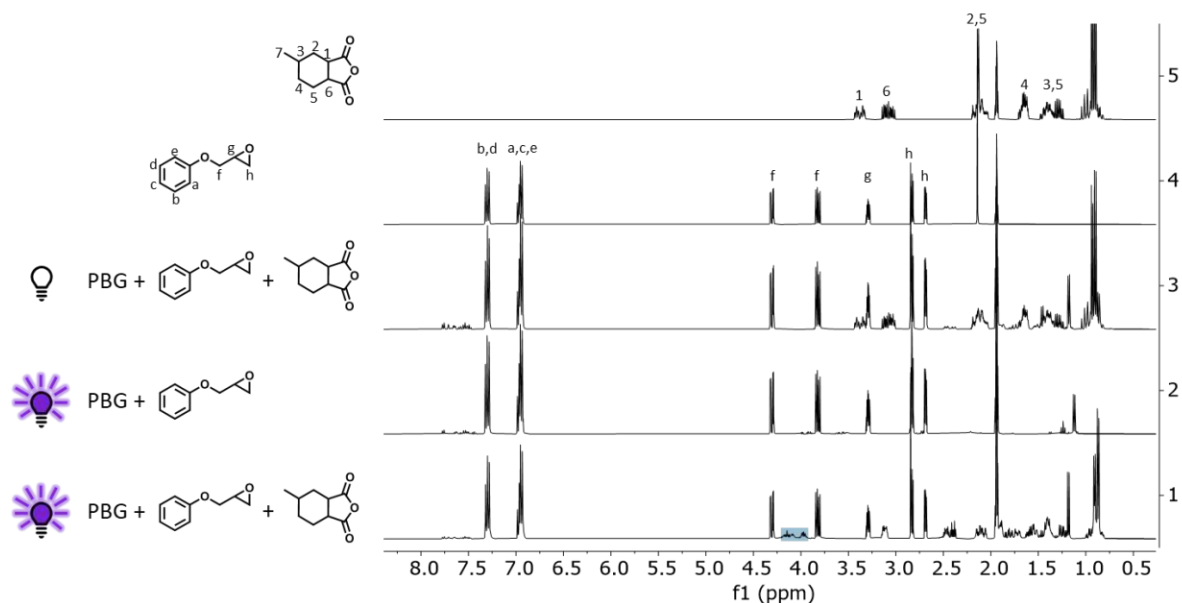
Figure S10. ¹H-NMR of PBG-catalyzed systems cured at 50 °C. 1) MHHPA, PGE + PBG cured at 50 °C. 2) PGE + PBG cured at 50 °C. 3) MHHPA, PGE + PBG formulation before irradiation. 4) PGE. 5) MHHPA.
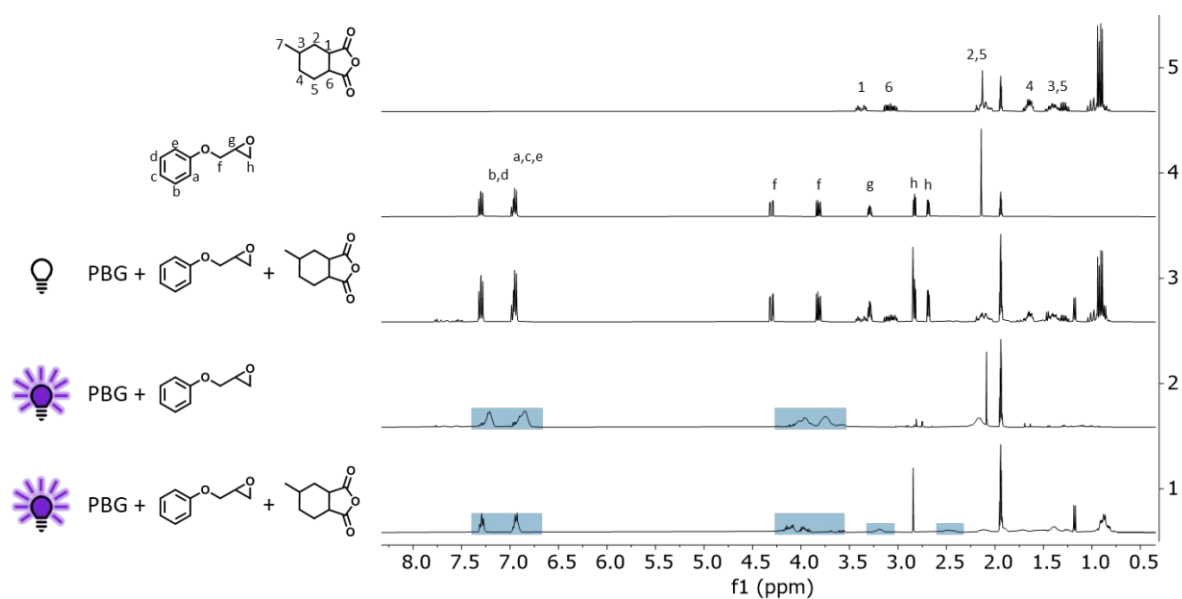
Figure S11. ¹H-NMR of PBG-catalyzed systems cured at 150 °C. 1) MHHPA, PGE + PBG cured at 150 °C. 2) PGE + PBG cured at 150 °C. 3) MHHPA, PGE + PBG formulation before irradiation. 4) PGE. 5) MHHPA.
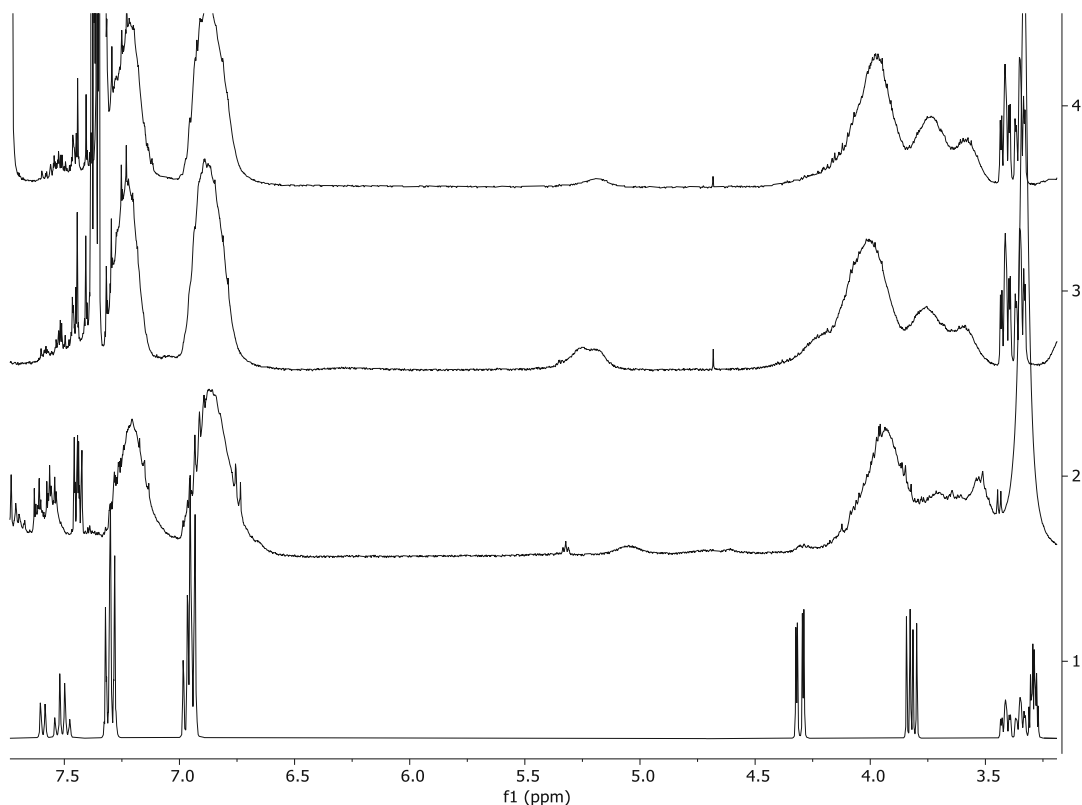
Figure S12. ^{1}H-NMR zoom of methine -COOCH$_2$-CH- signal formed during copolymerization. 1) MHHPA, GPE + PAG formulation before irradiation. 2) MHHPA, GPE + PAG cured at 150 °C. 3) MHHPA, GPE + PAG cured at 100 °C. 4) MHHPA, GPE + PAG cured at 50 °C.
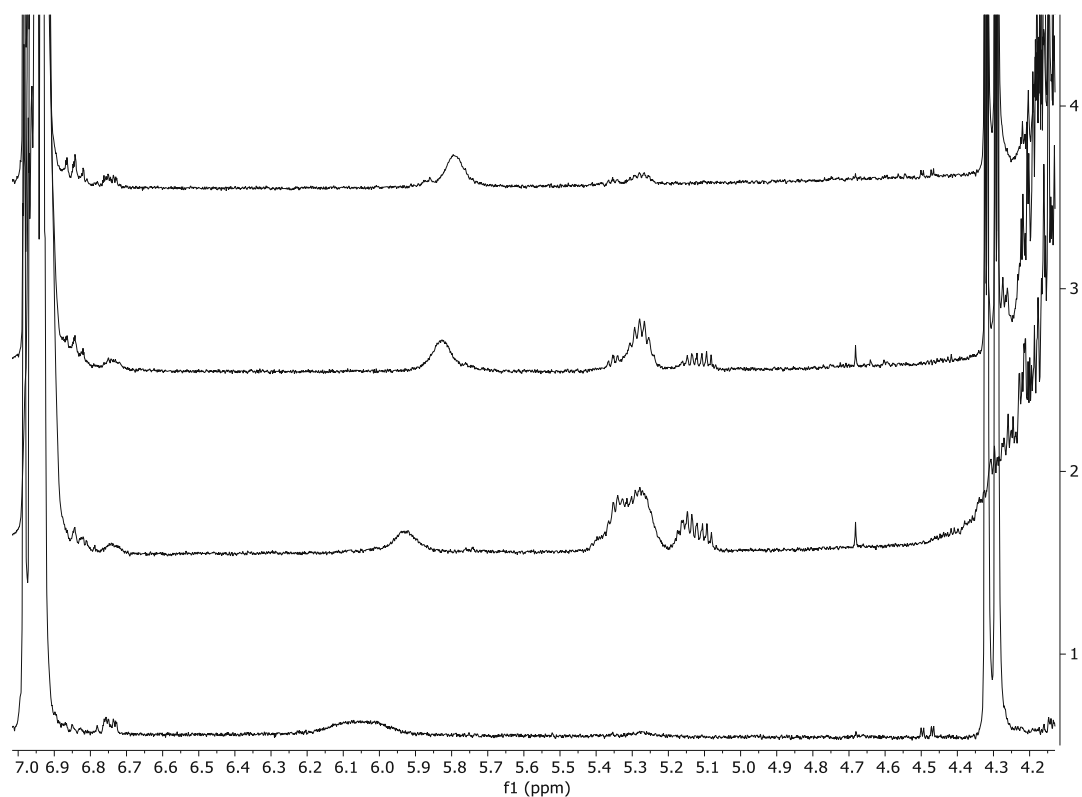
Figure S13. ^{1}H-NMR zoom of methine -COOCH$_2$-CH- signal formed during copolymerization. 1) MHHPA, GPE + PBG formulation before irradiation. 2) MHHPA, GPE + PBG cured at 150 °C. 3) MHHPA, GPE + PBG cured at 100 °C. 4) MHHPA, GPE + PBG cured at 50 °C.

TLC

Figure S14. TLC for determining the mobile phase for the purification of THPMTGE using MPLC.

Tables

Elucidation of Polymerization Behavior

Table S9. qNMR analysis results for determining the ratio copolymerization/homopolymerization by using monomer conversions. Samples contain PGE/MHHPA 1/1 (fg%/fg%) + 2.5 mol% catalyst.

	PAG			PBG		
	Uncured	Cured 50 °C	Cured 100 °C	Uncured	Cured 50 °C	Cured 100 °C
Sample weight (mg)	10.04	11.83	11.03	9.82	11.48	11.29
EC weight (mg)	8.02	7.80	7.75	8.63	9.08	9.02
Peak integral EC[a]	40.00	40.00	40.00	40.00	40.00	40.00
Peak integral PGE[b]	2.87	0.37	0.04	2.97	3.15	1.32
Peak integral MHHPA[c]	2.71	2.85	1.78	2.53	2.40	0.60
Amount PGE (wt%)	39.10	4.16	0.48	44.51	42.49	17.99
Amount MHHPA (wt%)	41.35	35.89	23.89	42.47	36.26	9.16
Conversion PGE (%)	0.00	89.36	98.77	0.00	4.54	59.60
Conversion MHHPA (%)	0.00	13.19	42.23	0.00	14.62	78.44

[a] 4.500-4.410 ppm (-CH_2-CH_2-)

[b] 4.328-4.280 ppm for PAG, 3.850-3.790 ppm for PBG (-O-CH_2-Epoxy)

[c] 3.445-3.320 ppm (>CH-CH$_2$-CH<)

Table S10. ^{1}H-NMR analysis results for determining the ratio copolymerization/homopolymerization by using monomer conversion. Samples contain PGE/MHHPA 1/1 (fg%/fg%) + 2.5 mol% catalyst.

	PAG: PGE			PAG: PGE + MHHPA		
	50 °C	100 °C	150 °C	50 °C	100 °C	150 °C
Peak integral PGE[a]	0.59	0.15	/	0.11	0.04	0.02
Constant peak integral PGE[b]	10.00	10.00	/	10.00	10.00	10.00
Peak integral polyester[c]	0.01	0.00	/	0.33	0.06	0.11
Conversion PGE (%)	82.30	95.50	/	96.70	98.80	99.40
Amount polyester (wt %)	0.30	0.00	/	9.90	1.80	3.30
Percentage copolymerization (%)	0.36	0.00	/	10.24	1.82	3.32
	PBG: PGE			**PBG: PGE + MHHPA**		
	50 °C	100 °C	150 °C	50 °C	100 °C	150 °C
Peak integral PGE[a]	3.27	2.91	0.00	2.72	0.85	0.03
Constant peak integral PGE[b]	10.00	10.00	10.00	10.00	10.00	10.00
Peak integral polyester[c]	0.01	0.01	0.01	0.03	0.47	1.54
Conversion PGE (%)	1.90	12.70	100.00	18.40	74.50	99.10
Amount polyester (wt %)	0.30	0.30	0.30	0.90	14.10	46.20
Percentage copolymerization (%)	15.79	2.36	0.30	4.89	18.93	46.62

[a]4.328-4.280 ppm for PAG, 3.850-3.790 ppm for PBG (-O-$\underline{CH_2}$-Epoxy)

[b]7.000-6.820 ppm (H2, H4, H6)

[c]5.400-5.050 ppm for PAG, 5.450-5.050 ppm for PBG (-COOCH_2-$\underline{CH}$-)

Table S11. Comparison of monomer conversions calculated from qNMR and ^{1}H-NMR for samples containing PGE/MHHPA 1/1 (fg%/fg%) + 2.5 mol% catalyst.

	qNMR PAG			qNMR PBG		
	Uncured	Cured 50 °C	Cured 100 °C	Uncured	Cured 50 °C	Cured 100 °C
Sample weight (mg)	10.04	11.83	11.03	9.82	11.48	11.29
EC weight (mg)	8.02	7.80	7.75	8.63	9.08	9.02
Peak integral EC[a]	40.00	40.00	40.00	40.00	40.00	40.00
Peak integral PGE[b]	2.87	0.37	0.04	2.97	3.15	1.32
Amount PGE (wt%)	39.10	4.16	0.48	44.51	42.49	17.99
Conversion PGE (%)	0.00	89.36	98.77	0.00	4.54	59.60
	^{1}H-NMR PAG			^{1}H-NMR PBG		
	/	Cured 50 °C	Cured 100 °C	/	Cured 50 °C	Cured 100 °C
Peak integral PGE[b]	/	0.37	0.04	/	3.15	1.32
Constant peak integral PGE[c]	/	10.91	8.16	/	9.22	8.86
Peak integral polyester[d]	/	0.01	0.24	/	-0.28	1.52
Conversion PGE (%)	/	89.83	98.53	/	-2.49	55.30
Amount polyester (wt %)	/	0.27	8.82	/	-9.11	51.47
Percentage copolymerization (%)	/	0.31	8.96	/	365.22	93.06

[a]4.500-4.410 ppm (-$\underline{CH_2}$-$\underline{CH_2}$-)

[b]4.328-4.280 ppm for PAG, 3.850-3.790 ppm for PBG (-O-$\underline{CH_2}$-Epoxy)

[c]7.000-6.820 ppm (H2, H4, H6)

[d]5.400-5.050 ppm for PAG, 5.400-5.130 ppm for PBG (-COOCH₂-$\underline{CH}$-)

Table S12. SEC data comparing the polymerization behavior of the model systems using PGE + MHHPA to the control system using only PGE when using either 2.5 mol% photoacid generator Irgacure 290 or 2.5 mol% photobase generator WPBG 266.

	Temperature (°C)	M_n (Da)	DP
	50	1940	12
PAG: PGE + MHHPA	100	2980	19
	150	3640	23
	50	1120	7
PAG: PGE	100	2160	14
	150	1750	12
	50	450	3
PBG: PGE + MHHPA	100	490	3
	150	620	4
	50	100	1
PBG: PGE	100	100	1
	150	1690	11

Table S13. qNMR analysis data of formulations containing PGE/MHHPA 1/1 (fg%/fg%) utilizing 2.5 mol% WPBG 266 + 0.25 mol% ITX to determine the stability of monomers in the formulation at 90 °C.

	time (min)	m sample (mg)	m EC (mg)	Peak integral EC[a]	Peak integral PGE[b]	Amount PGE (wt%)	Conversion PGE (%)
	0	13.37	3.91	40.00	9.03	45.04	0.00
	30	11.29	4.58	40.00	5.65	39.09	13.21
WPBG 266	60	11.29	4.70	40.00	4.90	33.94	24.64
	120	13.45	5.22	40.00	3.28	20.68	54.09
	240	9.83	4.86	40.00	0.74	5.80	87.11

[a]4.500-4.410 ppm (-CH_2-CH_2-)

[b]3.850-3.790 ppm (-O-CH_2-Epoxy)

Optimizing the Linear Model System

Table S14. qNMR analysis data of formulations containing PGE/MHHPA 1/1 (fg%/fg%) + 1 mol% of different PBGs to determine the effect of those different PBGs on the polymerization process.

	WPBG 266		WPBG 300		PDBN		KP2T		BP2T	
	Un-cured	Cured 100°C	Un-cured	Cured 100°C	Un-cured	Cured 100°C	Un-cured	Cured 100°C	Un-cured	Cured 100°C
Sample weight (mg)	12.53	10.78	12.48	11.14	12.46	11.36	12.64	11.48	12.93	12.20
EC weight (mg)	2.77	4.11	3.71	2.74	3.29	3.50	2.47	2.28	2.43	2.54
Peak integral EC[a]	40.00	40.00	40.00	40.00	40.00	40.00	40.00	40.00	40.00	40.00
Peak integral PGE[b]	12.40	5.50	9.37	8.76	10.32	7.67	14.09	5.42	14.65	11.78
Amount PGE (wt%)	46.75	35.76	47.50	36.75	46.47	40.30	46.96	18.36	46.95	41.83
Conversion PGE (%)	0.00	23.50	0.00	22.65	0.00	13.28	0.00	60.90	0.00	10.92

[a]4.500-4.410 ppm (-$\underline{CH_2}$-$\underline{CH_2}$-)

[b]3.850-3.790 ppm for PBG (-O-$\underline{CH_2}$-Epoxy)

Table S15. qNMR analysis data of formulations containing PGE/MHHPA 1/1 (fg%/fg%) utilizing 1 mol% of one respective PBG to determine the effect of PBG type on the stability of the formulation at 100 °C.

	time (min)	m sample (mg)	m EC (mg)	Peak integral EC[a]	Peak integral PGE[b]	Amount PGE (wt%)	Conversion PGE (%)
WPBG 266	0	11.36	2.47	40.00	13.10	48.58	0.00
	30	11.29	2.82	40.00	10.92	46.52	4.24
	60	13.97	2.77	40.00	12.26	41.46	14.65
	120	12.65	2.30	40.00	10.12	31.38	35.40
	240	15.68	2.55	40.00	6.28	17.42	64.14
WPBG 300	0	11.64	2.09	40.00	15.69	48.05	0.00
	30	12.36	2.33	40.00	14.39	46.26	3.71
	90	12.91	2.55	40.00	14.00	47.16	1.84
	120	11.05	2.18	40.00	13.61	45.79	4.69
	240	12.42	2.25	40.00	13.26	40.97	14.73
	360	13.19	2.35	40.00	12.02	36.52	23.98
PDBN	0	11.66	2.99	40.00	11.12	48.63	0.00
	30	11.59	2.73	40.00	10.36	41.62	14.42
	60	15.55	2.73	40.00	11.65	34.88	28.27
	120	15.18	2.54	40.00	7.51	21.43	55.93
BP2T	0	13.35	2.46	40.00	15.22	47.83	0.00
	30	12.22	2.21	40.00	15.44	47.62	0.44
	60	12.26	2.69	40.00	12.82	47.97	-0.30
	120	13.41	2.74	40.00	13.23	46.10	3.61
	240	12.35	2.73	40.00	11.56	43.58	8.89
	360	13.44	2.65	40.00	12.31	41.39	13.46
KP2T	0	11.81	2.12	40.00	15.56	47.64	0.00
	30	18.07	2.96	40.00	5.16	14.42	69.74
	90	10.10	2.93	40.00	1.51	7.47	84.32

[a] 4.500-4.410 ppm (-$\underline{CH_2}$-$\underline{CH_2}$-)

[b] 3.850-3.790 ppm (-O-$\underline{CH_2}$-Epoxy)

Table S16. Rheology data of formulations containing PGE/MHHPA 1/1 (fg%/fg%) utilizing 1 mol% of one respective PBG to determine the effect of PBG type on the stability of the formulation at 100 °C.

time (min)	Viscosity (Pa·s)				
	WPBG 266	WPBG 300	PDBN	BP2T	KP2T
0	0.0141±0.0001	0.0139±0.0001	0.0129±0.0001	0.0136±0.0001	0.0144±0.0001
30	0.0248±0.0001	0.0146±0.0001	0.0585±0.0001	0.0138±0.0001	2184±115
60	0.0503±0.0002	0.0145±0.0001	0.4628±0.0008	0.0139±0.0001	
120	0.4064±0.0005	0.0155±0.0000	116.4±0.5	0.0156±0.0001	
240	499.2±1.3	0.0356±0.0001		0.0195±0.0001	
360		0.0989±0.0001		0.0344±0.0004	

Table S17. qNMR analysis data of formulations containing PGE/MHHPA 1/1 (fg%/fg%) + different concentrations of WPBG 266 to determine the effect of those different PBG concentrations on the polymerization process.

	0.5 mol%		1 mol%		2.5 mol%	
	Uncured	Cured	Uncured	Cured	Uncured	Cured
Sample weight (mg)	12.55	10.87	12.53	10.78	11.58	11.47
EC weight (mg)	4.07	3.38	2.77	4.11	4.04	4.15
Peak integral EC[a]	40.00	40.00	40.00	40.00	40.00	40.00
Peak integral PGE[b]	8.44	7.48	12.40	5.50	7.53	2.63
Amount PGE (wt%)	46.68	39.67	46.75	35.76	44.80	16.23
Conversion PGE (%)	0.00	15.02	0.00	23.50	0.00	63.78

[a]4.500-4.410 ppm (-CH_2-CH_2-)

[b]3.850-3.790 ppm for PBG (-O-CH_2-Epoxy)

Table S18. qNMR analysis data of formulations containing PGE/MHHPA 1/1 (fg%/fg%) + different concentrations of WPBG 300 to determine the effect of those different PBG concentrations on the polymerization process.

	0.5 mol%		1 mol%		2.5 mol%	
	Uncured	Cured	Uncured	Cured	Uncured	Cured
Sample weight (mg)	14.21	10.85	12.48	11.14	11.51	12.09
EC weight (mg)	2.86	3.70	3.71	2.74	2.30	2.50
Peak integral EC[a]	40.00	40.00	40.00	40.00	40.00	40.00
Peak integral PGE[b]	13.70	7.00	9.37	8.76	13.56	6.97
Amount PGE (wt%)	47.02	40.71	47.50	36.75	46.21	24.58
Conversion PGE (%)	0.00	13.43	0.00	22.65	0.00	46.81

[a]4.500-4.410 ppm (-CH_2-CH_2-)

[b]3.850-3.790 ppm for PBG (-O-CH_2-Epoxy)

Table S19. SEC analysis data of formulations containing PGE/MHHPA 1/1 (fg%/fg%) + WPBG 266 or WPBG 300 in different concentrations for determining the effect of those different PBG concentrations on the polymerization process.

PBG	Concentration PBG (mol%)	M_n (Da)	DP
WPBG 266	0.5	610	4
	1	740	5
	2.5	490	3
WPBG 300	0.5	1340	8
	1	1750	11
	2.5	1850	12

Table S20. qNMR analysis data of formulations containing PGE/MHHPA 1/1 (fg%/fg%) + 2.5 mol% WPBG 266 to determine the effect of different curing temperatures on the polymerization process

PBG	Uncured	Cured 50 °C	Cured 60 °C	Cured 70 °C	Cured 80 °C	Cured 90 °C	Cured 100 °C
Sample weight (mg)	11.58	11.55	12.32	10.13	11.04	13.16	11.47
EC weight (mg)	4.04	4.52	4.03	4.42	4.34	4.43	4.15
Peak integral EC[a]	40.00	40.00	40.00	40.00	40.00	40.00	40.00
Peak integral PGE[b]	7.53	6.63	7.90	5.58	5.45	5.29	2.63
Amount PGE (wt%)	44.80	44.25	44.07	41.52	36.54	30.37	16.23
Conversion PGE (%)	0	1.24	1.63	7.32	18.45	32.21	63.78

[a]4.500-4.410 ppm (-$\underline{CH_2}$-$\underline{CH_2}$-)

[b]3.850-3.790 ppm for PBG (-O-$\underline{CH_2}$-Epoxy)

Table S21. SEC analysis data of formulations containing PGE/MHHPA 1/1 (fg%/fg%) + 2.5 mol% WPBG 266 to determine the effect of different curing temperatures on the polymerization process

Temperature (°C)	M_n (Da)	DP
50	120	1
60	120	1
70	120	1
80	120	1
90	1080	7
100	1590	10

Table S22. qNMR analysis data of formulations containing PGE/MHHPA 1/1 (fg%/fg%) + 2.5 mol% WPBG 300 to determine the effect of different higher curing temperatures on the polymerization process

	PGE + MHHPA				PGE			
	Uncured	Cured 120 °C	Cured 130 °C	Cured 140 °C	Uncured	Cured 120 °C	Cured 130 °C	Cured 140 °C
sample weight (mg)	11.83	11.36	11.62	11.97	13.14	11.17	11.27	11.21
EC weight (mg)	3.47	3.04	3.83	3.08	2.92	2.85	2.86	3.23
Peak integral EC[a]	40.00	40.00	40.00	40.00	40.00	40.00	40.00	40.00
Peak integral PGE[b]	8.94	0.24	0.05	0.08	22.21	12.89	16.36	10.25
Amount PGE (wt%)	44.72	1.10	0.28	0.35	84.17	56.09	70.80	50.37
Conversion PGE (%)	0.00	97.55	99.37	99.22	0.00	33.36	15.88	40.16

[a]4.500-4.410 ppm (-$\underline{CH_2}$-$\underline{CH_2}$-)

[b]3.850-3.790 ppm for PBG (-O-$\underline{CH_2}$-Epoxy)

Table S23. SEC analysis data of formulations containing PGE/MHHPA 1/1 (fg%/fg%) + 2.5 mol% WPBG 300 to determine the effect of different higher curing temperatures on the polymerization process

	Temperature (°C)	M_n (Da)	DP
PGE/MHHPA	120	2290	14
	130	2720	17
	140	2110	13
PGE	120	140	1
	130	550	3
	140	560	4

Table S24. Comparison of monomer conversions calculated from qNMR and ^{1}H-NMR for samples containing PGE/MHHPA 1/1 (fg%/fg%) + 2.5 mol% WPBG 300 to determine the effect of different higher curing temperatures on the copolymerization selectivity.

	qNMR				
	Uncured	**Cured 100 °C**	**Cured 120 °C**	**Cured 130 °C**	**Cured 140 °C**
Sample weight (mg)	11.83	See Table S18	11.36	11.62	11.97
EC weight (mg)	3.47		3.04	3.83	3.08
Peak integral EC[a]	40.00		40.00	40.00	40.00
Peak integral PGE[b]	8.94		0.24	0.05	0.08
Amount PGE (wt%)	44.72		1.10	0.28	0.35
Conversion PGE (%)	0.00		97.55	99.37	99.22

	^{1}H-NMR				
	/	**Cured 100 °C**	**Cured 120 °C**	**Cured 130 °C**	**Cured 140 °C**
Peak integral PGE[b]	/	6.97	0.24	0.05	0.08
Constant peak integral PGE[c]	/	36.34	21.31	12.32	6.27
Peak integral polyester[d]	/	3.89	2.56	1.41	0.44
Conversion PGE (%)	/	42.26	96.62	98.78	96.17
Amount polyester (wt %)	/	32.11	36.04	34.33	21.05
Percentage copolymerization (%)	/	75.63	37.30	34.76	21.89

[a]4.500-4.410 ppm (-CH_2-CH_2-)

[b]3.850-3.790 ppm (-O-CH_2-Epoxy)

[c]7.000-6.820 ppm (H2, H4, H6)

[d]5.400-5.130 ppm for PBG (-COOCH$_2$-CH-)

Table S25. qNMR analysis data of formulations containing PGE/MHHPA 1/1 (fg%/fg%) + 2.5 mol% WPBG 300 to determine the effect of different irradiation intensities on the polymerization process

Intensity (mW cm^{-2})	0	21	59	91	121	159
Sample weight (mg)	12.28	10.92	11.06	11.63	11.36	11.21
EC weight (mg)	2.16	2.32	2.32	2.56	2.33	2.77
Peak integral EC[a]	40.00	40.00	40.00	40.00	40.00	40.00
Peak integral PGE[b]	15.69	7.54	6.53	5.23	5.13	3.09
Amount PGE (wt%)	47.07	27.32	23.36	19.63	17.94	13.02
Conversion PGE (%)	0.00	41.96	50.37	58.29	61.87	72.33

[a]4.500-4.410 ppm (-CH_2-CH_2-)

[b]3.850-3.790 ppm for PBG (-O-CH_2-Epoxy)

Table S26. SEC analysis data of formulations containing PGE/MHHPA 1/1 (fg%/fg%) + 2.5 mol% WPBG 300 to determine the effect of different irradiation intensities on the polymerization process

Intensity (mW cm^{-2})	M$_n$ (Da)	DP
0	2050	13
21	1980	12
59	2280	14
121	2420	15
159	2460	15

Table S27. qNMR analysis data of formulations containing PGE/anhydride 1/1 (fg%/fg%) + 2.5 mol% of WPBG 300 to determine the effect of different anhydrides on the polymerization process.

	MHHPA		GA		DMGA		DMSA	
	Uncured	Cured 100 °C	Uncured	Cured 100 °C	Uncured	Cured 100 °C	Uncured	Cured 100 °C
Sample weight (mg)	11.06	10.73	12.03	12.00	12.08	11.68	12.31	11.24
EC weight (mg)	2.74	3.57	3.72	3.79	3.13	3.44	3.12	3.18
Peak integral EC[a]	40.00	40.00	40.00	40.00	40.00	40.00	40.00	40.00
Peak integral PGE[b]	10.98	3.70	10.06	7.61	11.32	8.06	5.88	2.75
Amount PGE (wt%)	46.39	20.99	53.05	40.99	50.02	40.48	51.00	40.43
Conversion PGE (%)	0.00	54.74	0.00	22.74	0.00	19.07	0.00	20.73

[a]4.500-4.410 ppm (-$\underline{CH_2}$-$\underline{CH_2}$-)

[b]3.850-3.790 ppm for PBG (-O-$\underline{CH_2}$-Epoxy)

Post-Curing Behavior

Table S28. qNMR analysis data of formulations containing PGE/MHHPA 1/1 (fg%/fg%) + different concentrations of WPBG 300 to investigate the post-curing behavior of these cured samples.

	1 mol% WPBG 300			
	Uncured	*Immediate quench.*	*48 h r.t.*	*48 h 100 °C*
Sample weight (mg)	11.36	11.52	11.62	11.46
EC weight (mg)	3.15	2.83	3.43	2.76
Peak integral EC[a]	40.00	40.00	40.00	40.00
Peak integral PGE[b]	10.05	8.71	5.22	0.11
Amount PGE (wt%)	47.53	36.49	26.28	0.45
Conversion PGE (%)	0.00	23.22	44.71	99.05

	2.5 mol% WPBG 300			
	Uncured	*Immediate quench.*	*48 h r.t.*	*48 h 100 °C*
Sample weight (mg)	12.28	11.63	12.03	12.79
EC weight (mg)	2.16	2.56	2.64	2.67
Peak integral EC[a]	40.00	40.00	40.00	40.00
Peak integral PGEb	15.69	5.23	3.32	0.08
Amount PGE (wt%)	47.07	19.63	12.43	0.28
Conversion PGE (%)	0.00	58.29	73.60	99.39

[a]4.500-4.410 ppm (-$\underline{CH_2}$-$\underline{CH_2}$-)

[b]3.850-3.790 ppm for PBG (-O-$\underline{CH_2}$-Epoxy)